Study on the structure of weak intensity tropical cyclones over Bay of Bengal using WRF model.

M. Sc. Thesis

BY

FLORA RAHMAN

DEPARTMENT OF PHYSICS

KHULNA UNIVERSITY OF ENGINEERING & TECHNOLOGY

KHULNA-9203, BANGLADESH

August-2017

Study on the structure of weak intensity tropical cyclones over Bay of Bengal using WRF model.

M. Sc. Thesis

BY

FLORA RAHMAN

ROLL NO: 1655501

SESSION: January-2016

A thesis submitted in partial fulfillment of the requirements for the degree of Master of Science in the Department of Physics, Khulna University of Engineering & Technology, Khulna-9203

DEPARTMENT OF PHYSICS

KHULNA UNIVERSITY OF ENGINEERING & TECHNOLOGY

KHULNA-9203, BANGLADESH

August-2017

DECLARATION

This is to certify that the thesis work entitled "***Study on the structure of weak intensity tropical cyclones over Bay Bengal using WRF model"*** has been carried out by FLORA RAHMAN in the Department of Physics, Khulna University of Engineering & Technology, Khulna, Bangladesh. The above thesis work or any part of this work has not been submitted anywhere for the award of any degree or diploma.

Signature of Supervisor — Signature of Candidate

(Professor Dr. Md. Abdullah Elias Akhter) — FLORA RAHMAN

DEDICATED TO
MY PARENTS

Acknowledgements

With my great manner it is a pleasure for me to express my deepest sense of gratitude and indebtedness to my reverend supervisor Dr. Md. Abdullah Elias Akhter, Professor, Department of Physics, Khulna University of Engineering & Technology, Khulna, for his kind guidance and supervision and for his constant encouragement throughout the research work. His inspiration and friendly cooperation has accelerated my works.

I am indebted to Professor Dr. Shibendra Shekher Sikder, Head, Department of Physics, Khulna University of Engineering & Technology for his strong support in various ways during the entire period of my study in this department. I express my heartfelt gratitude and thanks to Professor Dr. Md. Mahbub Alam Department of Physics, Khulna University of Engineering & Technology. Many thanks for their inspiration and advices from the beginning of my study. I gratefully acknowledge Mr. Md. Kamrul Hasan Reza, Associate Professors, Department of Physics, KUET for his cooperation during my theatrical study. I also gratefully acknowledge Mr. Sujit Kumar Shil, Md. Alamgir Hossain, Assistant Professors, Department of Physics, KUET for their cooperation regarding writing the thesis.

My personal thankful greetings are to my good friends and well wishers for their help and cooperation. There are numerous people who could not be mentioned individually but their interesting discussions have prompted much thought on various aspects, I would also like to thank them. I would like to express my heart full thanks to my parents for their inspiration, encouragement and multifaceted supports to carry out this thesis work.

I am grateful to the KUET authority for approval of the project in the 43rd meeting of CASR, agenda no. 43/23/1 and providing me the relevant facilities to complete this research work. The Author is grateful to National Centre for Atmospheric Research (NCAR), USA for making the WRF (WRF-ARW) model available to modeling community. I am grateful to the authors of the Grid Analysis and Display System software (GrADS) which is used for analytical purposes and displaying Figures. India Meteorological Department (IMD) is acknowledged for providing necessary data over India. Finally, I want to express my gratitude to almighty Creator for his mercy.

Flora Rahman

CONTENTS

			Page No.
Title Page			i
Declaration Page			iii
Acknowledgement			v
Contents			vi
List of Figures			ix
List of Tables			xiv
Nomenclature			xvi
Abstract			xvii
Chapter I:	**Introduction**		1
	1.1	**Introduction**	1
	1.2	**Objective and scope of the research work**	3
	1.3	**Social and economic benefit of the research work**	3
	1.4	**Structure of the Thesis**	4
Chapter II	**Review of Literature**		5
	2.1.1	**Tropical Cyclone**	5
	2.1.2	**Classification of Tropical Cyclones**	5
	2.1.3	**Life Cycle of Tropical Cyclones**	6
2.2	**Parameter of Tropical Cyclones**		7
	2.2.1	**Minimum Sea level pressure**	**7**
	2.2.2	**Wind speed**	8
	2.2.3	**Wind speed at 10m**	8
	2.2.4	**Vorticity**	9
	2.2.5	**Temperature anomaly**	10
	2.2.6	**Relative Humidity**	10
	2.2.7	**Water vapor mixing ratio**	11
2.3	**Weather Research & Forecasting Model**		12
	2.3.1	**Microphysics schemes in WRF-ARW Model**	12
	2.3.1.1	**WSM 6-class scheme**	13
	2.3.2	**Cumulus Parameterization**	13
	2.3.2.1	**Kain-Fritsch scheme**	14
	2.3.2.2	**Betts-Miller-Janjic scheme**	14

	2.3.2.3	**Grell–Freitas (GF)**	15
	2.3.2.4	**Grell-Devenyi ensemble schemes**	15
	2.3.2.5	**Grell-3 scheme**	16
	2.3.2.6	**Old Kain-Fritsch (OKF)**	16
	2.3.3	**Planetary boundary layer (PBL)**	17
	2.3.3.1	**Yonsei University (YSU) scheme**	17
	2.3.4	**Radiation schemes**	18
	2.3.4.1	**Long wave radiation**	18
	2.3.4.2	**Shortwave radiation**	18
	2.3.5	**Map Projection**	18
	2.3.5.1	**Mercator Projection**	19
	2.3.6	**Computation method**	19
	2.3.6.1	**Arakawa Staggered C-grids**	19
Chapter III	**Model Description and Methodology**		20
	3.1	**Model Description**	20
	3.2	**Model Domain and Configuration**	20
	3.3	**Data and Methodology**	21
Chapter IV	**Results and Discussion**		23
4.1	**Tropical Cyclone Rashmi**		23
	4.1.1	**Description of Tropical Cyclone Rashmi**	23
	4.1.2	**Minimum sea level pressure of Tropical Cyclone Rashmi**	24
	4.1.3	**Maximum wind speed of TC Rashmi**	26
	4.1.4	**Vorticity of TC Rashmi**	35
	4.1.5	**Temperature anomaly of TC Rashmi**	40
	4.1.6	**Relative humidity of TC Rashmi**	42
	4.1.7	**Relative humidity at 2m of TC Rashmi**	43
	4.1.8	**Water vapor mixing ratio of TC Rashmi**	44
4.2	**Tropical Cyclone Viyaru**		46
	4.2.1	**Description of Tropical Cyclone Viyaru**	46
	4.2.2	**Minimum sea level pressure of Tropical Cyclone Viyaru**	46
	4.2.3	**Maximum wind speed of TC Viyaru**	49
	4.2.4	**Vorticity of TC Viyaru**	57

	4.2.5	**Temperature anomaly of TC Viyaru**	61
	4.2.6	**Relative humidity of TC Viyaru**	64
	4.2.7	**Relative humidity at 2m of TC Viyaru**	65
	4.2.8	**Water vapor mixing ratio of TC Viyaru**	66
4.3	**Tropical Cyclone Nilam**		68
	4.3.1	**Description of Tropical Cyclone Nilam**	68
	4.3.2	**Minimum sea level pressure of Tropical Cyclone Nilam**	68
	4.3.3	**Maximum wind speed of TC Nilam**	71
	4.3.4	**Vorticity of TC Nilam**	80
	4.3.5	**Temperature anomaly of TC Nilam**	85
	4.3.6	**Relative humidity of TC Nilam**	87
	4.3.7	**Relative humidity at 2m of TC Nilam**	88
	4.3.8	**Water vapor mixing ratio of TC Nilam**	89
4.4	**Tropical Cyclone Khaimuk**		91
	4.4.1	**Description of Tropical Cyclone Khaimuk**	91
	4.4.2	**Minimum sea level pressure of Tropical Cyclone Khaimuk**	92
	4.4.3	**Maximum wind speed of TC Khaimuk**	95
	4.4.4	**Vorticity of TC Khaimuk**	104
	4.4.5	**Temperature anomaly of TC Khaimuk**	107
	4.4.6	**Relative humidity of TC Khaimuk**	110
	4.4.7	**Relative humidity at 2m of TC Khaimuk**	111
	4.4.8	**Water vapor mixing ratio of TC Khaimuk**	112
Chapter V	**Conclusions**		114
	References		116

List of Figures

Fig. No.	Description	Page
Fig. 1:	The WRF–ARW domain set up for the study.	21
Fig. 2:	Evolution of WRF model simulated (a) MSLP and (b) MWS at 10m level using six different cumulus schemes and that of observed of the TC Rashmi.	24
Fig. 3:	WRF model simulated SLP of TC Rashmi at different cumulus scheme.	25
Fig. 4:	WRF model simulated (a) East West and (b) North South cross sectional view of SLP of TC Rashmi at different cumulus scheme with fixed latitude and longitude respectively.	26
Fig. 5:	WRF model simulated MWS of TC Rashmi at different cumulus scheme	28
Fig. 6:	East west cross sectional view of WRF model simulated Wind speed (m/s) of TC Rashmi at different cumulus scheme with fixed latitude.	29
Fig. 7:	North south cross sectional view of WRF model simulated wind speed (m/s) of TC Rashmi at different cumulus scheme with fixed longitude.	29
Fig. 8:	WRF model simulated Wind vector and magnitude at 850 hPa levels at different cumulus scheme.	31
Fig. 9:	WRF model simulated Wind vector and magnitude at 200 hPa levels at different cumulus scheme.	31
Fig. 10:	WRF model simulated Radial wind (m/s) of TC Rashmi at different cumulus scheme	33
Fig. 11:	WRF model simulated tangential wind (m/s) of TC Rashmi at different cumulus scheme.	34
Fig. 12:	WRF model simulated Vertical wind (m/s) of TC Rashmi at different cumulus scheme.	34
Fig. 13:	WRF model simulated Horizontal wind (m/s) of TC Rashmi at different cumulus scheme.	35
Fig. 14:	Evolution of model simulated vorticity with time at different cumulus scheme for 1000,950,850,500 and 300 hPa level of TC Rashmi.	36
Fig. 15:	WRF Model simulated vorticity field of 850 hPa levels at different cumulus scheme.	38
Fig. 16:	WRF Model simulated vorticity field of 200 hPa levels at different cumulus scheme	38
Fig. 17:	WRF model simulated north south vertical distribution of relative vorticity with fixed longitude of TC Rashmi through the centre at different cumulus scheme.	39
Fig. 18:	WRF model simulated east west vertical distribution of relative vorticity with fixed latitude of TC Rashmi through the centre at different cumulus scheme.	39
Fig. 19:	WRF model simulated vertical distribution of temperature anomaly in the east-west direction of TC Rashmi at different cumulus scheme.	41

Fig. 20:	Evolution of model simulated (a) RH and (b) RH at 2m with time at different cumulus scheme of TC Rashmi	42
Fig. 21:	WRF model simulated vertical distribution of relative humidity (%) in the east-west direction of TC Rashmi at different cumulus.	42
Fig. 22:	WRF model simulated spatial distribution of relative humidity at 2m (%) in the east-west direction of TC Rashmi at different cumulus.	43
Fig. 23:	WRF model simulated vertical distribution of water vapor mixing ratio along the east-west cross section of the centre of TC Rashmi at different cumulus.	44
Fig. 24:	WRF model simulated horizontal distribution of water vapor mixing ratio at 950 hPa of TC Rashmi at different cumulus.	45
Fig. 25:	Evolution of WRF model simulated (a) MSLP and (b) MWS at 10m level using six different cumulus schemes and that of observed of the TC VIiyaru.	47
Fig. 26:	WRF model simulated SLP of TC Viyaru at different cumulus scheme	48
Fig. 27:	WRF model simulated (a) East West and (b) North South cross sectional view of SLP of TC Viyaru at different cumulus scheme with fixed latitude and longitude respectively.	49
Fig. 28:	WRF model simulated MWS of TC Viyaru at different cumulus scheme	50
Fig. 29:	East west cross sectional view of WRF model simulated wind speed (m/s) of TC Viyaru at different cumulus scheme with fixed latitude.	51
Fig. 30:	North south cross sectional view of WRF model simulated wind speed (m/s) of TC Viyaru at different cumulus scheme with fixed longitude.	52
Fig. 31:	WRF model simulated Wind vector and magnitude at 850 hPa levels at different cumulus scheme.	53
Fig. 32:	WRF model simulated Wind vector and magnitude at 200 hPa levels at different cumulus scheme.	54
Fig. 33:	WRF model simulated Radial wind (m/s) of TC Viyaru at different cumulus scheme	56
Fig. 34:	WRF model simulated Tangential wind (m/s) of TC Viyaru at different cumulus scheme.	56
Fig. 35:	WRF model simulated Vertical wind (m/s) of TC Viyaru at different cumulus scheme.	57
Fig. 36:	WRF model simulated Horizontal wind (m/s) of TC Viyaru at different cumulus scheme.	57
Fig. 37:	Evolution of model simulated vorticity with time at different cumulus scheme for 1000,950,850,500 and 300 hPa level of TC Viyaru.	58
Fig. 38:	WRF Model simulated vorticity field of 850 hPa levels at different cumulus scheme.	60
Fig. 39:	WRF Model simulated vorticity field of 200 hPa levels at different cumulus scheme.	60

Fig. 40:	WRF model simulated east west vertical distribution of relative vorticity with fixed longitude of TC Viyaru through the centre at different cumulus scheme.	61
Fig. 41:	WRF model simulated east west vertical distribution of relative vorticity with fixed latitude of TC Viyaru through the centre at different cumulus scheme.	61
Fig. 42:	WRF model simulated vertical distribution of temperature anomaly in the east-west direction of TC Viyaru at different cumulus scheme.	63
Fig. 43:	Evolution of model simulated (a) RH and (b) RH at 2m with time at different cumulus scheme of TC Viyaru	64
Fig. 44:	WRF model simulated vertical distribution of Relative humidity (%) in the east-west direction of TC Viyaru at different cumulus.	64
Fig. 45:	WRF model simulated spatial distribution of relative humidity at 2m (%) in the east-west direction of TC Viyaru at different cumulus.	65
Fig. 46:	WRF model simulated vertical distribution of water vapor mixing ratio along the east-west cross section of the centre of TC Viyaru at different cumulus.	66
Fig. 47:	WRF model simulated horizontal distribution of water vapor mixing ratio at 950 hPa of TC Viyaru at different cumulus.	67
Fig. 48:	Evolution of WRF model simulated (a) MSLP and (b) MWS at 10m level using six different cumulus schemes and that of observed of the TC Nilam.	69
Fig. 49:	WRF model simulated SLP of TC Nilam at different cumulus scheme.	70
Fig. 50:	WRF model simulated (a) East West and (b) North South cross sectional view of SLP of TC Nilam at different cumulus scheme with fixed latitude and longitude respectively.	71
Fig. 51:	WRF model simulated MWS of TC Nilam at different cumulus scheme.	73
Fig. 52:	East West cross sectional view of WRF model simulated wind speed (m/s) of TC Nilam at different cumulus scheme with fixed latitude.	74
Fig. 53:	North south cross sectional view of WRF model simulated Wind speed (m/s) of TC Nilam at different cumulus scheme with fixed longitude.	74
Fig. 54:	WRF model simulated Wind vector and magnitude at 850 hPa levels at different cumulus scheme	76
Fig. 55:	WRF model simulated Wind vector and magnitude at 200 hPa levels at different cumulus scheme	76
Fig. 56:	WRF model simulated Radial wind (m/s) of TC Nilam at different cumulus scheme	78
Fig. 57:	WRF model simulated Tangential wind (m/s) of TC Nilam at different cumulus scheme.	79
Fig. 58:	WRF model simulated Vertical wind (m/s) of TC Nilam at different cumulus	79

	scheme.	
Fig. 59:	WRF model simulated Horizontal wind (m/s) of TC Nilam at different cumulus scheme.	80
Fig. 60:	Evolution of model simulated vorticity with time at different cumulus scheme for 1000, 950, 850, 500 and 300 hPa level of TC Nilam.	81
Fig. 61:	WRF Model simulated vorticity field of 850 hPa levels at different cumulus scheme.	83
Fig. 62:	WRF Model simulated vorticity field of 200 hPa levels at different cumulus scheme.	83
Fig. 63:	WRF model simulated east west vertical distribution of relative vorticity with fixed longitude of TC Nilam through the centre at different cumulus scheme.	84
Fig. 64:	WRF model simulated east west vertical distribution of relative vorticity with fixed latitude of TC Nilam through the centre at different cumulus scheme.	84
Fig. 65:	WRF model simulated vertical distribution of temperature anomaly in the east-west direction of TC Nilam at different cumulus scheme.	86
Fig. 66:	Evolution of model simulated (a) RH and (b) RH at 2m with time at different cumulus scheme of TC Nilam.	87
Fig. 67:	WRF model simulated vertical distribution of Relative humidity (%) in the east-west direction of TC Nilam at different cumulus.	87
Fig. 68:	WRF model simulated spatial distribution of Relative humidity at 2m (%) in the east-west direction of TC Nilam at different cumulus.	88
Fig. 69:	WRF model simulated vertical distribution of water vapor mixing ratio along the east-west cross section of the centre of TC Nilam at different cumulus.	89
Fig. 70:	WRF model simulated horizontal distribution of water vapor mixing ratio at 950 hPa of TC Nilam at different cumulus.	90
Fig. 71:	Evolution of WRF model simulated (a) MSLP and (b) MWS at 10m level using six different cumulus schemes and that of observed of the TC Khaimuk.	92
Fig. 72:	WRF model simulated SLP of TC Khaimuk at different cumulus scheme.	93
Fig. 73:	WRF model simulated (a) East West and (b) North South cross sectional view of SLP of TC Khaimuk at different cumulus scheme with fixed latitude and longitude respectively	94
Fig. 74:	WRF model simulated MWS of TC Khaimuk at different cumulus scheme	96
Fig. 75:	East West cross sectional view of WRF model simulated wind speed (m/s) of TC Khaimuk at different cumulus scheme with fixed latitude.	97
Fig. 76:	North south cross sectional view of WRF model simulated Wind speed (m/s) of TC Khaimuk at different cumulus scheme with fixed longitude.	98
Fig. 77:	WRF model simulated Wind vector and magnitude at 850 hPa levels at different cumulus scheme.	99
Fig. 78:	WRF model simulated Wind vector and magnitude at 200 hPa levels at different cumulus scheme.	100
Fig. 79:	WRF model simulated Radial wind (m/s) of TC Khaimuk at different cumulus scheme	102

Fig. 80:	WRF model simulated Tangential wind (m/s) of TC Khaimuk at different cumulus scheme.	102
Fig. 81:	WRF model simulated Vertical wind (m/s) of TC Khaimuk at different cumulus scheme.	103
Fig. 82:	WRF model simulated Horizontal wind (m/s) of TC Khaimuk at different cumulus scheme.	103
Fig. 83:	Evolution of model simulated vorticity with time at different cumulus scheme for 1000, 950, 850, 500 and 300 hPa level of TC Khaimuk.	104
Fig. 84:	WRF Model simulated vorticity field of 850 hPa levels at different cumulus scheme.	106
Fig. 85:	WRF Model simulated vorticity field of 200 hPa levels at different cumulus scheme.	106
Fig. 86:	WRF model simulated east west vertical distribution of relative vorticity with fixed longitude of TC Khaimuk through the centre at different cumulus scheme	107
Fig. 87:	WRF model simulated north-south vertical distribution of relative vorticity with fixed latitude of TC Khaimuk through the centre at different cumulus scheme.	107
Fig. 88:	WRF model simulated vertical distribution of temperature anomaly in the east-west direction of TC Khaimuk at different cumulus scheme.	109
Fig. 89:	Evolution of model simulated (a) RH and (b) RH at 2m with time at different cumulus scheme of TC Khaimuk	110
Fig 90:	WRF model simulated vertical distribution of Relative humidity (%) in the east-west direction of TC Khaimuk at different cumulus.	110
Fig. 91:	WRF model simulated spatial distribution of Relative humidity at 2m (%) in the east-west direction of TC Khaimuk at different cumulus.	111
Fig. 92:	WRF model simulated vertical distribution of water vapor mixing ratio along the east-west cross section of the centre of TC Khaimuk at different cumulus.	112
Fig. 93:	WRF model simulated horizontal distribution of water vapor mixing ratio at 950 hPa of TC Khaimuk at different cumulus.	113

List of Table

Table	Name of the Table	Page
Table 1:	WRF Model and Domain Configurations	22
Table 2:	WRF model simulated maximum wind speed (m/s) at different cumulus scheme of 850, 500, 300 and 200 hPa pressure levels of TC Rashmi	30
Table 3:	WRF model simulated radial wind, tangential wind, vertical velocity and horizontal wind (cm/s) of TC Rashmi at different cumulus.	33
Table 4:	WRF Model simulated maximum vorticity ($x10^{-5}$ s^{-1}) at different pressure levels associated with TC Rashmi at different cumulus scheme.	37
Table 5:	WRF Model simulated temperature anomaly (^oC), relative humidity (%) and water vapor mixing ratio (kg/kg $x10^{-2}$) associated with TC Rashmi at different cumulus.	41
Table 6:	WRF model simulated wind speed (m/s) at different cumulus scheme of 850, 500, 300 and 200 hPa pressure levels of TC Viyaru	53
Table 7:	WRF model simulated radial wind, tangential wind, vertical velocity and horizontal wind (cm/s) of TC Viyaru at different cumulus.	55
Table 8:	WRF Model simulated maximum vorticity ($x10^{-5}$ s^{-1}) at different pressure levels associated with TC Viyaru at different cumulus scheme.	59
Table 9:	WRF Model simulated temperature anomaly (^oC), relative humidity (%) and water vapor mixing ratio (kg/kg $x10^{-2}$) associated with TC Viyaru at different cumulus.	63
Table 10:	WRF model simulated wind speed (m/s) at different cumulus scheme of 850, 500, 300 and 200 hPa pressure levels of TC Nilam.	75
Table 11:	WRF model simulated maximum radial wind, tangential wind, vertical velocity and horizontal wind (m/s) of TC Nilam at different cumulus.	78
Table 12:	WRF Model simulated maximum vorticity ($x10^{-5}$ s^{-1}) at different pressure levels associated with TC Nilam at different cumulus scheme.	82
Table 13:	WRF Model simulated temperature anomaly (^oC), relative humidity (%) and water vapor mixing ratio (kg/kg $x10^{-2}$) associated with TC Nilam at different cumulus.	86
Table 14:	WRF model simulated wind speed (m/s) at different cumulus scheme of 850, 500, 300 and 200 hPa pressure levels of TC Khaimuk.	99
Table 15:	WRF model simulated maximum radial wind, tangential wind, vertical velocity and horizontal wind (m/s) of TC Khaimuk at different cumulus.	101
Table 16:	WRF Model simulated maximum vorticity ($x10^{-5}$ s^{-1}) at different pressure levels associated with TC Khaimuk at different cumulus scheme.	105
Table 17:	WRF Model simulated temperature anomaly (^oC), relative humidity (%) and water vapor mixing ratio (kg/kg $x10^{-2}$) associated with TC Khaimuk at different cumulus.	109

Nomenclature

AFWA	:	Air force weather agency
ARW	:	Advanced Research WRF
BMJ	:	Betts-Miller-Janjic
CAPE	:	Convective available potential energy
CIN	:	Convective inhibition
CS	:	Cyclonic storm
CSLP	:	Central sea level pressure
DLHF	:	Downward long wave heat flux
DSHF	:	Downward shortwave heat flux
DSSF	:	Down-welling surface shortwave radiation flux
FAA	:	The Federal Aviation Administration
FE	:	Ferrier scheme
FNL	:	Final Reanalysis
FSL	:	The Forecast Systems Laboratory
G3	:	Grell-3
GD	:	Grell-Devenyi
GF	:	Greel-Freitas
IMD	:	India Meteorological Department
ITCZ	:	Inter-tropical convergence zone
JTWC	:	Join typhoon warning center
lat	:	Latitude
lon	:	Longitude
MSLP	:	Minimum sea level pressure
MODIS	:	Moderate Resolution Imaging Spectroradiometer
MWS	:	Maximum wind speed
NCAR	:	National Center for Atmospheric Research
NCEP	:	National Center for Environmental Prediction
NWP	:	Numerical weather prediction
OKF	:	Old Kain-Fritsch
OLR	:	Outgoing long wave radiation
PBL	:	Planetary Boundary Layer
RH	:	Relative humidity
RRTM	:	Rapid radiative transfer model
SCS	:	Severe Cyclonic storm
SST	:	Sea surface temperature
TC	:	Tropical Cyclones
TH	:	Thomson
UTC	:	Universal Time Co-ordinate
VSCS	:	Very severe cyclonic storm
WSM6	:	WRF Single-moment 6-class
YSU	:	Yonsei University Scheme

ABSTRACT

- Comprehensive sensitivity analysis on Cumulus parameterization schemes of Weather Research and Forecasting model (WRF version 3.80) has been carried out for the effects on structure of weak intensity Tropical Cyclones Rashmi, Viyaru, Nilam and Khaimuk those formed in the Bay of Bengal and crossed Bangladesh, Bangladesh, Sri Lanka and Indian coast during 21 UTC of 26 October to 0300 UTC of 27 October 2008, around 0800 UTC of 16 May 2013, 0900 to 1200 UTC of 31October 2012 and during 2200 to 2300 UTC of 15 November 2008 respectively. The initial and boundary conditions of tropical cyclone (TC) are drawn from the global operational analysis and forecast products of National Center for Environmental Prediction (NCEP-GFS) available for the public at $1°\times1^{o}$ resolution. The model was run by using WSM6-class graupel microphysics (MP) schemes with different cumulus (Kain-Fritsch, Betts-Miller-Janjic, Grell- Fritsch, Grell-3, Grell-Denenyi and Old Kain-Fritsch) parameterization (CP). Different cumulus schemes have been used to study the effects on system intensification and structure of TC. The model domain consists of $3\text{-}27^{o}$N and $75\text{-}98^{o}$E and has 9 km horizontal resolution with 32 vertical sigma levels. The model is run for 96 hours using initial conditions at 0000 UTC of 24 October 2008 for TC Rashmi, 0000 UTC of 13 May 2013 for TC Viyaru, 0000 UTC of 28 October 2012 for TC Nilam and 0000 UTC of 13 November 2008 for TC khaimuk. Single domain ($3\text{-}27^{o}$N & $75\text{-}98^{o}$E) is considered to examine the effect on structure of weak intensity TC. In this research the Minimum sea level pressure (MSLP), Maximum wind speed (MWS), Vorticity, Temperature anomaly, Relative humidity, Relative humidity at 2m and Water vapor mixing ratio have been analyzed to observe the impact on these parameters of weak intensity TC. Using different CP options, variation of MSLP is around -20 to 10 hPa compared to observed value for all cyclones except Viyaru. Temperature anomaly from 3-12 ^{0}C is obtained. Around 100 km cyclone eye is also observed. It may be concluded that the different CP options have their own impact on the structure of weak intensity cyclonic Rashmi, Viyaru, Nilam and Khaimuk with more or less value with the available observed value.

Chapter 1

Introduction

1.1 Introduction

Tropical cyclones are known to cause enormous damage and destruction in the coastal regions. The cyclones form over the Bay of Bengal generally move in the northwest direction, recurve and crossed Bangladesh, Myanmar and eastern coast of India. Cyclones generally form over the Bay of Bengal in the pre-monsoon and post-monsoon seasons and have the tendency to cross Bangladesh coast. Tropical cyclone (TC) is a system of rapidly rotating storm with low pressure center, strong winds and spiral arrangement that produce significant natural disaster. For this reason, coastal regions are particularly vulnerable to damage from a tropical cyclone as compared to inland regions. Heavy rain, significant flooding inland, and storm surges can produce extensive coastal flooding up to 40 km from the coastline. The importance of the sea surface temperature (SST) in the genesis and intensity of tropical cyclones has become well established. It is known that tropical cyclones usually develop over waters in which the SST is 26°C or higher.

Tropical Cyclones are among the most devastating weather systems on the Earth. They cause considerable damage and destruction of lives and property due to strong gale winds, torrential rain and associated storm surge. The TC over the Bay of Bengal (BoB) form primarily in pre-monsoon season (March - May) and post-monsoon season (October - December) unlike in the other ocean basins which occur around late summer to early fall.

Understanding TC genesis, development and associated characteristic features has been a challenging subject in meteorology over the last several decades. In recent years, attempts to associate TC trends with climate change resulting from greenhouse warming has led to additional attention being paid to TC prediction (Emanuel, 1987; Evans, 1992; Lighthill *et al*., 1994).

The prediction of structure, movement and intensity of TC is very much essential in context of landfall and intensity. To improve the prediction, there is need of basic understanding of physics and dynamics involved in the genesis, intensity change, structure and track of TC. The concept of Conditional Instability of Second Kind (Charney and Eliassen, 1964) indicated that cyclonic inflow in lower tropospheric boundary layer is essential for

development of TCs. Gray (1968) indicated that developing and non-developing cyclones are associated with different upper tropospheric circulation patterns e.g. non-developing TCs have uni-directional upper tropospheric flow which causes vertical shear above the cloud clusters relatively strong and the developing TCs normally have multidirectional outflow that results in weak vertical shear above the cyclones. The study of Holland and Merrill (1984) concluded that not only upper tropospheric interactions but also the inner core convective heating may directly affect intensity change while lower tropospheric interactions will produce a size change which may indirectly affect the intensity or strength of TC. Craig and Gray (1996) showed that the intensification of numerically simulated TCs is due to Wind Induced Surface Heat Exchange (WISHE). Holland (1983) demonstrated that nonlinear combination of two processes: 1) an interaction between the cyclone and its basic current (steering current) and 2) an interaction with the Earth's vorticity field, is responsible for movement of TCs.

TC is the generic term for a non-frontal warm core synoptic scale low-pressure system originating over tropical or sub-tropical waters with organized convection and definite cyclonic surface wind circulation - counterclockwise in the Northern Hemisphere and clockwise in the Southern Hemisphere (Henderson-Sellers *et al.,* 1998). The 1970 Bhola Cyclone was the deadliest TC on record, killing over 200,000 people after striking the densely populated Ganges Delta region of Bangladesh on 12 November, 1970. Thus study of the TCs, their vertical structure including spatial anomalies, energetic and tracks will contribute towards understanding of the physics and dynamics of these processes and help predicting these systems in advance of time. Among many other advanced tools of atmospheric research, WRF model is one of the most advanced tools of atmospheric research. With the advancement in the computer technology, several simulation studies have been conducted to study the TCs (different categories such as strong and weak) over the North Indian Ocean (NIO) using high resolution mesoscale models (Pattanayak and Mohanty, 2008; Deshpande *et al*., 2010, 2012; Trivedi *et al*., 2006; *Osuri et al., 2012*, 2013; Srinivas *et al*., 2007, 2010; Raju *et al*., 2011; *Mukhopadhyay et al., 2011, Akhter et. al. 2011, 2017*). These studies are based on evaluating the model performance with respect to physics sensitivity, resolution, initial conditions and impact of data assimilation on the track and intensity forecast of very severe cyclones. In all the above studies, scientists have attempted simulation of strong TCs with rapid intensification. However, there is another class of TC which does not reach the stage of very severe cyclonic storm but attains lesser

intensity, named as weak cyclones. These weak cyclones, due to their slow motion and quasi-stationary nature, cause very heavy rainfall and in turn large amount of damage to the property. Very few studies have focused on simulating the weak intensity storms (*Osuri et al., 2012*; Srinivas *et al*., 2010), but the detailed evolutions of structural changes in the genesis parameters during development of the storm are hardly addressed. It is found that YSU as Planetary Boundary Layer (PBL) scheme and WSM6 as Microphysics scheme (Li and Pu, 2008; Efstathiou *et al*., 2012; Tao *et al*., 2011; *Mukhopadhyay et al., 2011*) and BMJ as Cumulus scheme (Kanase and Salvekar, 2011) give better track and intensity simulation of TCs. Therefore, in this study, structure of low intensity cyclones, will be simulated using different initial condition and different cumulus parameterization schemes.

In this research, 6 experiments have been conducted by using six different (Kain-Fritsch, Betts-Miller-Jamjic, Grell-Freitas, Grell-Deveneyi, Grell-3 and Old Kain-Fritsch) cumulus parameterization (CP) schemes for each TC. Finally, total 24 experiments have been conducted for 4 tropical cyclone Rashmi (2008), Viyaru (2013), Nilam (2008) and Khaimuk (2012) that formed in the Bay of Bengal and crossed Bangladesh, Bangladesh, Sri Lanka and India. Many meteorological parameters have been studied to see the effect of these parameters on the structure of tropical cyclones. These parameters are Minimum sea level pressure (MSLP), Maximum wind speed (MWS), Vorticity, Temperature anomaly, Relative humidity, Relative humidity at 2m, Water vapor mixing ratio and Mixing ratio.

1.2 Objective and scope of the research work

- To study the performance of different cumulus parameterization of WRF_ARW model for the simulation of different Tropical Cyclones (i.e. Rashmi, Viyaru, Nilam and Mala) in the BoB.
- To investigate different meteorological parameters of low intensity Tropical Cyclone.
- To investigate the structure of the Tropical Cyclone of low intensity.
- Then by identifying the structure, accurate forecasting of low intensity Tropical Cyclone will be possible with sufficient lead time.

1.3 Social and economic benefit of the research work

The tropical cyclones, tornadoes and other meso-scale activities cause severe damage to lives, properties, infrastructures and environment. Specially, low intensity or weak cyclone has slow motion and quasi-stationary nature and it causes very heavy rainfall and in turn

large amount of damage to the property. The weather activities of the country of Bangladesh are dominated by the southwest monsoon. In addition to this, Bangladesh is supposed to become the worst victim of the impacts of global warming and associated climate change. The climate change induced enhancement of nature disasters will cause its people to suffer innumerable loss to resources and livelihood. The model predicts the structure, intensity and probable areas and time of landfall of the selected tropical cyclone with high accuracy. Thus, the model may be used for operational prediction of cyclones of this area. And as a result the lives and properties of the urban people of the Bay of Bengal region will be saved.

1.4 Structure of the Thesis

The thesis has been constructed with the following structure:

Chapter 1 contains general introduction, objectives, scope of the research work, explains how the research results will be of social and economic benefit and structure of the thesis.

Chapter 2 contains introduction of Tropical Cyclone, Classification of Tropical Cyclones, Life Cycle of Tropical Cyclones, Different parameter of Tropical cyclone (MSLP, MWS, Vorticity, Temperature anomaly, RH, RH at 2m, and Water vapour mixing ratio etc.) and Weather Research & Forecasting Model.

Chapter 3 contains Model Description and Methodology, Model Description, Model Domain and configuration, Data and methodology and table of Model and Domain configuration.

Chapter 4 contains the results and discussions of the study of tropical cyclone events. It deals the MSLP, MWS, Vorticity, and Temperature anomaly, RH, RH at 2m and Water vapor mixing ratio of selected tropical cyclones using different cumulus of WRF model.

Chapter 5 contains the conclusion of the research and reference.

Chapter 2

Literature Review

This chapter is based on the review of the literatures for the TC, meteorological parameters related to tropical cyclone and WRF model.

2.1.1 Tropical Cyclone

TC is defined as a non-frontal low pressure system of synoptic scale that is developing over warm waters having organized convection and a maximum wind speed of 34 knots (gale force) or greater extending more than half-way around near the centre and persisting for at least six hours. The gale force winds can extend hundreds of kilometers from the cyclone centre. If the sustained winds around the centre reach 90-117 km/h, then the system is called a severe tropical cyclone. These are referred to as hurricanes in Atlantic Ocean and typhoons in Pacific Ocean. The circular eye or centre of a TC is an area characterized by light winds and often by clear skies. Eye diameters are typically 40 km but can range from under 10 km to over 100 km. The eye is surrounded by a dense ring of cloud about 16 km high known as the eye wall which marks the belt of strongest winds and heaviest rainfall. In addition to strong winds and rain, TCs are capable of generating high waves, damaging storm surge, and tornadoes. They typically weaken rapidly over land where they are cut off from their primary energy source of water. For this reason, coastal regions are particularly vulnerable to damage from a TC as compared to inland regions. Heavy rains, however, can cause significant flooding inland, and storm surges can produce extensive coastal flooding up to 40 kilometers from the coastline. Though their effects on human populations are often devastating, TCs can relieve drought conditions. They also carry heat energy away from the tropics and transport it toward temperate latitudes, which may play an important role in modulating regional and global climate.

2.1.2 Classification of Tropical Cyclones

Cyclonic disturbances in the North Indian Ocean are classified according to their intensity. The following nomenclature is in use:

- Low: Wind speed < 31 km/hr.
- Well marked low: Wind speed equals to 31 km/hr.

- Depression: Wind speed ranges from 32 - 48 km/hr.
- Deep Depression: Wind speed ranges from 49 - 62 km/hr.
- Cyclonic Storm: Wind speed ranges from 63 - 88 km/hr.
- Severe Cyclonic Storm: Wind speed ranges from 89 - 117 km/hr.
- SCS with a core of hurricane intensity: Winds speed 118-220 km/hr.
- Super Cyclone Winds speed ≥ 221 km/hr.

2.1.3 Life Cycle of Tropical Cyclones

The life span of tropical cyclones with full cyclonic intensity averages at about 6 days from the time they form until the time they enter land or recurve into the Temperate Zone. Some storms last only a few hours; a few as long as two weeks. The evolution of the average storm from birth to death has been divided into four stages.

- **Formative Stage:** Tropical storms form only in near pre-existing weather systems. Deepening can be a slow process, requiring days for the organization of a large area with diffuse winds. It can also produce a well-formed eye within 12 hours. Wind speed usually remains below hurricane force in the formative stage. Unusual fall of pressure over 24 hours by 2 - 3 hPa or more takes place in the center of the vorticity concentration.

- **Immature Stage:** A large number of formative cyclones die within 24 hours. Others travel long distances as shallow depressions. Wind of cyclonic force forms a tight band around the center. The cloud and rain pattern changes from disorganised squalls to narrow organised bands, spiralling inward. Only a small area is as yet involved, though there may be a large outer envelope. The eye is usually visible but ragged and irregular in shape.

- **Mature Stage:** The force of cyclonic winds may blow within a 30 - 50 km radius during immature stage. This radius can increase to over 300 km in mature storms. On the average, the mature stage occupies the longest part of the cycle and most often lasts several days. The eye is prominent and circular and the cloud pattern is almost circular and smooth. The surface pressure at the center is no longer falling and the maximum wind speeds no longer increasing. At this stage, heating from convective clouds furnishes the largest amount of energy for cyclone maintenance. Pressure gradient is largest at the surface. Wind speed range is between 128 - 322 km/hr.

- **Terminal Stage:** Nearly, all cyclones weaken substantially upon entering land, because they lose the energy source furnished by the underlying ocean surface. The decay is especially rapid where the land is mountainous. Movement of a cyclone over land cuts off the surface energy source and increases the surface friction, especially when the land is mountainous. Some cyclones die out over sea and this event can be related to their moving over a cold ocean current or being invaded by a surface cold air mass behind a cold front or by a cold center at high levels moving over their top.

2.2 Parameter of Tropical cyclone

The different meteorological parameters of related to TC structure are written in the following sub-sections**:**

2.2.1 Minimum Sea level pressure (MSLP)

The sea level pressure (SLP) is the atmospheric pressure at sea level at a given location. When observed at a reporting station that is not at sea level (nearly all station), it is a correction of the station pressure to sea level. This correction takes into account the standard variation of pressure with height on the pressure. The temperature used in the sea level correction is a twelve hour mean, eliminating diurnal effect. The mean sea level pressure (MSLP) is the atmospheric pressure at sea level. This is the atmospheric pressure normally given in weather reports on radio, television, and newspapers or on the Internet. When barometers in the home are set to match the local weather reports, they measure pressure adjusted to sea level, not the actual local atmospheric pressure. The altimeter setting in aviation is an atmospheric pressure adjustment. Average SLP is 1013.25 mbar (101.325 kPa; 29.921 inHg; 760.00 mmHg). In aviation weather reports (METAR), QNH is transmitted around the world in millibars or hectopascals (1 hectopascal = 1 millibar), except in the United States, Canada, and Colombia where it is reported in inches (to two decimal places) of mercury. The United States and Canada also report SLP, which is adjusted to sea level by a different method, in the remarks section, not in the internationally transmitted part of the code, in hectopascals or millibars. However, in Canada's public weather reports, sea level pressure is instead reported in kilopascals. In the US weather code remarks, three digits are all that are transmitted; decimal points and the one or two most significant digits are omitted: 1013.2 mbar (101.32 kPa) is transmitted as 132; 1000.0 mbar (100.00 kPa) is transmitted as 000; 998.7 mbar is transmitted as 987; etc. The highest SLP on Earth occurs in Siberia, where the Siberian High often attains a SLP above 1050 mbar (105 kPa; 31 inHg), with record highs close to 1085 mbar (108.5 kPa; 32.0 inHg). The

lowest measurable SLP is found at the centers of tropical cyclones and tornadoes, with a record low of 870 mbar (87 kPa; 26 inHg).

2.2.2 Wind speed

Wind speed, or wind flow velocity is a fundamental atmospheric quantity. Wind speed is caused by air moving from high pressure to low pressure, usually due to changes in temperature. Wind speed affects weather forecasting, aircraft and maritime operations, construction projects, growth and metabolism rate of many plant species, and countless other implications. Wind speed is now commonly measured with an anemometer but can also be classified using the older Beaufort scale which is based on people's observation of specifically defined wind effects.

In meteorology, winds are often referred to according to their strength, and the direction from which the wind is blowing. Short bursts of high speed wind are termed gusts. Strong winds of intermediate duration (around one minute) are termed squalls. Long-duration winds have various names associated with their average strength, such as breeze, gale, storm, and hurricane. Wind occurs on a range of scales, from thunderstorm flows lasting tens of minutes, to local breezes generated by heating of land surfaces and lasting a few hours, to global winds resulting from the difference in absorption of solar energy between the climate zones on Earth. The two main causes of large-scale atmospheric circulation are the differential heating between the equator and the poles, and the rotation of the planet (Coriolis Effect). Within the tropics, thermal low circulations over terrain and high plateaus can drive monsoon circulations. In coastal areas the sea breeze/land breeze cycle can define local winds; in areas that have variable terrain, mountain and valley breezes can dominate local winds.

2.2.3 Wind speed at 10m

In most of the world, the standard height above the surrounding vegetation for measuring open wind speed is ten meters (33 feet); in the United States, it is measured 20 feet above the surrounding vegetation (20-ft wind speed). Multiply 20-foot wind speed by 1.15 to estimate 10 m wind speed, alternately, divide 10-meter wind speed by 1.15 to estimate 20-foot wind speed (Turner and Lawson 1978).

2.2.4 Vorticity

Vorticity the microscopic measure of rotation in a fluid is a vector field defined as the curl of wind velocity. The definition can be expressed by the vector analysis formula: $\omega \rightarrow \equiv \nabla \times u$ .where ∇ is the del operator.

Mathematically, the vorticity of a three-dimensional flow is a pseudovector field, usually denoted by $\omega\rightarrow$, defined as the curl or rotational of the velocity field, $v\rightarrow$ describing the continuum motion. In Cartesian coordinates:

$$\omega \rightarrow = \nabla \times v = \omega_x i + \omega_y j + \omega_z k = (\frac{\partial w}{\partial y} - \frac{\partial v}{\partial z})i + (\frac{\partial u}{\partial z} - \frac{\partial w}{\partial x})j + (\frac{\partial v}{\partial x} - \frac{\partial u}{\partial y}) k.$$

The vorticity is the microscopic measurement of the rotation of a small air parcel. Air parcel has vorticity when the parcel spins as it moves along its path. Although the axis of the rotation can extend in any direction, meteorologists are primarily concerned with the rotational motion about an axis that is perpendicular to the earth's surface. If it does not spin, it is said to have zero vorticity. In the Northern Hemisphere, the vorticity is positive when the parcel has a counterclockwise or cyclonic rotation. It is negative when the parcel has clockwise or anticyclonic rotation. For turning of the atmosphere, vorticity may be imbedded in the total flow and not readily identified by a flow pattern. The rotation of the Earth imparts vorticity to the atmosphere; absolute vorticity is the combined vorticity due to this rotation and vorticity due to circulation relative to the Earth (relative vorticity). The negative vorticity is caused by anticyclonic turning; it is associated with downward motion of the air. The positive vorticity is caused by cyclonic turning; it is associated with upward motion of the air. Also the relative vorticity is the air relative to the Earth, disregarding the component of vorticity resulting from Earth's rotation. The absolute vorticity μ_a is given by the curl of the absolute velocity, while the relative vorticity μ is given by the curl of the relative velocity:

$$\mu_a \rfloor \overline{\ } \mid \overline{V_a} \qquad\qquad \mu \rfloor \overline{\ } \mid \overline{V}$$

In meteorology, the general concerned only with the vertical components of absolute and relative vorticity:

$$\zeta = \hat{k}\cdot\nabla\times\vec{V}_a \qquad \zeta = \hat{k}\cdot\nabla\times\vec{V}$$

In particular, the vertical component of relative vorticity ζ is highly correlated with synoptic scale weather disturbances. Large positive ζ tends to occur in association with cyclonic storms in the Northern Hemisphere. Furthermore, ζ tends to be conserved following the motion in the middle troposphere. Thus, analysis of the ζ field and its evolution due to advection forms the basis for the simplest dynamical forecast scheme.

2.2.5 Temperature anomaly

The term temperature anomaly means a departure from a reference value or long-term average. A positive anomaly indicates that the observed temperature was warmer than the reference value, while a negative anomaly indicates that the observed temperature was cooler than the reference value.

When researching global climate changes and temperature data, temperature anomaly is observed in this case. That is the difference between the long-term average temperature (sometimes called a reference value) and the temperature that is actually occurring. In other words, the long-term average temperature is one that would be expected; the anomaly is the difference between what you would expect and what is happening.

2.2.6 Relative Humidity

Relative Humidity is the most commonly used measurements of moisture content in the air. The Relative Humidity is the amount of water vapor (moisture) in the air compared to the maximum amount that the air could hold at a given temperature. The relative humidity is:

$$f = \frac{\mu}{\mu_s} \times 100 = \frac{\omega}{\omega_s} \times 100 = \frac{q}{q_s} \times 100 = \frac{e}{e_s} \times 100$$

Here q is specific humidity and q_s is specific humidity at saturation point, ω is mixing ratio and ω_s is mixing ratio at saturation point.

If the relative humidity is 100%, the air is saturated. If the relative humidity is 50%, the air contains half the water vapor required for it to be saturated. If the amount of water vapor in the air increases, the relative humidity increases, and if the amount of water vapor in the air decreases, the relative humidity decreases. However, relative humidity is dependent on air temperature, too. If the water vapor content remains the same and the temperature drops, the relative humidity increases. If the water vapor content remains the same and the

temperature rises, the relative humidity decreases. This is because colder air doesn't require as much moisture to become saturated as warmer air. Warm air can hold more water vapor than cool air, so a particular amount of water vapor will yield a lower relative humidity in warm air than it does in cool air. In the summer, the relative humidity is actually higher in the morning than in the afternoon. This is because the cooler morning air is closer to saturation than the hot afternoon air, even with the same amount of water vapor. Surprisingly, there is no significant difference in daily average relative humidity between summer and winter. Since warm air is less dense than cold air, there is more room for water vapor in warm summer air as compared with cold winter air. At a given vapor pressure (or mixing ratio), relative humidity with respect to ice is higher than that with respect to water. Water is known by different names in different states. If the maximum amount of water vapor has been reached and more water is introduced into the air, an equal amount of water must transform back to liquid or solid form through condensation. At this point, the air is said to be saturated with water, and the relative humidity is 100%. On the other end of the scale, when there is no water vapor in the air, the relative humidity is 0% whatever the temperature. In other words, relative humidity always lies between 0 and 100%. As mentioned, the ability of air to hold water vapor is strongly dependent on temperature. This means that relative humidity is also strongly temperature dependent.

2.2.7 Water Vapor mixing ratio

Mixing ratio (w) is the amount of water vapor that is in the air. w is the grams of vapor per kg of dry air. w is an absolute measure of the amount of water vapor in the air.

The mixing ratio is defined as the weight of water vapor contained in mixture with a unit weight of dry air, expressed in grams per gram or gram per kilogram. It differs from specific humidity only in that it is related to dry air instead of to the total of dry air plus water vapor. Designating it as ω, we have

$$\mu \; X \; \frac{\circ_{w}}{\circ_{d}} \; X \; \frac{m_{w}}{m_{d}}$$

Mixing ratio mass of water vapor in a fixed mass of remaining dry air. Since there are so few molecules of water vapor in a volume of air, as compared to N_2 and O_2, the value of the mixing ratio is similar to the specific humidity. Changing the temperature of the air parcel does not affect the parcels mixing ratio.

2.3 Weather Research & Forecasting Model

The Weather Research and Forecasting (WRF) Model is a next-generation mesoscale numerical weather prediction system designed to serve both atmospheric research and operational forecasting needs. It features two dynamical cores, a data assimilation system, and a software architecture facilitating parallel computation and system extensibility. The model serves a wide range of meteorological applications across scales from tens of meters to thousands of kilometers. The effort to develop WRF began in the latter part of the 1990's and was a collaborative partnership principally among the National Center for Atmospheric Research (NCAR), the National Oceanic and Atmospheric Administration (NOAA) represented by the National Centers for Environmental Prediction (NCEP) and the Forecast Systems Laboratory (FSL) the Air Force Weather Agency (AFWA), the Naval Research Laboratory, the University of Oklahoma, and the Federal Aviation Administration (FAA).

WRF offers two dynamical solvers for its computation of the atmospheric governing equations, and the variants of the model are known as WRF-ARW and WRF-NMM. The Advanced Research WRF (ARW) is supported to the community by the NCAR Mesoscale and Microscale Meteorology Division. The WRF-NMM solver variant was based on the Eta Model, and later Non hydrostatic Mesoscale Model, developed at NCEP. The WRF-NMM is supported to the community by the Developmental Test bed Center.

There are many options in the model such as physics option, map projection and computation methods. Descriptions of all of items used for the present study are written in the following sub-section. Again, there are many Physics option in the model such as microphysics, cumulus physics, radiation Physics and planetary boundary Layer Physics. Each physics option has many parameterization schemes. Descriptions of the parameterization schemes used for the present study are written as follows:

2.3.1 Microphysics schemes in WRF-ARW Model

Microphysics includes explicitly resolved water vapor, cloud and precipitation processes. The model is general enough to accommodate any number of mass mixing-ratio variables, and other quantities such as number concentrations. Four-dimensional arrays with three spatial indices and one species index are used to carry such scalars. Memory, i.e., the size of the fourth dimension in these arrays, is allocated depending on the needs of the scheme

chosen, and advection of the species also applies to all those required by the microphysics option. In the current version of the ARW, microphysics is carried out at the end of the time-step as an adjustment process, and so does not provide tendencies.

The rationale for this is that condensation adjustment should be at the end of the time-step to guarantee that the final saturation balance is accurate for the updated temperature and moisture. However, it is also important to have the latent heating forcing for potential temperature during the dynamical sub-steps and this is done by saving the microphysical heating as an approximation for the next time-step as described.

2.3.1.1 WSM 6-class scheme

The WRF-single-moment-6-class (WSM6) microphysics scheme has been one of the options of microphysical process in the WRF model. This scheme predicts the mixing ratios for water vapor, cloud water, cloud ice, snow, rain, and graupel. We attempt to improve such existing deficiencies in the WSM6 scheme by incorporating the prediction of number concentrations for warm rain species. A new method for representing mixed-phase particle fall speeds for the snow and graupel by assigning a single fall speed to both that is weighted by the mixing ratios, and applying that fall speed to both sedimentation and accumulation processes is introduced of the three WSM schemes, the WSM6 scheme is the most suitable for cloud-resolving grids, considering the efficiency and theoretical backgrounds (Hong *et al*., 2006). The WSM6 scheme has been developed by adding additional process related to graupel to the WSM5 scheme (Hong and Lim, 2006).

2.3.2 Cumulus Parameterization

These schemes are responsible for the sub-grid-scale effects of convective and/or shallow clouds. The schemes are intended to represent vertical fluxes due to unresolved updrafts and downdrafts and compensating motion outside the clouds. They operate only on individual columns where the scheme is triggered and provide vertical heating and moistening profiles. Some schemes provide cloud and precipitation field tendencies in the column, and future schemes may provide momentum tendencies due to convective transport of momentum. The schemes all provide the convective component of surface rainfall. Cumulus parameterizations are theoretically only valid for coarser grid sizes, (e.g., greater than 10 km), where they necessary to properly release latent heat on a realistic time scale in the convective columns. Where the assumptions about the convective eddies being entirely sub-

grid-scale break down for finer grid sizes, sometimes these schemes have been found to be helpful in triggering convection in 5-10 km grid applications. Generally they should not be used when the model can resolve the convective eddies itself. These schemes are responsible for the sub-grid-scale effects of convective and shallow clouds. The schemes are intended to represent vertical fluxes due to unresolved updrafts and downdrafts and compensating motion outside the clouds.

2.3.2.1 K**ain-Fritsch scheme**

In the KF scheme the condensates in the updraft are converted into precipitation when their amount exceeds threshold value. In this scheme the convection consumes the convective available potential energy in a certain time scale. The KF scheme also includes the shallow convection other than deep convection. The shallow convection creates non-perceptible condensates and the shallowness of the convection is determined by a vertical extent of the cloud layer that is known by a function of temperature at LCL of rising air parcel. The KF scheme was derived from the Fritsch–Chappell, and its fundamental framework and closure assumptions are described by Fritsch and Chappell (1980). KF (1990, 1993) modified the updraft model in the scheme and later introduced numerous other changes, so that it eventually became distinctly different from the Fritsch–Chappell scheme. It was distinguished from its parent algorithm by referring to the more elaborate code as the KF scheme, beginning in the early 1990s. This is also deep and shallow convection sub-grid scheme using a mass flux approach with downdrafts and CAPE removal time scale. Updraft generates condensate and dump condensate into environment downdraft evaporates condensate at a rate that depends on RH and depth of downdraft leftover condensate accumulates at surface as precipitation.

2.3.2.2 Betts-Miller-Janjic scheme

The BMJ cumulus parameterization scheme is a nudging type adjustment of temperature and humidity in grid scale. The scheme adjusts the sounding towards a pre-determined, post convective profile derived from climatology. This post convective profile has been defined by points at the cloud base, cloud top and freezing level. In this scheme there is no explicit updraft or downdraft and no cloud detrainment occur. Convection is initiated when soundings are moist through a deep layer and when CAPE and convective cloud depth thresholds are exceeded. Betts and Miller proposed a convective adjustment scheme that

includes both deep and shallow convection. The deep convection in the Betts–Miller scheme is similar to the other adjustment schemes except that it uses empirically based quasi-equilibrium thermodynamic profiles as a reference state rather than a moist adiabatic. The basic shape of these quasi-equilibrium reference profiles is based on the numerous observations. The construction of the reference profiles and the specification of the relaxation timescale are two major components of the Betts–Miller scheme (Janjic, 1994).

These points and thresholds can vary by season and between the tropics and extra tropics. Compared with the original sounding, the sounding modified to the post convective profile will note a net change in perceptible water as well as changes in net heating and cooling. Convection is initiated when soundings are moist through a deep layer and when CAPE and convective cloud depth thresholds are exceeded. Important vertical structures may be eliminated since the reference profiles are based on climatology. Convection only initiated for soundings with deep moisture profile. When convection is initiated the scheme often rains out to much water. This is because the reference profile is too dry for the forecast scenario or the transition to the reference profile was too rapid. Scheme does not account for the strength of CAPE inhibiting convective development. Scheme does not account for any changes below the cloud base.

2.3.2.3 Grell–Freitas (GF)

Arakawa et al. (2011) build a unified convective parameterization for use at all horizontal scales, Grell and Freitas (GF, 2011) introduced a scale-aware approach into a pre-existing scheme based on a stochastic approach. Development and testing of the GF parameterization are partially supported by the National Weather Service Research to operations initiative. Interest in this scheme by Environmental Modeling Center (EMC) and the Next Generation Global Prediction System (NGGPS) Program Office has led to the implementation and testing for potential use in the NCEP operational global model. We implemented the GF parameterization in a developmental version of the NOAA Environmental Modeling System (NEMS)-based Global Spectral Model (GSM), and ran experimental retrospective forecasts using the NEMS-GSM over a warm (June, July, and August 2015) and cool (December 2015, January, February 2016) season.

2.3.2.4 Grell-Devenyi ensemble schemes

Grell and Devenyi (2002) introduced an ensemble cumulus scheme in which effectively multiple cumulus schemes and variants are run within each grid box and then the results are averaged to give the feedback to the model. In principle, the averaging can be weighted to

optimize the scheme, but the default is an equal weight. The schemes are all mass-flux type schemes, but with differing updraft and downdraft entrainment and detrainment parameters, and precipitation efficiencies. These differences in static control are combined with differences in dynamic control, which is the method of determining cloud mass flux. The dynamic control closures are based on convective available potential energy (CAPE or cloud work function), low-level vertical velocity, or moisture convergence. Those based on CAPE either balance the rate of change of CAPE or relax the CAPE to a climatological value, or remove the CAPE in a convective time scale. The moisture convergence closure balances the cloud rainfall to the integrated vertical advection 71 of moisture. Another control is the trigger, where the maxi mum cap strength that permits convection can be varied. These controls typically provide ensembles of 144 members.

2.3.2.5 Grell-3 scheme

The Grell-3 scheme was first introduced in Version 3.0, and so is new, and not yet well tested in many situations. It shares a lot in common with the Grell-Devenyi in scheme, being based on an ensemble mean approach, but the quasi-equilibrium approach is no longer included among the ensemble members. The scheme is distinguished from other cumulus schemes by allowing subsidence effects to be spread to neighboring grid columns, making the method more suitable to grid sizes less than 10 km, while it can also be used at larger grid sizes where subsidence occurs within the same grid column as the updraft.

2.3.2.6 Old Kain-Fritsch (OKF)

The KF scheme was derived from the Fritsch–Chappell CPS, and its fundamental framework and closure assumptions are described by Fritsch and Chappell (1980). KF90 modified the updraft model in the scheme and later introduced numerous other changes, so that it eventually became distinctly different from the Fritsch–Chappell scheme. It was distinguished from its parent algorithm by referring to the more elaborate code as the KF scheme, beginning in the early 1990s (KF93). These early papers documented many details of the code. Additional details can be found in Bechtold et al. (2001); although this paper describes a significantly modified version of the KF scheme, it documents some sections of the KF code that are not available in print elsewhere; it thus provides a valuable additional reference. Furthermore, a less quantitative description of the code was recently presented in a paper that describes one of its unique applications (Kain et al. 2004). Here, a brief overview of the ‘‘old’’ versions of the code is presented to provide the context for the description of the recent modifications. The KF scheme is a mass flux parameterization. It

uses the Lagrangian parcel method (e.g., Simpson and Wiggert 1969; Kreitzberg and Perkey 1976), including vertical momentum dynamics (Donner 1993), to estimate whether instability exists, whether any existing instability will become available for cloud growth, and what the properties of any convective clouds might be. For the sake of this discussion, it is convenient to compartmentalize the KF scheme into three parts: 1) the convective trigger function, 2) the mass flux formulation, and 3) the closure assumptions. Each of these is discussed briefly below.

2.3.3 Planetary boundary layer (PBL)

The PBL is the layer in the lower part of the troposphere with thickness ranging from a few hundred meters to a few kilometers within which the effects of the Earth's surface are felt by the atmosphere. The PBL processes represent a consequence of interaction between the lowest layer of air and the underlying surface. The interactions can significant impact on the dynamics of the upper air flows. The influences of the small-scale eddy on large scale atmospheric circulations may be included in the model equations. Accurate depiction of meteorological conditions, especially within the PBL, is important for air pollution modeling, and PBL parameterization schemes play a critical role in simulating the boundary layer. It is a very important portion of the atmosphere to correctly model to provide accurate forecasts, e.g., air pollution forecasts (Deardorff 1972; Pleim 2007). As important as the PBL is, it has one basic property whose accurate and realistic prediction is paramount to its correct modeling: its height. After all, the height of the top of the PBL defines its upper boundary. This is critical since PBL parameterizations schemes in WRF-ARW models need to know the extent through which to mix properties such as heavy rainfall, relative humidity, outgoing long wave flux, downward long wave flux.

PBL schemes were developed to help resolve the turbulent fluxes of heat, moisture, and momentum in the boundary layer. Another important issue is the interaction between the atmosphere and the surface. The PBL schemes handle the latent and sensible heat fluxes into the atmosphere, the frictional effects with the surface and the strong sub–grid–scale mixing which takes place in the lower levels due to these processes.

2.3.3.1 Yonsei University (YSU) scheme

The Yonsei University (YSU) PBL is the next generation of the Medium Range Forecast (MRF), Non local-K scheme with explicit entrainment layer and parabolic K profile in

unstable mixed layer. The YSU scheme is a bulk scheme that expresses non-local mixing by convective large eddies. Non-local mixing is achieved by adding a non-local gradient adjustment term to the local gradient. At the top of the PBL, the YSU scheme uses explicit treatment of the entrainment layer, which is proportional to the surface layer flux (Shin and Hong 2011; Hong *et al*. 2006).

2.3.4 Radiation schemes

There are two types of radiation schemes: Long wave and short wave. The used schemes for these are describe as follows:

2.3.4.1 Long wave radiation

Rapid Radiative Transfer Model (RRTM) scheme: This RRTM, which is taken from MM5, is based on Mlawer et al., and is a spectral-band scheme using the correlated-k method. An accurate scheme using looking tables for efficiency. Accounts for multiple bands, trace gases and microphysics species.

2.3.4.2 Shortwave radiation

MM5 (Dudhia) scheme: This scheme is base on Dudhai and is taken from MM5. Simple downward integration allowing efficiently for clouds and clear-sky absorption and scattering. When used in high-resolution simulations, sloping and shadowing effects may be considered.

2.3.5 Map Projection

Commonly, a map projection is a systematic transformation of the latitudes and longitudes of locations on the surface of a sphere or an ellipsoid into locations on a plane. Map projections are necessary for creating maps. All map projections distort the surface in some fashion. Depending on the purpose of the map, some distortions are acceptable and others are not; therefore, different map projections exist in order to preserve some properties of the sphere-like body at the expense of other properties. There is no limit to the number of possible map projections. More generally, the surfaces of planetary bodies can be mapped even if they are too irregular to be modeled well with a sphere or ellipsoid. Even more generally, projections are the subject of several pure mathematical fields, including differential geometry and projective geometry. However, map projection refers specifically to a cartographic projection (Snyder *et al*. 1989).

2.3.5.1 Mercator Projection

The Mercator projection is a cylindrical map projection presented by the Flemish geographer and cartographer Gerardus Mercator in 1569. It became the standard map projection for nautical purposes because of its ability to represent lines of constant course, known as rhumb lines_ loxodromes, as straight segments which conserve the angles with the meridians. While the linear scale is equal in all directions around any point, thus preserving the angles and the shapes of small objects, the Mercator projection distorts the size and shape of large objects, as the scale increases from the Equator to the poles, where it becomes infinite. Although the Mercator projection is still used commonly for navigation, due to its unique properties, cartographers agree that it is not suited to general reference world maps due to its distortion of land area. Mercator himself used the equal-area sinusoidal projection to show relative areas. As a result of these criticisms, modern atlases no longer use the Mercator projection for world maps or for areas distant from the equator, preferring other cylindrical projection or forms of equal-area projection. The Mercator projection is still commonly used for areas near the equator, however, where distortion is minimal.

2.3.6 Computation method

2.3.6.1 Arakawa Staggered C-grids

The Arakawa grid system depicts different ways to represent and compute orthogonal physical quantities on rectangular grids used for Earth system models for meteorology and oceanography. For example, the Weather Research and Forecasting Model use the Arakawa Staggered C-Grid in its atmospheric calculations when using the ARW core. The staggered Arakawa C-grid further separates evaluation of vector quantities compared to the Arakawa B-grid. E.g., instead of evaluating both east-west (u) and north-south (v) velocity components at the grid center, one might evaluate the u components at the centers of the left and right grid faces, and the v components at the centers of the upper and lower grid faces (Arakawa and Lamb *et al* 1977)

Chapter 3

Model Description and Methodology

In the present study the Weather Research and Forecasting (WRF-ARW Version 3.80) model consists of fully compressible non-hydrostatic equations and different prognostic variables is utilized. The model vertical coordinate is terrain following hydrostatic pressure and the horizontal grid is Arakawa C-grid staggering. Third-order Runge-Kutta time integration is used in the model. The model description and methodology are given below:

3.1 Model Description

In the present study, the Weather Research and Forecasting (WRF-ARW Version 3.80) model consists of fully compressible non-hydrostatic equations and different prognostic variables is utilized. The model vertical coordinate is terrain following hydrostatic pressure and the horizontal grid is Arakawa C-grid staggering. A third-order Runge-Kutta time integration is used in the model. The model is configured in single domain, 9 km horizontal grid spacing with 290×316 grids in the west-east and north-south directions and 32 vertical levels. The six different cumulus parameterization (CP) schemes have been used in WRF model are Kain-Fritsch (KF), Betts-Miller-Janjic (BMJ), Grell–Freitas (GF), Grell-Devenyi (GD), Grell-3 and Old Kain-Fritsch (OKF) scheme. The CP schemes contain prognostic equations for cloud water, rainwater, cloud ice, snow, and graupel mixing ratio. The Ferrier scheme also contains prognostic equations for cloud water, rainwater and snow mixing ratio. Dudhia simple five-layer soil thermal diffusion scheme for soil processes, Rapid Radiative Transfer Model (RRTM) for long wave scheme and Dudhia for short wave radiation schems and Yonsei University scheme planetary boundary layer (PBL) have been used for the simulation of TC Rashmi, Viyaru, Nilam and Khaimuk. The model domain is given in Fig.1. The detail of the model and domain configuration is given in Table 1.

3.2 Model Domain and Configuration

In this study, the WRF–ARW model has been configured with single domain. For the analysis of structure and intensity, the model domain covers the region 3-27^{o}N & 75-98^{o}E and is shown in Figure 1.

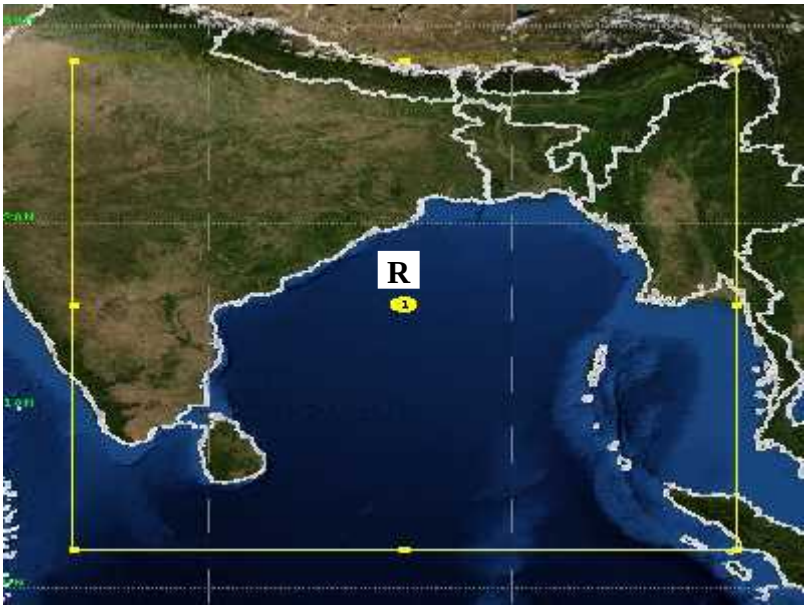

Fig. 1: The WRF-ARW domain set up for the study.

3.3 Data and Methodology

Weather Research and Forecasting (WRF) model with high resolution can be used for diagnosis weak intensity tropical cyclone which formed on the Bay of Bengal. This numerical model which is currently available in free of cost has been developed by the collaborative efforts of NCAR (National Center for Atmospheric Research) and NCEP (National Centers for Environmental Prediction). At first, few cyclone with low intensity have been selected which formed on the Bay of Bengal. The WRF model has been run using different cumulus (KF, BMJ, GF, G3, GD and OKF) of 96 hrs before the landfall time to simulate structure of low intensity tropical cyclones formed in the Bay of Bengal. The coverage area of the model domain is 3-27°N latitude and 75-98°E longitude and the level is 1000 to 100. Different cumulus parameterization schemes have been used to observe the sensitivity on the structure of cyclone. NCEP final reanalysis (FNL) data (1°×1° resolution) have been used as initial and lateral boundary conditions (LBCs) which are updated at six hourly intervals. The model results are presented in the graphical and tabular forms and compared with the IMD (Indian Meteorological Department) best track data to demonstrate the performance of the modeling exercise. For these purpose, Grid Analysis and Display System (GrADS) and Microsoft Excel soft ware will be used. The procedure will be mainly studied on the structure, track and landfall of selected low intensity cyclones in terms of different parameters viz. Minimum Sea Level Pressure (MSLP), Maximum Wind Speed

(MWS), Vorticity, Temperature anomaly, Relative humidity, Relative humidity at 2m and Water vapor mixing ratio. These parameters are directly related to the structure of TCs.

Table 1: WRF Model and Domain Configurations

Dynamics	Non-hydrostatic
Number of domain	1
Central points of the domain	Central Lat.: 15.4°N, Central Lon.: 86.5°E
Horizontal grid distance	9 km
Integration time step	30 s
Number of grid points	X-direction 290 points, Y-direction 316 points
Map projection	Mercator
Horizontal grid distribution	Arakawa C-grid
Nesting	One way
Vertical co-ordinate	Terrain-following hydrostatic-pressure co-ordinate (32 sigma levels up to 100 hPa)
Time integration	3rd order Runge-Kutta
Spatial differencing scheme	6th order centered differencing
Initial conditions	Three-dimensional real-data (FNL: 1° × 1°)
Lateral boundary condition	Specified options for real-data
Top boundary condition	Gravity wave absorbing
Bottom boundary condition	Physical or free-slip
Diffusion and Damping	Simple Diffusion
Microphysics	WSM 6-class graupel scheme
Radiation scheme	Dudhia for short wave radiation/ RRTM long wave (Mlawer et al., 1997)
Surface layer	Monin– Obukhov similarity theory scheme
Land surface parameterization	5 Layer Thermal diffusion scheme
Cumulus parameterization schemes	1) Kain-Fritsch (KF), (2)Betts-Miller-Janjic (BMJ), (3) Grell–Freitas (GF), (4) Grell-Devenyi (GD), (5) Grell-3 and (6) Old Kain-Fritsch (OKF) scheme.
PBL parameterization	Yonsei University Scheme

Chapter 4

Results and Discussion

The model simulated MSLP, maximum wind at 10 m level, Vorticity, Temperature anomaly, Relative humidity, Relative humidity at 2m and Water vapor mixing ratio with six CP schemes along with synoptic situation are discussed for the TC Rashmi, Viyaru, Nilam and Khaimuk in the following sub-sections:

4.1 Tropical Cyclone Rashmi

The model simulated MSLP, maximum wind at 10 m level, Vorticity, Temperature anomaly, Relative humidity, Relative humidity at 2m and Water vapor mixing ratio with six CP schemes along with synoptic situation are discussed for the TC Rashmi in the following sub-sections:

4.1.1 Description of Tropical Cyclone Rashmi

To analyze the low intensity of TC Rashmi, the WRF model has been run for 96 hrs with the initial field at 0000 UTC of 24 October 2008 using different cumulus. A low formed over west central Bay and adjoining area on 24 October 2008 and intensified into a well-marked low over the same area at 0000 UTC of 25 October 2008. At 0600 UTC of the same day the system concentrated into a depression over the same area (16.5°N, 86.5°E) and started to move in a northerly direction. At 0300 UTC of 26 October the system intensified into a DD over northwest Bay and adjoining west central Bay. After that the system changed its direction of movement and moved north-northeastwards and concentrated into a cyclonic storm ‘Rashmi’ at 1200 UTC of the same day over northwest Bay and adjoining area (20.2°N, 88.2°E). By moving rapidly towards the same direction the system started to cross Khulna-Barisal coast of Bangladesh near Patharghata at 2100 UTC of the same day and completed crossing the coast by 0300 UTC of 27 October and lay over south-central part of the country as a land depression. Using WRF models the different meteorological parameters are discussed for the intensity of the TC Rashmi in the following sub-section. The WRF model simulated data are compared with those obtained from Joint Typhoon Warning Centre (JTWC).

4.1.2 Minimum sea level pressure (MSLP)

The storm intensity forecasts for the TC Rashmi in terms of MSLP using six different cumulus schemes KF, BMJ, GF, G3, GD and OKF for 96 hours (every 3 hourly) along with observed MSLP are presented in Figure 2. The WRF model simulated and observed MSLP gradually drops with time and attains peak intensity just before the landfall and thereafter MSLP increases. The Model simulated MSLP of 980, 986, 964, 983, 994 and 984 hPa are obtained using KF, BMJ, GF, G3, GD and OKF schemes respectively and these simulated MSLP are obtained at 0600 UTC of 26, 1500 UTC of 26, 1500 UTC of 26, 0000 UTC of 27, 0000 UTC of 27 and 1500 UTC of 26 October 2008 respectively. The observed MSLP 984 hPa is obtained at 2100 UTC of 26 October 2008 according to IMD. So, simulated minimum MSLP (mature stage) are obtained later/earlier than that of observed. The observed MSLP is much higher than the simulated MSLP for all cumulus schemes with little exception. The pressure departure is found minimum for G3 scheme and maximum for GD schemes compared with IMD observed value. The simulated pressure fall for all cumulus schemes indicate that the system has attained the intensity of cyclonic storm and the observation also indicates that the system attained the intensity of cyclonic storm (984 hPa). Cumulus G3, OKF and BMJ match better than the others cumulus with the observed intensity. But Cumulus G3 simulates later than the observed and OKF and BMJ simulate earlier than the observed pressure. At first, Cumulus KF does not match with the observed value but with the progress of simulation time it matches finally with the observed value of pressure. Cumulus GF simulates more intensity than the observed. Intensity simulated by Cumulus GD is absolutely not matched with the observed value.

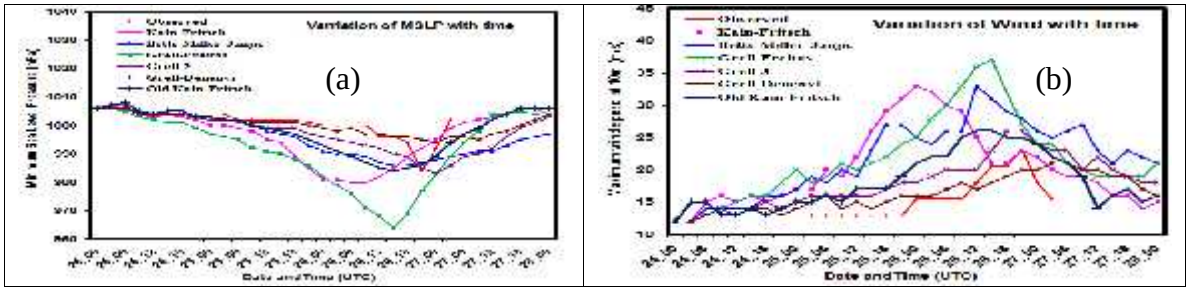

Figure 2: Evolution of WRF model simulated (a) MSLP and (b) MWS at 10m level using six different cumulus schemes and that of observed of the TC Rashmi.

Figure 3 shows the mature stage of spatial distribution of sea level pressure using six different cumulus schemes and it is obtained with different time and position with different intensity. The spatial distribution of sea level pressure at its mature stage for the TC Rashmi

using different cumulus schemes KF, BMJ, GF, G3, GD and OKF in WRF model is obtained at 0006 UTC of 26, 15 UTC of 26, 1500 UTC of 26, 0000 UTC of 27, 0000 UTC of 27 and 1500 UTC of 26 October respectively.

The lowest simulated MSLP (i.e. mature stage) for the TC Rashmi using different cumulus scheme KF, BMJ, GF, G3, GD and OKF in WRF models are obtained 980, 986, 964, 983, 994 and 984 hPa respectively. The observation also indicates that the system attained the intensity of cyclonic storm (984 hPa,). The OKF cumulus scheme has the same intensity of the observation. It is seen that GF cumulus scheme has very high intensity, and then the GD cumulus scheme has also very high intensity. The G3 cumulus scheme has almost the same intensity as that of the observation. The KF cumulus scheme has lower intensity than the observation and BMJ cumulus scheme has higher intensity than the observation.

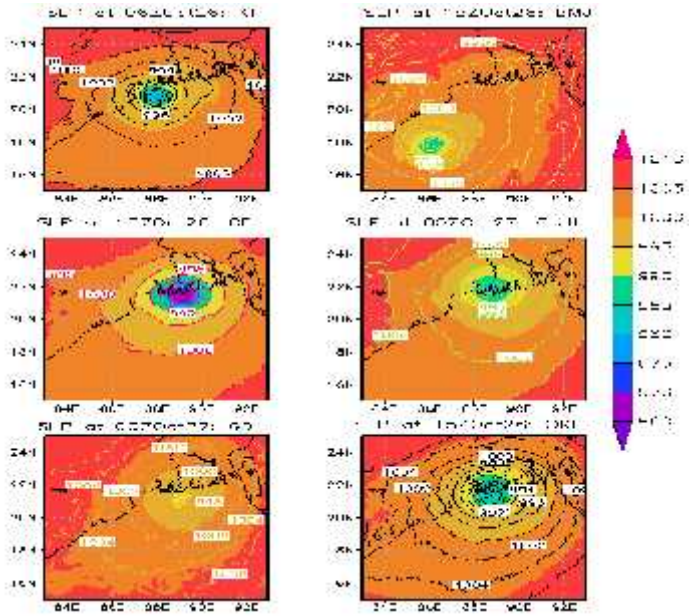

Figure 3: WRF model simulated SLP of TC Rashmi for different cumulus schemes.

In figure 3, it is observed that mature stage of spatial distribution of sea level pressure using different cumulus is obtained with different time and different positions. Position of mature stages using KF, BMJ, GF, G3, GD and OKF are located at 88^{o}E and 20.9^{o}N at 06 UTC of 26 October, 86.1^{o}E and 17.8^{o}N at 1500 UTC of 26, 89.1^{o}E and 21.4^{o}N at 1500 UTC of 26, 88.5^{o}E and 21.8^{o}N at 0000 UTC of 27, 89.13^{o}E and 21.15^{o}N at 0000 UTC of 27 and 88.6^{o}E and 21.35^{o}N at 1500 UTC of 26 October respectively. Intensity, position and time of mature stages are different for different cumulus schemes used in WRF model. The isobar has circular arrangement around the TC centre with some asymmetric features in the outer

periphery. The contour interval is different for different positions because of different intensity of the system. From Figure 3, the radius of the TC eye is found to be around 100 km for all cumulus according to all simulation.

The distribution of the sea level pressure of the TC Rashmi along east-west cross section and north-south cross section passing through its centre using different cumulus is shown in Figure 4. The position of the centre at mature stage using different cumulus schemes KF, BMJ, GF, G3, GD and OKF are located at 88^{o}E and 20.9^{o}N, 86.1^{o}E and 17.8^{o}N, 89.1^{o}E and 21.4^{o}N, 88.5^{o}E and 21.8^{o}N, 89.13^{o}E and 21.15^{o}N and 88.6^{o}E and 21.35^{o}N respectively. The Model simulated MSLP of 980, 986, 964, 983, 994 and 984 hPa are obtained at 0006 UTC of 26, 1500 UTC of 26, 1500 UTC of 26, 0000 UTC of 27, 0000 UTC of 27 and 1500 UTC of 26 October respectively and are shown in Figure 4. In Figure 4, the black, green, yellow, orange, magenta and the dark purple color represent KF, BMJ, GF, G3, GD and OKF scheme respectively. The figures demonstrate the moderate pressure gradient around the centre with maximum gradient at around 222 km below or above for all cumulus schemes from the centre. Variation of east-west and north-south elongated SLP at the center are clearly observed.

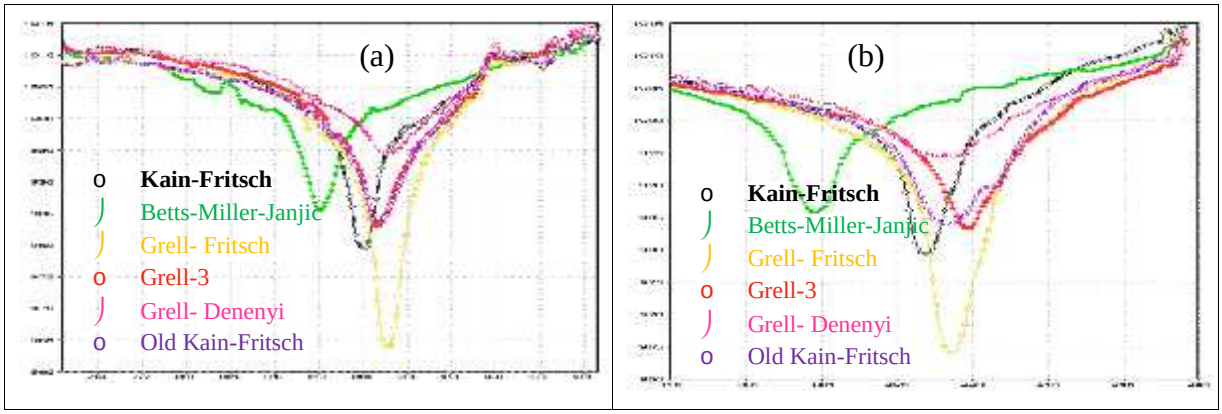

Figure 4: WRF model simulated (a) East West and (b) North South cross sectional view of SLP of TC Rashmi at different cumulus schemes with fixed latitude and longitude respectively.

4.1.3 Maximum Wind speed

The storm intensity forecasts for the TC Rashmi in terms of MWS using six different cumulus schemes KF, BMJ, GF, G3, GD and OKF for 96 hours (every 3 hourly) along with observed MWS are presented in Figure 2. The model simulated MWSs are obtained at the standard meteorological height at 10 m. The WRF Model simulated MWSs are higher than

the observed values through almost full forecast hours with few exceptions. Model simulated highest value of MWS using six different cumulus schemes are obtained at same the time and earlier. But for convenience, times of maximum intensity (mature stage) are considered as the time of obtained MSLP (this times are written in previous section).

The observed and simulated MWS by WRF decrease with time gradually after obtaining highest value of MWSs. The highest value of MWS for the TC Rashmi using different cumulus scheme KF, BMJ, GF, G3, GD and OKF in WRF models are 33, 33, 37, 26, 21 and 26 m/s respectively. Whereas the observed MWS is 23.15 m/s. the simulated and observation values indicate that the system attained the intensity of cyclonic storm (17.5 - 24.44 m/s). WRF model using different cumulus schemes simulate higher value of MWS than that of observed value. It is seen GF cumulus scheme has very high intensity, than the KF and BMJ cumulus scheme have also high intensity. The G3 and OKF cumulus schemes have slightly more intensity than the observation. Finally, GD cumulus scheme has lower intensity than the observation.

Figure 5 shows the spatial distribution of surface (10 m) wind speed using six different cumulus schemes and it is obtained with different time and position with different times and positions with different intensities. The spatial distribution of wind speed at its mature stage for the TC Rashmi using different cumulus schemes such as KF, BMJ, GF, G3, GD and OKF in WRF model is obtained at 0600 UTC of 26, 1500 UTC of 26, 1500 UTC of 26, 0000 UTC of 27, 0000 UTC of 27 and 1500 UTC of 26 October 2008 respectively and are shown in Figure 5. Figure 5 obtained from WRF model shows that the wind field of the TC is highly asymmetric in the horizontal distribution. At 0000 UTC of 24 October 2008 (i.e. at the initial time of simulation) the TC is in the sea with different cumulus schemes (not shown in figure). Gradually, TC is organized with strong wind bands around and the wind flow in the core region shows asymmetric feature with minimum wind speed at the centre. The spatial distribution of surface (10 m) wind speed is found maximum for GF scheme and minimum for G3 and GD scheme. The figure shows that the pattern has an asymmetric wind distribution with strong wind bands in the front right side, rear left and rear right sides close to the centre of north directed moving storm. In Figure 5, it is observed that mature stage of spatial distribution of wind speed using different cumulus is obtained with different times and different positions. Positions of mature stages using KF, BMJ, GF, G3, GD and OKF are located at 88^{o}E and 20.9^{o}N at 0006 UTC of 26 October, 86.1^{o}E and 17.8^{o}N at 1500

UTC of 26, 89.1°E and 21.4°N at 1500 UTC of 26, 88.5°E and 21.8°N at 0000 UTC of 27, 89.13°E and 21.15°N at 0000 UTC of 27 and 88.6°E and 21.35°N at 15 UTC of 26 October respectively. At this mature stage, the wind flow in the core region shows a near circular feature with minimum wind speed at the centre.

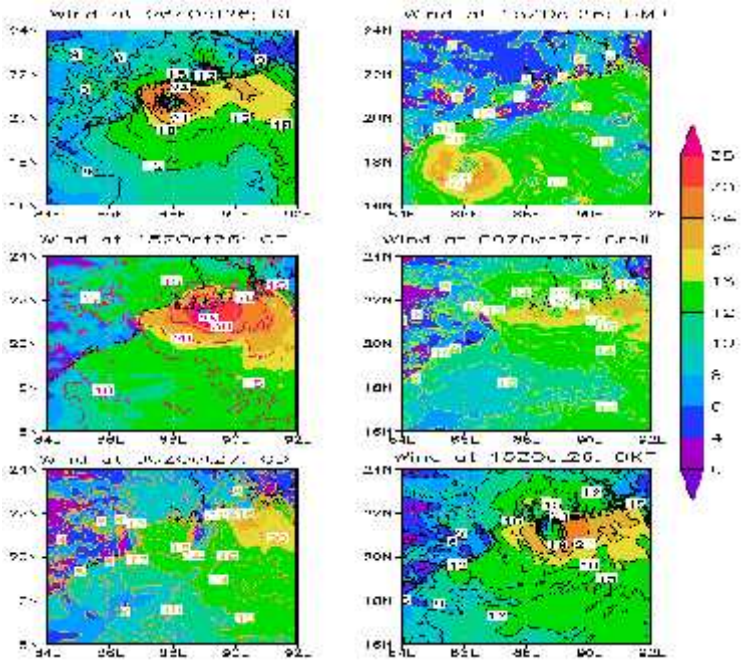

Figure 5: WRF model simulated MWS of TC Rashmi at different cumulus schemes.

The distribution of the surface wind of the TC Rashmi along east-west cross section and north-south cross section passing through its centre at mature stage using different cumulus schemes is shown in Figures 6 and 7 respectively. The positions of the centre at mature stage using different cumulus schemes KF, BMJ, GF, G3, GD and OKF are located at 88°E and 20.9°N, 86.1°E and 17.8°N, 89.1°E and 21.4°N, 88.5°E and 21.8°N, 89.13°E and 21.15°N and 88.6°E and 21.35°N respectively. The model simulated wind speeds of 33, 33, 37, 26, 21 and 26 m/s are obtained at 0000 UTC of 26, 1200 UTC of 26, 1500 UTC of 26, 1800 UTC of 26, 0000 UTC of 27 and 1500 UTC of 26 October 2008 respectively. But the model simulated wind speeds of 30, 31, 37, 24, 20 and 26 m/s are obtained at 0600 UTC of 26, 1500 UTC of 26, 1500 UTC of 26, 0000 UTC of 27, 0000 UTC of 27 and 1500 UTC of 26 October 2008 respectively at mature stage (that is at the minimum SLP position). The figures demonstrate that a calm region is found inside the eye of the system and maximum wind ~~was~~ is found in the eye wall. The simulated value of wind at the centre using different cumulus schemes has a wide variety. In Figure 6 the value is less than 8 m/s and in Figure 7 the value is less than 9 m/s. In Figure 6, the KF, BMJ and GF cumulus scheme show better

result than the other cumulus scheme. And in Figure 7, the KF, BMJ, GF and G3 cumulus scheme show better results than the other cumulus schemes. In both figures, the performance of GD cumulus scheme is the worst. The radius of maximum wind of the TC Rashmi is found to be just lower than 80 km according to the simulation. Variation of east-west and north-south elongated wind at the center is clearly observed.

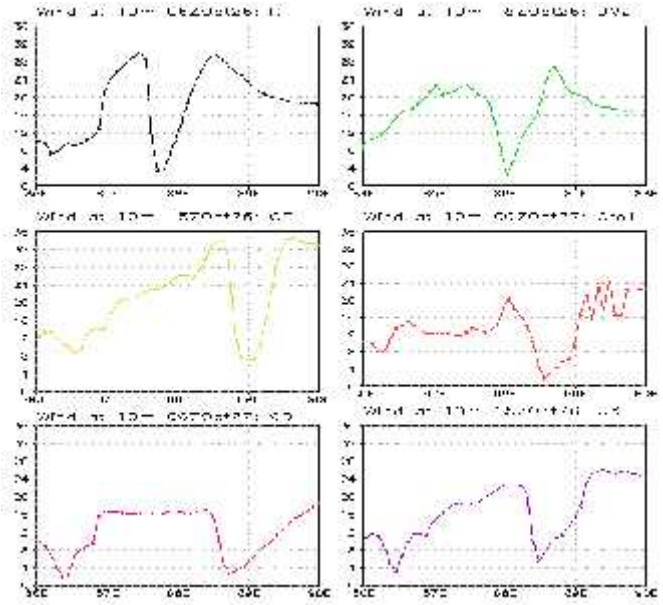

Figure 6: WRF model simulated East West cross sectional view of wind speed of TC Rashmi at different cumulus schemes with fixed latitude.

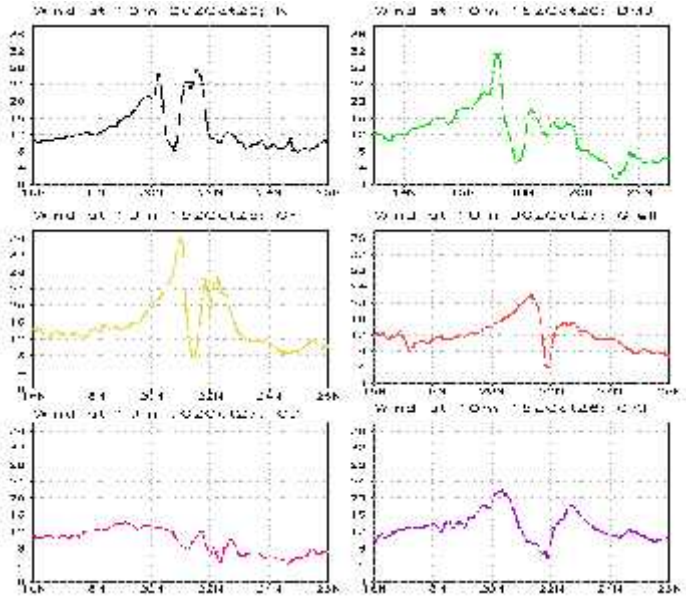

Figure 7: WRF model simulated North-south cross sectional view of wind speed of TC Rashmi at different cumulus schemes with fixed longitude.

The horizontal distribution of vector wind field at its mature stage for the levels 850, 500, 300 and 200 hPa of the TC Rashmi using different cumulus is tabulated in Table 2 and figure of this only for the levels 850 and 200 hPa are shown in Figures 8 and 9 respectively.

From the Figure 8, a well organized TC circulation with strong winds encircling the centre is found at the 850 hPa levels. It is noted that the strong wind is confined to the right of the direction of the movement of the system. From the Figure 9, at 200 hPa level strong outflow is evident from the central part of the TC. So, using simulated results obtained from WRF models, Figure 8 and Figure 9 demonstrate inflow in the lower level and outflow in the upper level respectively. WRF model simulated maximum winds at the mature stage (0600 UTC of 26, 1500 UTC of 26, 1500 UTC of 26, 0000 UTC of 27, 0000 UTC of 27 and 1500 UTC of 26 October 2008) are about 50, 40, 60, 50, 30, 50 m/s and 30, 40, 40, 40, 30, 30 m/s for different cumulus (KF, BMJ, GF, G3, GD and OKF) schemes at 850 and 200 hPa levels respectively. The wind speed at 850 hPa level is found minimum for GD scheme and maximum for GF schemes. And the wind speed at 200 hPa levels is found minimum for KF, GD and OKF scheme and maximum for BMJ, GF and G3 schemes. The mature stages are obtained at different time and position. The values of wind speed for mature stage at the levels 500 and 300 hPa are obtained different with different cumulus schemes.

Table 2: WRF model simulated maximum wind speed (m/s) at different cumulus scheme of 850, 500, 300 and 200 hPa pressure levels of TC Rashmi

Pressure level (hPa)	Maximum Wind Speed (m/s) at different time					
	06 UTC on 26 October at KF	15 UTC on 26 October at BMJ	15 UTC on 26 October at GF	00 UTC on 27 October at Greel	00 UTC on 27 October at GD	15 UTC on 26 October at OKF
850	50	40	60	50	30	50
500	40	30	50	30	30	40
300	50	30	50	40	30	40
200	30	40	40	40	30	30

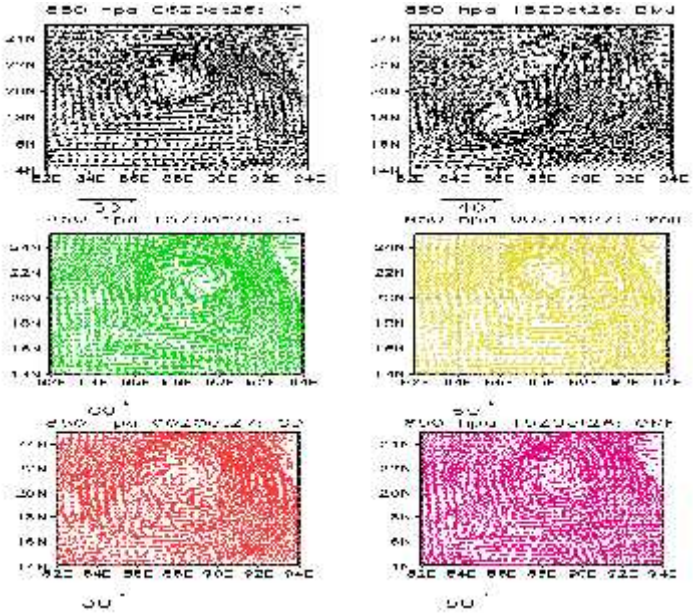

Figure 8: WRF model simulated Wind vector and magnitude at 850 hPa levels at different cumulus schemes.

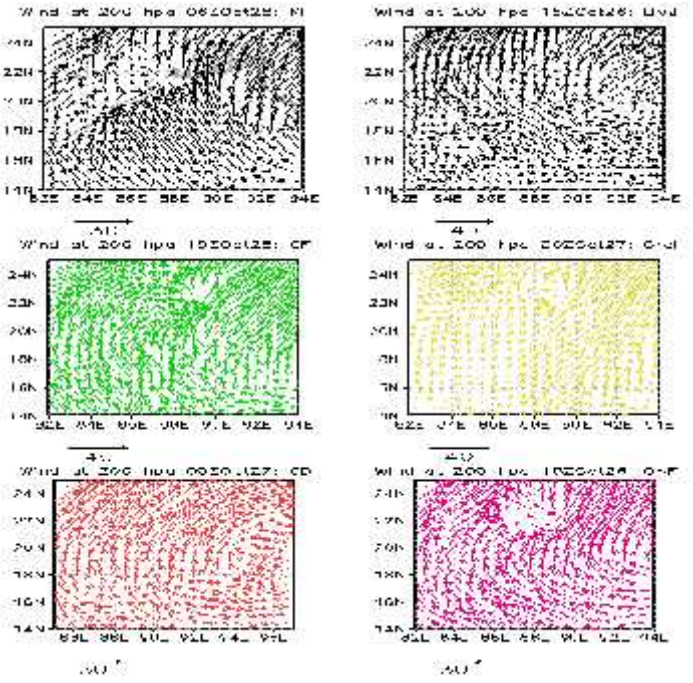

Figure 9: WRF model simulated Wind vector and magnitude at 200 hPa levels at different cumulus schemes.

The Vertical profile of Radial, Tangential, Vertical and Horizontal wind fields at its mature stage for the TC Rashmi using different cumulus schemes KF, BMJ, GF, G3, GD and OKF in WRF model are obtained at 0600 UTC of 26, 1500 UTC of 26, 1500 UTC of 26, 0000

UTC of 27, 0000 UTC of 27 and 1500 UTC of 26 October 2008 respectively and shown in Figures 10, 11, 12and 13 respectively. Model simulated results are also tabulated in Table 3, for different cumulus mentioned in the Table. From the table it is clear that the value of the vertical profiles of radial, tangential, vertical and horizontal winds of TC Rashmi obtained using different cumulus (KF, BMJ, GF, G3, GD and OKF) scheme are different for different cumulus schemes. The strong wind with different speeds (Table 3) is confined to the different levels in lower troposphere and extended up to 100 hPa level in the left side of the system.

From the Figure 10, it is found that vertical profile of radial wind is much more organized and it is also clearly seen that the system has strong inflow in the lower levels which bring the air to the system through the boundary level and lower level and outflow in the upper level. The radial wind is found minimum for KF and OKF schemes and maximum for GF schemes.

The vertical profile of tangential wind flows in a northerly direction at the eastern side of the system and in a southerly direction at the western side. For this reason, tangential wind shows positive value at the right side (east side) of the centre and negative value at the left side (west side) of the centre. The tangential wind is found minimum for GD scheme and maximum for GF schemes.

The values of the vertical profile of vertical wind are different in magnitude for different cumulus and the values such as 2.1, 1.3, 0.8, 0.5, 1.2 and 0.6 m/s are simulated by KF, BMJ, GF, G3, GD and OKF cumulus respectively. It indicates that the vertical wind is found minimum for OKF scheme and maximum for BMJ schemes. These values are along the eye wall and other parts of the system which feed moisture into the system. It is noted that Rashmi has very weak updraft motion at the eye wall throughout mid and upper troposphere. The downward motion is visible in the central parts of the TC and other areas in between rain bands.

The vertical profile of horizontal wind of the system at its mature stage shows the distribution of strong winds up to 100 hPa for KF, GF and GD cumulus scheme and up to 200 hPa for BMJ, G3 and OKF cumulus scheme around the centre of TC. It further confirms that the maximum winds are confined to the right of the direction of the movement of the system. This value decreases with the radial distance from both sides of the eye. Calm wind zone is sharp and narrow and little bit tilted to the westward and get expanded towards upper levels. This is in agreement with the previous studies of Rao and Prasad (2006) and

Goswami *et al.* (2006) on Orissa TC. Cyclonic circulation is generally seen up to about 300 hPa level and anticyclone circulation with divergence fields aloft. In case of TC Rashmi, cyclonic circulation is also seen up to about 300 hPa level for cumulus KF and G3 scheme, 400 hPa levels for cumulus BMJ, GF and OKF scheme, 600 hPa levels for GD cumulus scheme and anticyclone circulation with divergence fields aloft. And the horizontal wind is found minimum for GD scheme and maximum for GF scheme.

Table 3: WRF model simulated maximum radial wind, tangential wind, vertical velocity and horizontal wind (m/s) of TC Rashmi at different cumulus schemes.

Component of wind	Simulated maximum wind speed (m/s) at different time					
	06 UTC of 26 October at KF	15 UTC of 26 October at BMJ	15 UTC of 26 October at GF	00 UTC of 27 October at Grell 3	00 UTC of 27 October at GD	15 UTC of 26 October at OKF
Radial wind	12	15	35	18	15	12
Tangential wind	32	30	52	32	27	38
Vertical velocity	2.1	1.3	0.8	0.5	1.2	0.6
Horizontal wind	40	40	60	40	30	40

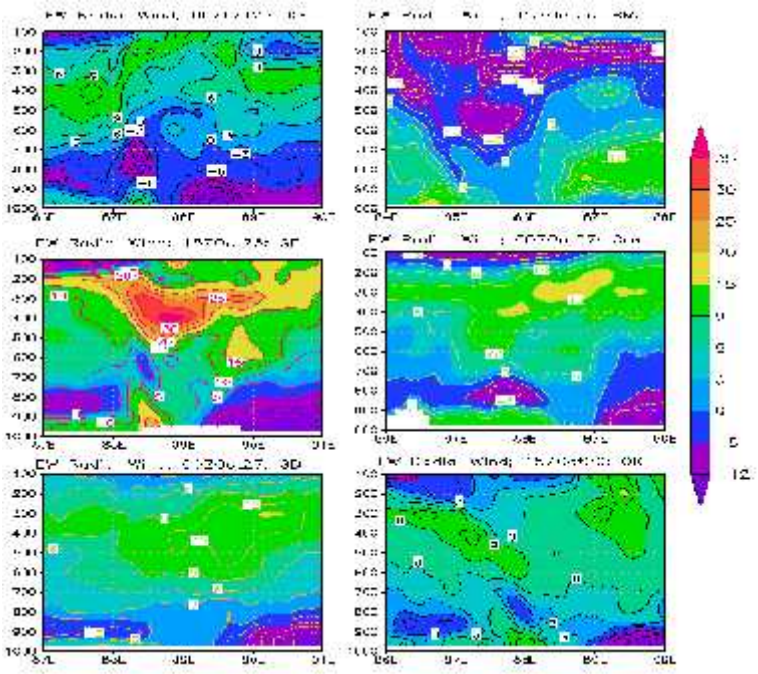

Figure 10: WRF model simulated Radial wind (m/s) of TC Rashmi at different cumulus schemes.

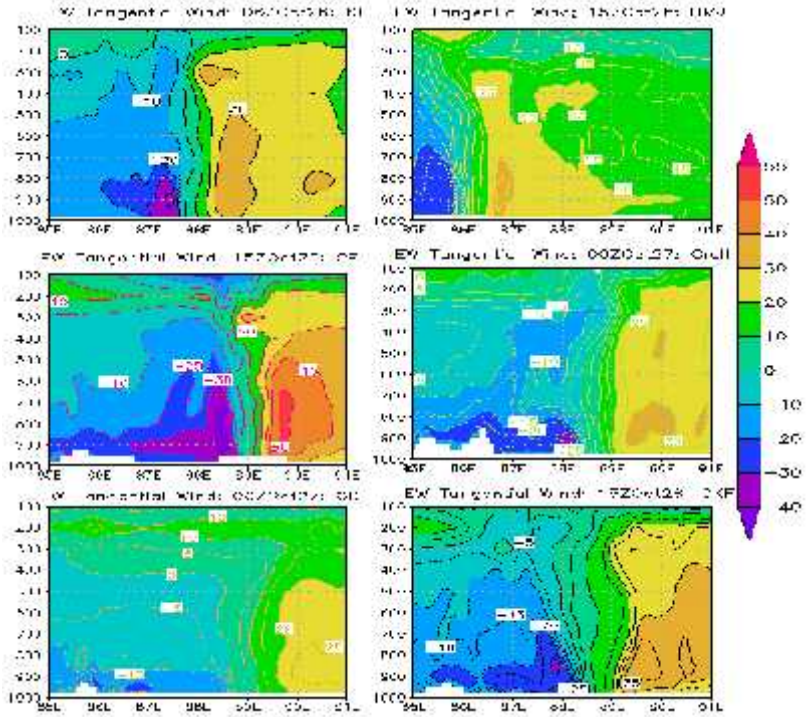

Figure 11: WRF model simulated tangential wind (m/s) of TC Rashmi at different cumulus schemes.

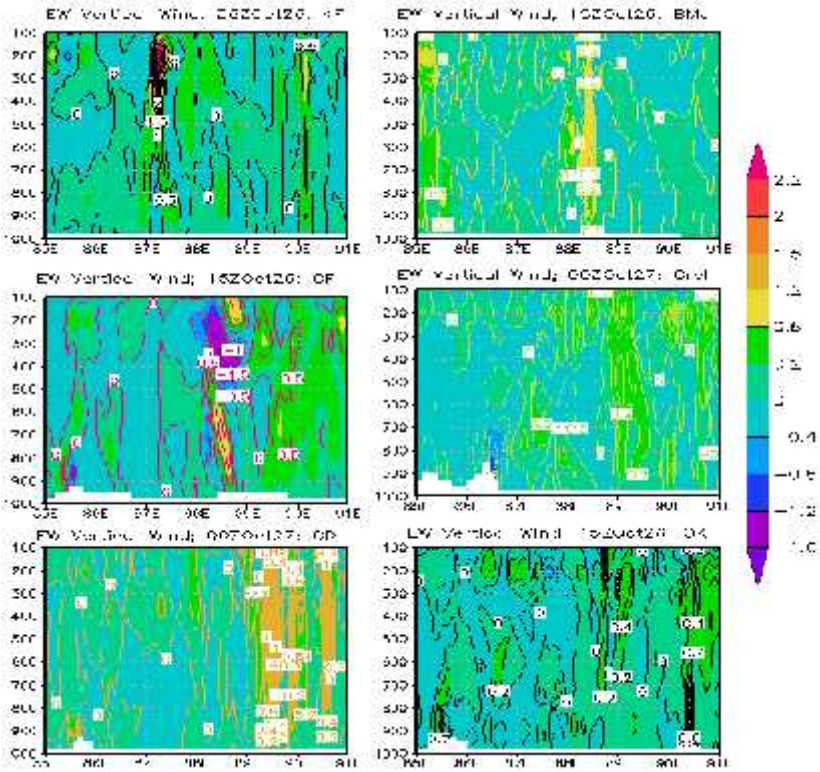

Figure 12: WRF model simulated Vertical wind (m/s) of TC Rashmi at different cumulus schemes.

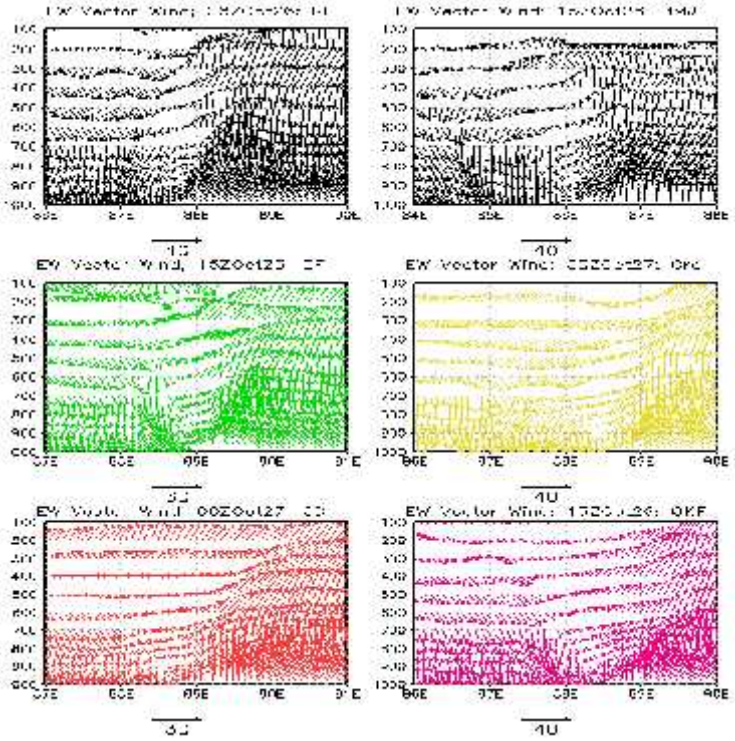

Figure 13: WRF model simulated Horizontal wind (m/s) of TC Rashmi at different cumulus schemes.

4.1.4 Vorticity

To know the WRF model simulated relative vorticity at 1000,950,850,500 and 300 hPa at six cumulus KF, BMJ, GF, G3, GD and OKF scheme for 96 hours (every 3 hourly) are presented in Figure 14. The values of relative vorticity are increased with the increase of time (i.e. in the development of the TC) at all levels for all cumulus schemes and increased to a maximum value. Thereafter the value shows a fall. From the figure it is observed that at 1000, 500 and 300 hPa, the vorticity is found maximum for cumulus BMJ scheme. And 950 hPa level the vorticity is found maximum for cumulus KF and GF schemes. And 850 hPa level the vorticity is found maximum for cumulus GF scheme. The vorticity is found more than zero for all levels using all schemes. So, from the simulated value of vorticity it is seen that system intensification is satisfied more or less by all cumulus schemes.

Simulated the horizontal distribution of the relative vorticity obtained for TC Rashmi at 850 and 200 hPa levels are shown in the Figures 15 and 16 respectively. It is seen from the figures that the vorticity is distributed with maximum value at the centre and these values for the levels 850, 500, 300 and 200 hPa are tabulated in Tables 4 for different cumulus (KF, BMJ, GF, G3, GD and OKF) schemes respectively. At 850 hPa, the distribution

maintains circular pattern with some asymmetric features in the outer periphery. Negative vorticity field is situated far from the centre. This distance of the negative vorticity from the centre is increased due to development of TC (not shown). Low level relative vorticity fields confirm the strong cyclonic circulation at low levels with different time and distance in feeding the moisture into the system to sustain its intensity. The values of relative vorticity are increased with the development of TC. At 200 hPa level, the weak positive vorticity embedded with negative vorticity field is visible at 200 hPa level. Negative vorticity is found at the centre of the TC. It is clear from the figure that relative vorticity is more organized in the mature stage. The vorticity is found maximum or minimum for 850, 500, 300 and 200 hPa levels at different times using different cumulus schemes.

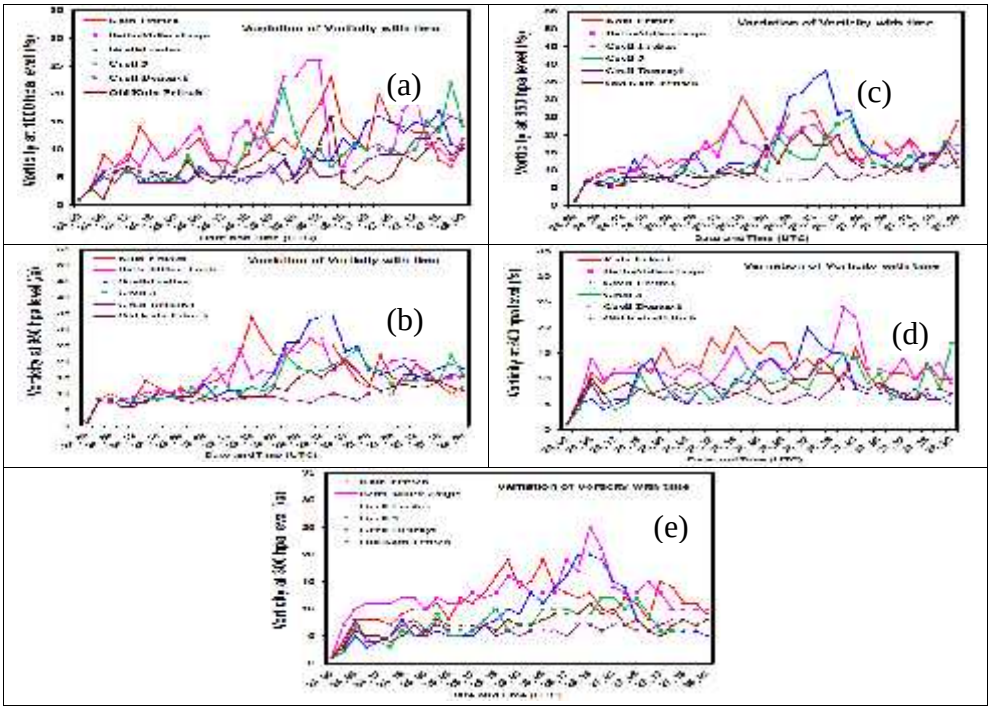

Figure 14: Evolution of model simulated vorticity with time at different cumulus schemes for 1000,950,850,500 and 300 hPa level of TC Rashmi.

Vertical distribution of the relative vorticity with fixed latitude (along east-west direction) and fixed longitude (along north-south direction) are obtained from WRF model and are shown in Figures 17 and 18 respectively and the values are tabulated in Table 4. Simulated results at 0600 UTC of 26, 1500 UTC of 26, 1500 UTC of 26, 0000 UTC of 27, 0000 UTC of 27 and 1500 UTC of 26 October 2008 for different cumulus scheme KF, BMJ, GF, G3, GD and OKF are located at 88^{o}E and 20.9^{o}N, 86.1^{o}E and 17.8^{o}N, 89.1^{o}E and 21.4^{o}N, 88.5^{o}E and 21.8^{o}N, 89.13^{o}E and 21.15^{o}N and 88.6^{o}E and 21.35^{o}N respectively.

In figure 17 the system has the positive vorticity along the centre up to 200 hPa level with higher value for all cumulus. For KF, BMJ, GF, G3, GD and OKF the higher value up to 200, 300, 300, 400, 400 and 400 levels respectively. So the strong cumulus scheme is Kain-Fritsch scheme. In figure 18 the system has the positive vorticity along the centre up to 100 hPa level with higher value for all cumulus. For KF, BMJ, GF, G3, GD and OKF the higher value up to 100, 350, 250, 200, 350 and 300 hPa levels respectively. So the strong cumulus scheme is KF scheme. Both Figures the greatest vorticity is GF cumulus scheme.

Table 4: WRF Model simulated maximum vorticity ($x10^{-5}$ s^{-1}) at different pressure levels associated with TC Rashmi at different cumulus schemes.

Pressure level (hPa)	Maximum Vorticity ($x10^{-5}$ s^{-1}) at different times					
	06 UTC on 26 October at KF	15 UTC on 26 October at BMJ	15 UTC on 26 October at GF	00 UTC on 27 October at Greel	00 UTC on 27 October at GD	15 UTC on 26 October at OKF
850	180	100	250	120	50	160
500	60	30	30	40	20	40
300	60	30	90	20	40	40
200	40	40	30	40	10	20
Position of TC centre	20.9°N and 88°E	17.8°N and 86.1°E	21.4°N and 89.1°E	21.8°N and 88.5°E	21.15°N and 89.1°E	21.35°N and 88.6°E
Vertical distribution with fixed latitude	15	12	15	12	9	10
Vertical distribution with fixed longitude	16	10	18	9	5	8

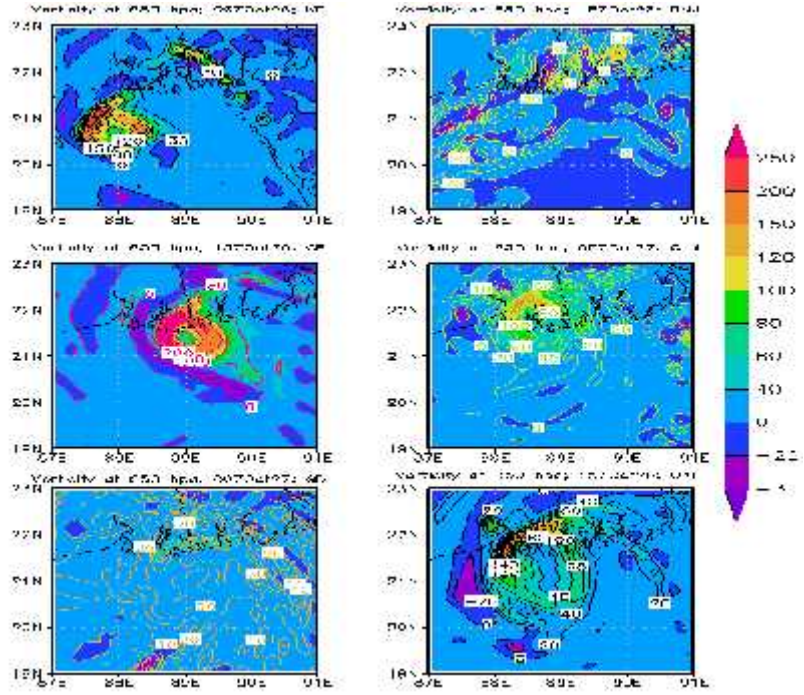

Figure 15: WRF Model simulated vorticity field of 850 hPa levels at different cumulus schemes.

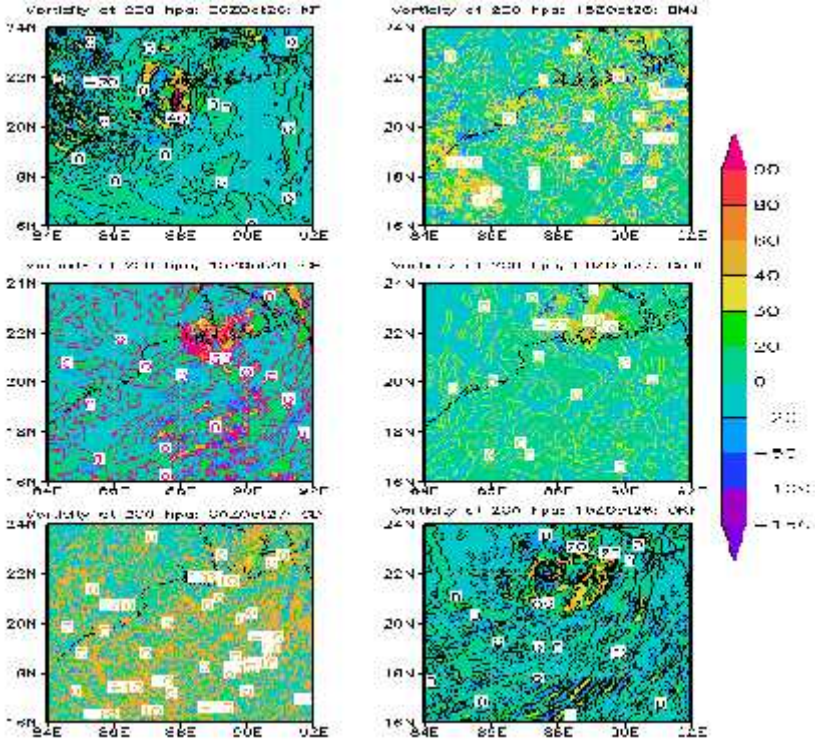

Figure 16: WRF Model simulated vorticity field of 200 hPa levels at different cumulus schemes.

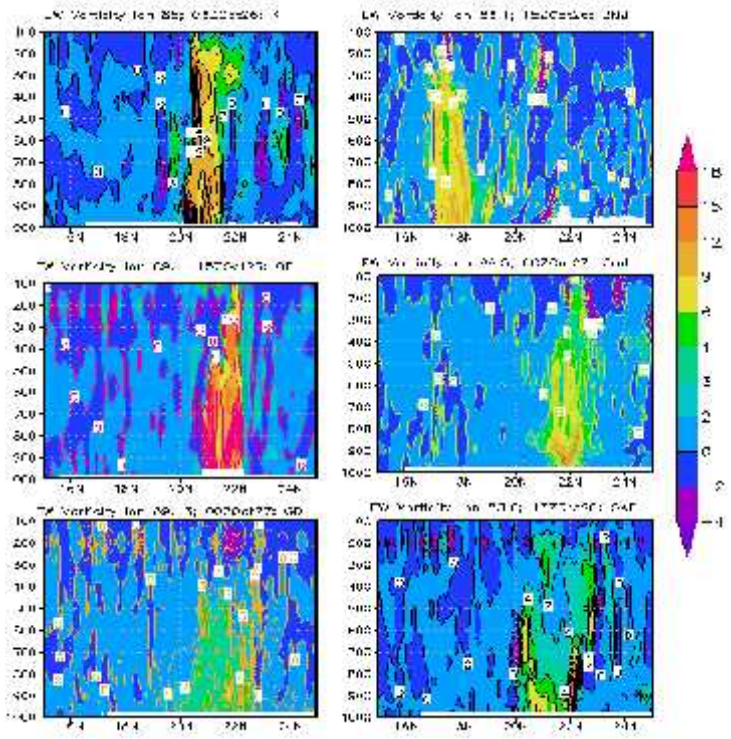

Figure 17: WRF model simulated north south vertical distribution of relative vorticity with fixed longitude of TC Rashmi through the centre at different cumulus schemes.

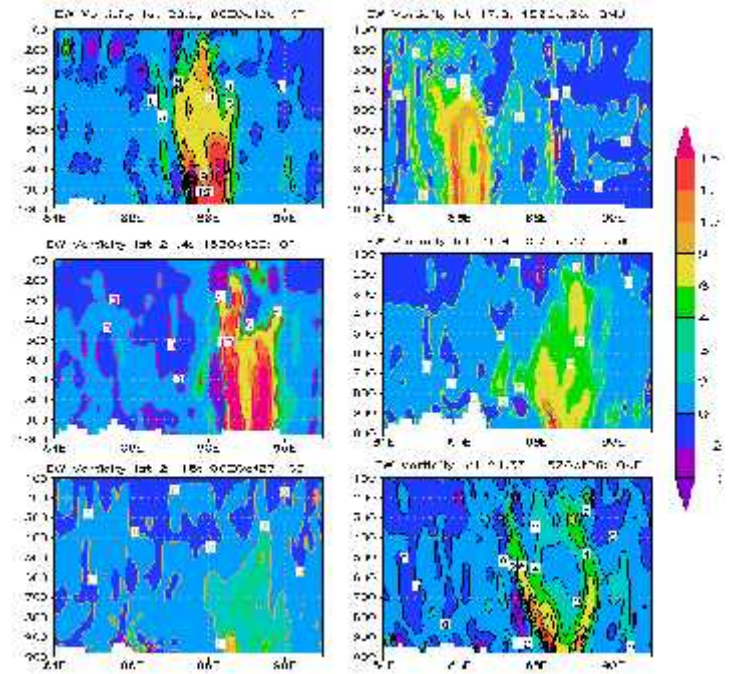

Figure 18: WRF model simulated east west vertical distribution of relative vorticity with fixed latitude of TC Rashmi through the centre at different cumulus schemes.

4.1.5 Temperature anomaly

The WRF model simulated temperature anomaly at 0600 UTC of 26, 1500 UTC of 26, 1500 UTC of 26, 0000 UTC of 27, 0000 UTC of 27 and 1500 UTC of 26 October 2008 (i.e. its mature stage) for different cumulus (KF, BMJ, GF, G3, GD and OKF) schemes is shown in Figure 19 and the values are tabulated in Table 5. Here, temperature anomaly is the difference of temperature from its mean value at a certain time in a vertical cross section. It is noted that the warm core region is slightly expanded up to 200 hPa level all most for all cumulus schemes.

For KF cumulus scheme, at 0600 UTC of 26 October 2008, a warm core with 6^{o}C is observed in 300-200 hPa layer. It is noted that the warm core region is expanded outward at 600-200 hPa level. The greatest anomaly is observed around 250 hPa level. The simulated temperature anomaly demonstrates that the warm core is visible mainly at upper troposphere.

For BMJ cumulus scheme at 1500 UTC of 26 October 2008, a warm core with 5^{o}C is observed in 800-380 hPa layer. It is noted that the warm core region is expanded outward at 800-200 hPa level. The greatest anomaly is observed around 600 hPa level. The simulated temperature anomaly demonstrates that the warm core is visible mainly at middle troposphere.

For GF cumulus scheme at 1500 UTC of 26 October 2008, a warm core with 10^{o}C is observed in 510-380 hPa layer. It is noted that the warm core region is expanded outward at 700-200 hPa level. The greatest anomaly is observed around 450 hPa level. The simulated temperature anomaly demonstrates that the warm core is visible mainly above middle troposphere.

For G3 cumulus scheme at 0000 UTC of 27 October 2008, a warm core with 6^{o}C is observed in 400-300 hPa layer. It is noted that the warm core region is expanded outward at 500-200 hPa level. The greatest anomaly is observed around 400 hPa level. The simulated temperature anomaly demonstrates that the warm core is visible mainly at above middle troposphere.

For GD cumulus scheme at 0000 UTC of 27 October 2008, a warm core with 4^{o}C is observed in 600-200 hPa layer. It is noted that the warm core region is expanded outward at 500-300 hPa level. The greatest anomaly is observed around 400 hPa level. The simulated temperature anomaly demonstrates that the warm core is visible mainly above middle troposphere.

For OKF cumulus scheme at 0600 UTC of 26 October 2008, a warm core with 5^{o}C is observed in 580-200 hPa layer. It is noted that the warm core region is expanded outward at

500-200 hPa level. The greatest anomaly is observed around 400 hPa level. The simulated temperature anomaly demonstrates that the warm core is visible mainly at upper troposphere.

Finally, the greatest anomaly is occurred at cumulus GF scheme around 450 hPa levels. The simulated temperature anomaly demonstrates that the warm core is visible mainly at middle troposphere for all cumulus schemes with little exception. Negative temperature anomalies are also seen at the upper levels and lower levels.

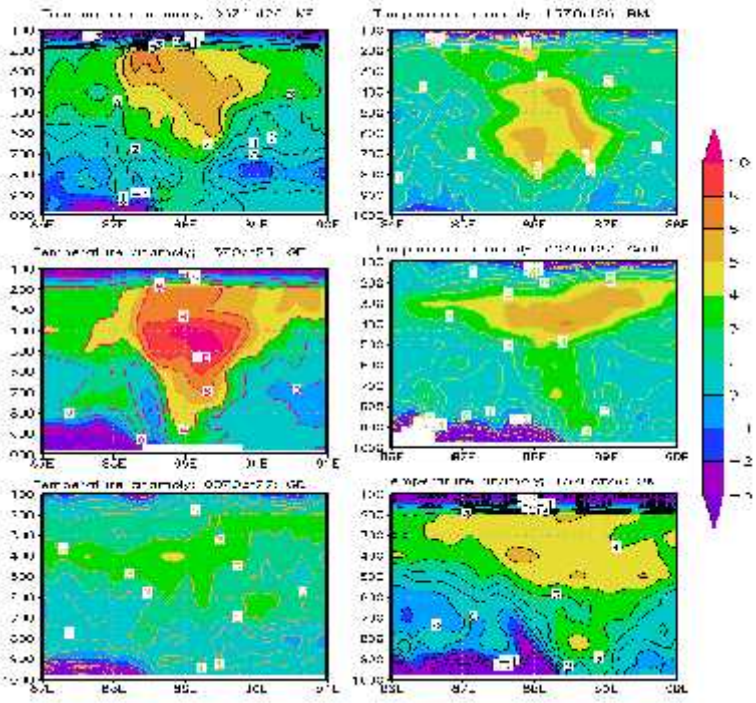

Figure 19: WRF model simulated vertical distribution of temperature anomaly in the east-west direction of TC Rashmi at different cumulus schemes.

Table 5: WRF Model simulated maximum temperature anomaly (°C), Relative Humidity (%) and Water vapor mixing ratio (g/kg) associated with TC Rashmi at different cumulus schemes.

Parameter	06 UTC of 26 October at KF	15 UTC of 26 October at BMJ	15 UTC of 26 October at GF	00 UTC of 27 October at G3	00 UTC of 27 October at GD	15 UTC of 26 October at OKF
Maximum Temperature	6	5	10	6	4	5
Relative Humidity	95	100	95	95	95	95
Water vapor mixing ratio	2	2	2.2	2	2	2

4.1.6 Relative humidity

The horizontal distribution of relative humidity of TC Rashmi obtained from WRF model at 0600 UTC of 26, 1500 UTC of 26, 1500 UTC of 26, 0000 UTC of 27, 0000 UTC of 27 and 1500 UTC of 26 October 2008 (i.e. its mature stage) for different cumulus (KF, BMJ, GF, G3, GD and OKF) schemes is shown in Figure 20. Time variation of relative humidity at surface is obtained around 100% with few exceptions. But the relative humidity at 850 levels for all cumulus is 100% of the cyclones (not shown in figure). These values satisfy the condition for the intensification of cyclone through convection.

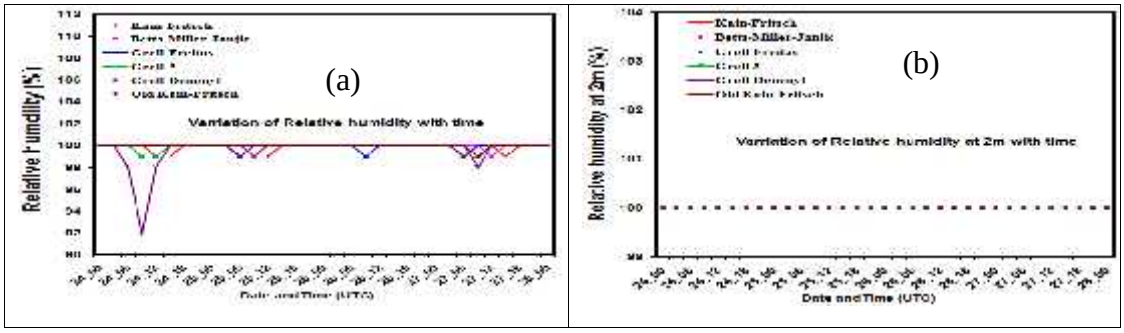

Figure 20: Evolution of model simulated (a) RH and (b) RH at 2m with time at different cumulus schemes of TC Rashmi.

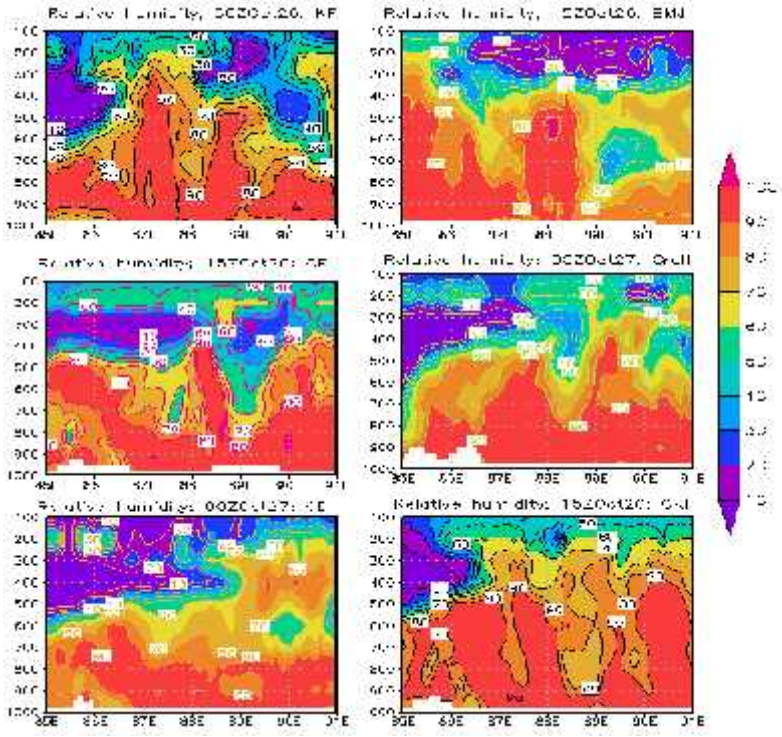

Figure 21: WRF model simulated vertical distribution of relative humidity (%) in the east-west direction of TC Rashmi at different cumulus schemes.

The vertical cross section of relative humidity of TC Rashmi obtained from WRF model at 0600 UTC of 26, 1500 UTC of 26, 1500 UTC of 26, 0000 UTC of 27, 0000 UTC of 27 and 1500 UTC of 26 October 2008 (i.e. its mature stage) for different cumulus (KF, BMJ, GF, G3, GD and OKF) schemes from surface to 100 hPa levels is shown in Figure 21 and its values are tabulated in Table 5. It is noted that high relative humidity (more than 90%) spreads in outer range of eye wall up to 350, 550, 400, 500, 600 and 450 hPa levels for the cumulus (KF, BMJ, GF, G3, GD and OKF) schemes respectively. High relative humidity bands are also found in the rain band of the system situated at both sides of the system in the wider range throughout 980-700 hPa level. From the Table 5 and the figure, it is observed that highest relative humidity of 100% is observed using BMJ cumulus scheme.

4.1.7 Relative humidity at 2m

The time evolution of relative humidity at 2m of TC Rashmi obtained from WRF model at 0600 UTC of 26, 1500 UTC of 26, 1500 UTC of 26, 0000 UTC of 27, 0000 UTC of 27 and 1500 UTC of 26 October 2008 (i.e. its mature stage) for different cumulus (KF, BMJ, GF, G3, GD and OKF) schemes is shown in Figure 20. It is noted that high relative humidity at 2m (around 100%) spreads in outer range of eye wall up for all cumulus schemes without any exception. It is the good indication for the intensification of cyclone.

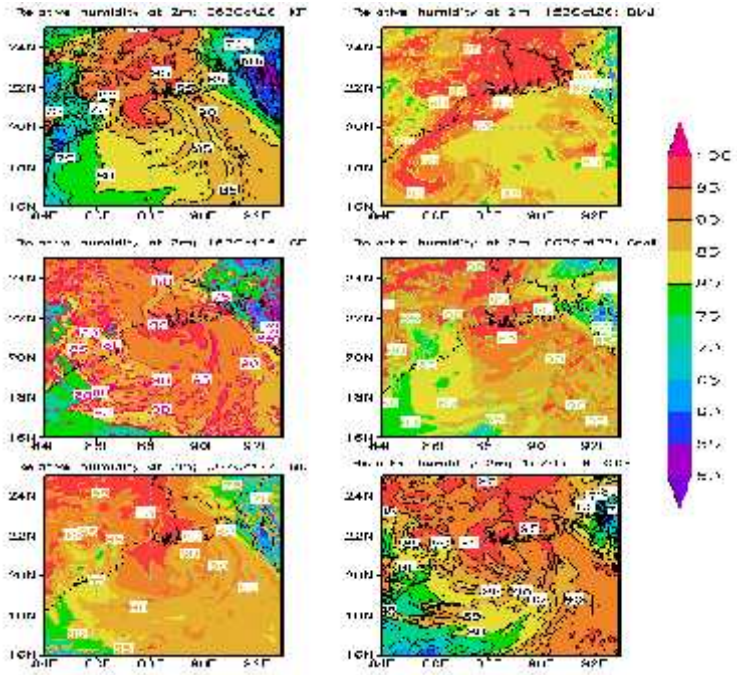

Figure 22: WRF model simulated spatial distribution of relative humidity at 2m (%) in the east-west direction of TC Rashmi at different cumulus schemes.

The spatial distribution of relative humidity at 2m of TC Rashmi obtained from WRF at 0600 UTC of 26, 1500 UTC of 26, 1500 UTC of 26, 0000 UTC of 27, 0000 UTC of 27 and 1500 UTC of 26 October 2008 (i.e. its mature stage) for different cumulus (KF, BMJ, GF, G3, GD and OKF) schemes is shown in Figure 22. The values of the relative humidity at 2m of TC Rashmi around the centre are about 100% or less for all cumulus schemes. This status of the relative humidity is satisfied the convection for the cyclone intensification.

4.1.8 Water vapor mixing ratio

The vertical distribution of water vapor mixing ratio obtained from WRF model along the east-west cross section of the centre at 0600 UTC of 26, 1500 UTC of 26, 1500 UTC of 26, 0000 UTC of 27, 0000 UTC of 27 and 1500 UTC of 26 October 2008 (i.e. its mature stage) for different cumulus (KF, BMJ, GF, G3, GD and OKF) schemes respectively of TC Rashmi from surface to 100 hPa level is shown in Figure 23 and its values are tabulated in Table 5. It shows that the highest moisture content more than around 2.2 g/kg or more is found at the centre of the system at 950 hPa level and it decreases upwards to 400 hPa levels or more. For the development of the system this upward level goes up to 350 hPa level (i.e. its mature stage). Performance of all cumulus schemes for the simulation of vertical distribution of water vapor mixing ratio are comparable.

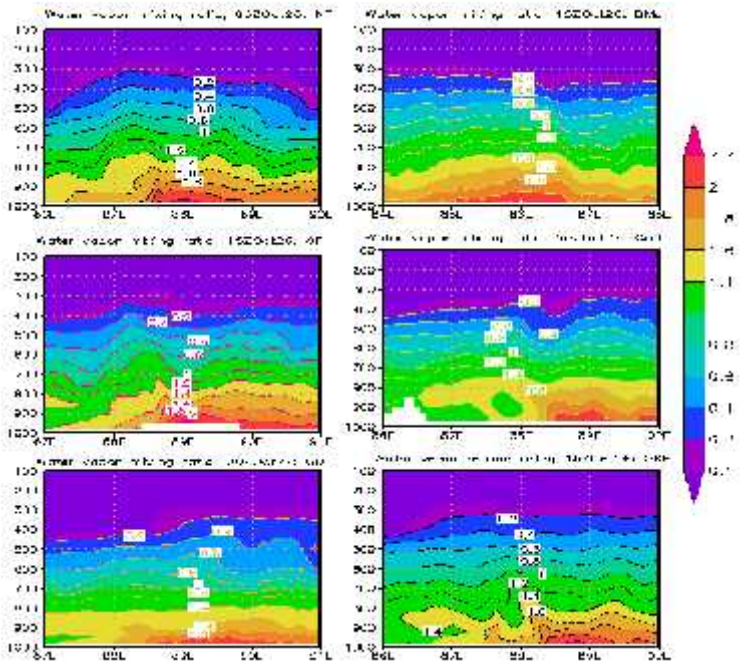

Figure 23: WRF model simulated vertical distribution of water vapor mixing ratio along the east-west cross section of the centre of TC Rashmi at different cumulus.

The horizontal distribution of water vapor mixing ratio of TC Rashmi at 950 hPa level at 0600 UTC of 26, 1500 UTC of 26, 1500 UTC of 26, 0000 UTC of 27, 0000 UTC of 27 and 1500 UTC of 26 October 2008 (i.e. its mature stage) for different cumulus (KF, BMJ, GF, G3, GD and OKF) schemes are obtained from WRF model is shown in the Figure 24. The maxing ratio shows a highly asymmetric character in the horizontal distribution. In Figure 24, maximum water vapor mixing ratio of 2 g/kg is obtained. It is noted that the highest mixing ratio is obtained at 950 hPa level close to the near of Bangladesh.

It is noted that the high moisture flux comes from the southern side covering a large area of the Bay of Bengal which feeds the system along its southeastern side through the boundary layer. The value of high moisture flux increases slightly with development of the system.

Maximum value of water vapor mixing ratio is 2.2 gm/Kg and it is situated mainly at and around the centre of the cyclone. These maximum values cover large area of sea and small area of Bangladesh for all cumulus schemes except GD scheme. The south and western parts of Bangladesh ~~is~~ are covered with more value of water vapor mixing ratio (but less than 2.2 gm/Kg) finally, it may be concluded that all the schemes satisfy the intensification of the cyclone.

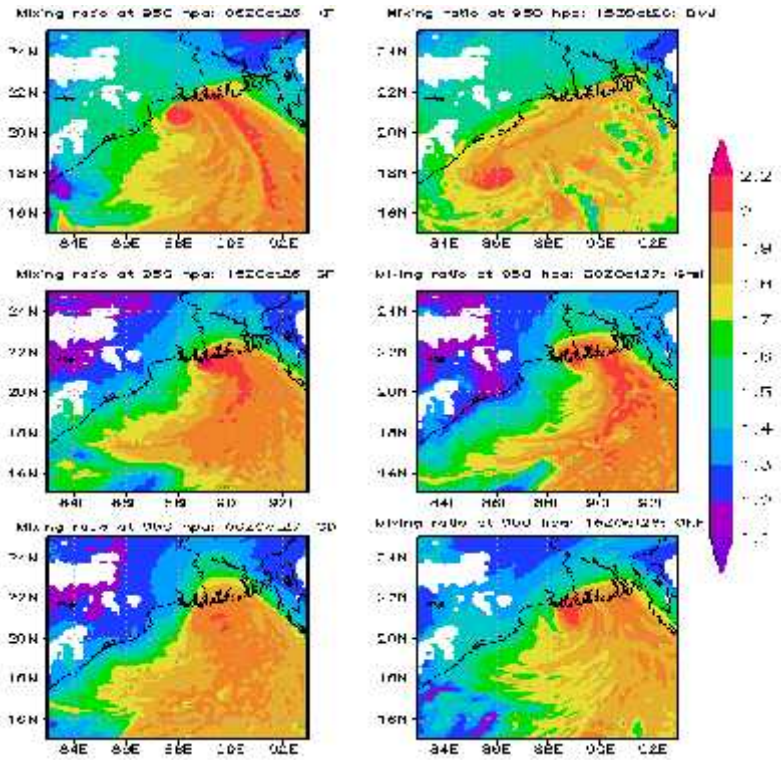

Figure 24: WRF model simulated horizontal distribution of water vapor mixing ratio at 950 hPa of TC Rashmi at different cumulus.

4.2 Tropical Cyclone Viyaru

The model simulated MSLP, maximum wind at 10 m level, Vorticity, Temperature anomaly, Relative humidity, Relative humidity at 2m and Water vapor mixing ratio with six CP schemes along with synoptic situation have been discussed for the TC Viyaru in the following sub-sections:

4.2.1 Description of Tropical Cyclone Viyaru

To analyze the low intensity of TC Viyaru, the WRF model has been run for 96 hrs with the initial field at 0000 UTC of 13 May 2013 using different cumulus. A depression formed over southeast Bay of Bengal at 0900 UTC of 10th May 2013 near latitude 5.0°N and longitude 92.0°E. It moved northwestwards and intensified into a deep depression in the evening of the same day. Continuing its northwestward movement, it further intensified into a cyclonic storm, Mahasen in the morning of 11th May 2013. Under the influence of the anticyclonic circulation lying to the east, the cyclonic storm changed its direction of movement initially from northwesterly to northerly and then to north northeasterly on 13th and 14th May respectively. On 15th May, it further came under the influence of the midlatitude westerly trough running roughly along 77°E, which further helped in enhancing the north-northeastward speed of the cyclonic storm. The cyclonic storm crossed Bangladesh coast near lat.22.8°N and long. 91.4°E, about 30 km south of Feni around 0800 UTC of 16th May 2013 with a sustained maximum surface wind speed of about 85-95 kmph. After the landfall, it continued to move north-northeastwards and weakened gradually due to interaction with land surface. It weakened into a deep depression over Mizoram in the evening and into a depression over Manipur around mid-night of 16th. It further weakened into a well marked low pressure area over Nagaland in the early morning and moved away towards Myanmar as a low pressure area in the morning of 17th May. Using WRF models the different meteorological parameters are discussed for the intensity of the TC Viyaru in the following sub-section. The WRF model simulated data are compared with those obtained from Joint Typhoon Warning Centre (JTWC).

4.2.2 Minimum sea level pressure (MSLP)

The storm intensity forecasts for the TC Viyaru in terms of MSLP using six different cumulus schemes KF, BMJ, GF, G3, GD and OKF for 96 hours (every 3 hourly) are presented in Figure 25. The WRF model simulated and observed MSLP gradually drops with time and attains peak intensity just before the landfall and thereafter MSLP increases. The model simulated MSLP values of 947, 963, 952, 949, 967 and 942 hPa are obtained using KF, BMJ, GF, G3, GD and OKF schemes respectively and these simulated MSLP are obtained at 0000 UTC of 15, 0900 UTC of 16, 1200 UTC of 15, 0300 UTC of 15, 0000

UTC of 16 and 2100 UTC of 15 May 2013 respectively. The observed MSLP of 990 hPa is obtained at 0600 UTC of 15 May 2013 according to IMD. So, simulated MSLP values are obtained later than that of observed. The observed MSLP is higher than the simulated MSLP for all cumulus schemes. The pressure departure is found minimum for OKF scheme and maximum for G3 schemes as compared with IMD observed. The simulated pressure fall for all cumulus schemes indicate that the system has attained the intensity of cyclonic storm and the observation also indicates that the system attained the intensity of cyclonic storm (990 hPa). All Cumulus schemes simulates later than the observed. The intensity using different cumulus scheme is extremely high to the observed intensity throughout the simulation time.. Cumulus BMJ and GD intensity is found to match much well than other cumulus.

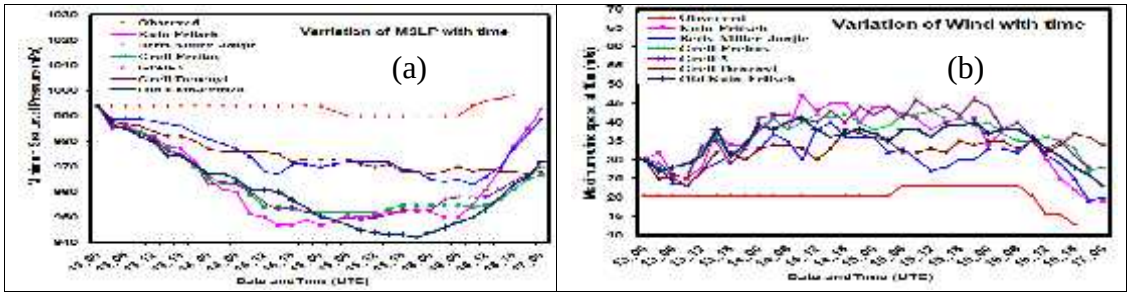

Figure 25: Evolution of WRF model simulated (a) MSLP and (b) MWS at 10m level using six different cumulus schemes and that of observed of the TC Viyaru.

Figure 26 shows the mature stage of spatial distribution of sea level pressure using six different cumulus schemes and it is obtained with different times and positions with different intensities. The spatial distribution of sea level pressure at its mature stage for the TC Viyaru using different cumulus schemes KF, BMJ, GF, G3, GD and OKF in WRF model is obtained at 0000 UTC of 15, 0900 UTC of 16, 1200 UTC of 15, 0300 UTC of 15 , 0000 UTC of 16 and 2100 UTC of 15 May 2013 respectively.

The lowest simulated MSLP values (i.e. mature stage) for the TC Viyaru using different cumulus schemes KF, BMJ, GF, G3, GD and OKF in WRF models are 947, 963, 952, 949, 967 and 942 hPa respectively. The observation also indicates that the system attained the intensity of cyclonic storm (990 hPa,). The intensity using different cumulus schemes is not close to the observed intensity. It is seen that OKF, KF and G3 cumulus schemes have very high intensity, and then the GF, BMJ and GD cumulus schemes have also very high intensity. In Figure 26, it is observed that mature stage of spatial distribution of sea level pressure using different cumulus is obtained with different time and different positions.

Positions of mature stages using KF, BMJ, GF, G3, GD and OKF are located at 87.42°E and 17.61°N at 0000 UTC of 15, 89.9°E and 22°N at 0900 UTC of 16, 88.45°E and 18.40°N at 1200 UTC of 15, 87.6°E and 17.5°N at 0300 UTC of 15, 87.36°E and 18.5°N at 0000 UTC of 16 May and 88.3°E and 19.75°N with time and 2100 UTC of 15 May 2013 respectively. Intensity, position and time of mature stages are different for different cumulus schemes used in WRF model. The isobar has circular arrangement around the TC centre with some asymmetric features in the outer periphery. The contour interval is different for different positions because of different intensity of the system. From the Figure 26, the radius of the TC eye is found to be around 100 km for all cumulus according to all simulation.

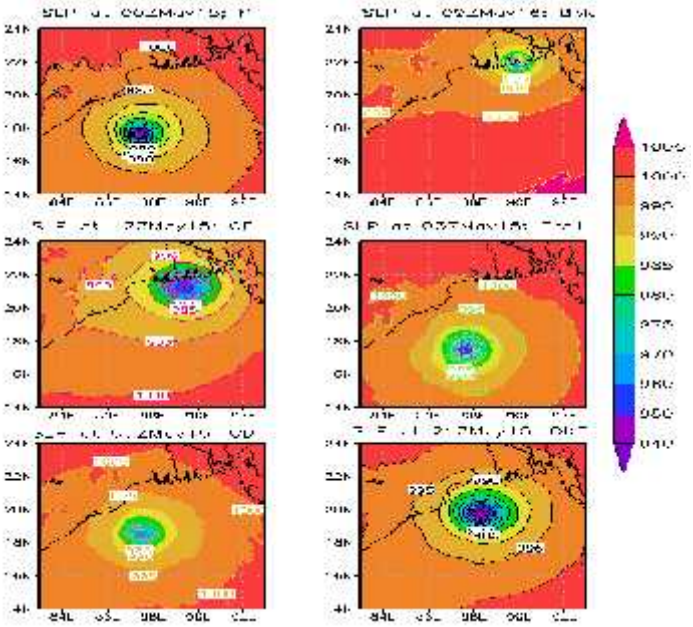

Figure 26: WRF model simulated SLP of TC Viyaru at different cumulus schemes.

The distribution of the sea level pressure of the TC Viyaru along east-west cross section and north-south cross section passing through its centre using different cumulus is shown in Figure 27. The positions of the centre at mature stage using different cumulus schemes KF, BMJ, GF, G3, GD and OKF are located at 87.42°E and 17.61°N, 89.9°E and 22°N, 88.45°E and 18.40°N, 87.6°E and 17.5°N, 87.36°E and 18.5°N and 88.3°E and 19.75°N respectively. The model simulated MSLP values of 947, 963, 952, 949, 967 and 942 hPa are obtained 0000 UTC of 15, 0900 UTC of 16, 1200 UTC of 15, 0300 UTC of 15, 0000 UTC of 16 and 2100 UTC of 15 May 2013 respectively and shown in Figure 27. In Figure 27, the black, green, yellow, orange, magenta and the dark purple color represent KF, BMJ, GF, G3, GD and OKF scheme respectively. The figures demonstrate the moderate pressure

gradient around the centre with maximum gradient at around 120 km below or above for all cumulus schemes from the centre. Variations of east-west and north-south elongated SLP at the center are clearly observed.

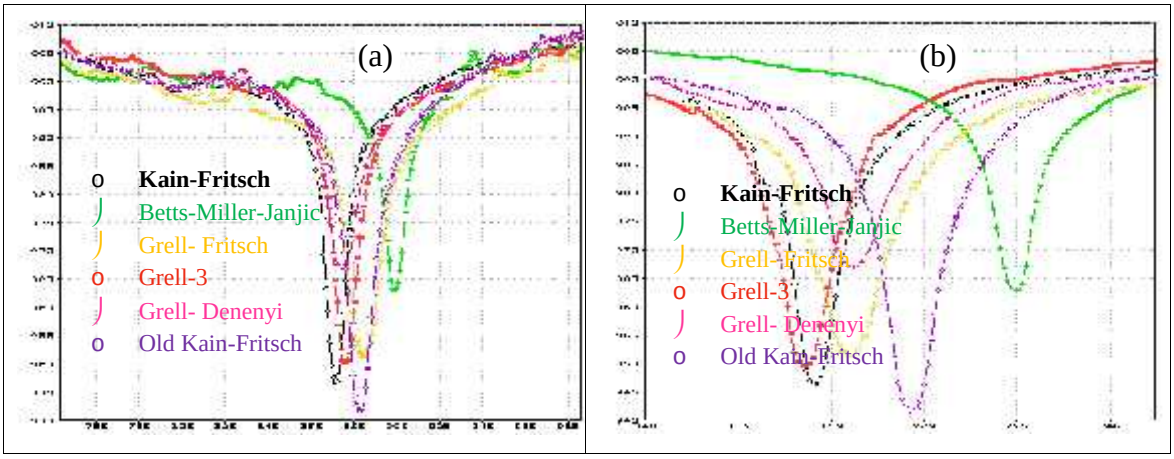

Figure 27: WRF model simulated (a) East West and (b) North South cross sectional view of SLP of TC Viyaru at different cumulus schemes with fixed latitude and longitude respectively.

4.2.3 Maximum Wind speed

The storm intensity forecasts for the TC Viyaru in terms of MWS using six different cumulus schemes KF, BMJ, GF, G3, GD and OKF for 96 hours (every 3 hourly) along with observed MWS are presented in Figure 25. The model simulated MWS are obtained at the standard meteorological height of 10 m. The WRF model simulated MWSs are higher than the observed values. Model simulated highest value of MWSs using six different cumulus schemes are obtained earlier. The observed and simulated MWSs by WRF decrease with time gradually after obtained highest value of MWS. The highest value of MWS for the TC Viyaru using different cumulus schemes of KF, BMJ, GF, G3, GD and OKF in WRF models are 47, 40, 43, 46, 38 and 41 m/s respectively. Whereas the observed MWS is 23.15 m/s. The observation value indicates that the system attained the intensity of cyclonic storm (17.5-24.44 m/s) and simulated values indicate that the system attained the intensity of SCS with a core of hurricane ($\geq$ 33.5 m/s). WRF model using different cumulus schemes simulate value of MWS than that of observed value. It is seen that KF cumulus scheme has very high intensity, then the GF and G3 cumulus scheme has also high intensity, then the BMJ, GD and OKF cumulus schemes has intensity.

Figure 28 shows spatial distribution of surface (10 m) wind speed at mature stage using six different cumulus schemes and it is obtained with different times and positions with different intensities. The spatial distribution of wind speed at its mature stage for the TC

Viyaru using different cumulus schemes KF, BMJ, GF, G3, GD and OKF in WRF model is obtained at 0000 UTC of 15, 0900 UTC of 16 , 1200 UTC of 15, 0300 UTC of 15, 0000 UTC of 16 and 2100 UTC of 15 May 2013 respectively and shown in Figure 28. The Figure 28 obtained from WRF model shows that the wind field of the TC is highly asymmetric in the horizontal distribution. At 0000 UTC of 13 May 2013 (i.e. at the initial time of simulation) the TC is in the sea with different cumulus schemes (not shown in figure). Gradually, TC is organized with strong wind bands around and the wind flow in the core region shows asymmetric feature with minimum wind speed at the centre. The spatial distribution of surface (10 m) wind speed is found maximum for KF scheme and minimum for BMJ and GD scheme. The figure shows that the pattern has an asymmetric wind distribution with strong wind bands in the front right side, rear left and rear right sides close to the centre of north directed moving storm. In Figure 28, it is observed that mature stage of spatial distribution of wind speed using different cumulus is obtained with different times and different positions. Positions of mature stages using KF, BMJ, GF, G3, GD and OKF are located at 87.42^{o}E and 17.61^{o}N at 0000 UTC of 15, 89.9^{o}E and 22^{o}N at 0900 UTC of 16, 88.45^{o}E and 18.40^{o}N at 1200 UTC of 15, 87.6^{o}E and 17.5^{o}N at 0300 UTC of 15, 87.36^{o}E and 18.5^{o}N at 0000 UTC of 16 and 88.3^{o}E and 19.75^{o}N at and 2100 UTC of 15 May 2013 respectively. At this mature stage, the wind flow in the core region shows a near circular feature with minimum wind speed at the centre.

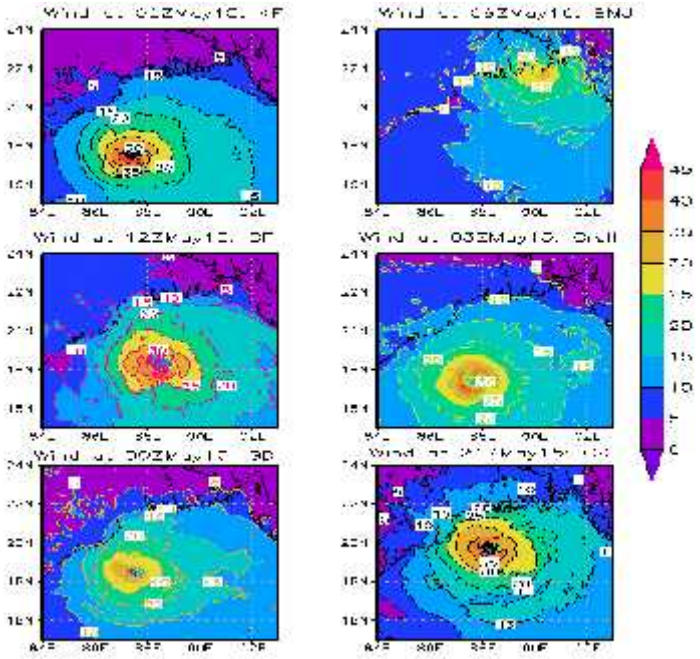

Figure 28: WRF model simulated MWS of TC Viyaru at different cumulus schemes.

The distributions of the surface wind of the TC Viyaru along east-west cross section and north-south cross section passing through its centre at mature stage using different cumulus are shown in Figures 29 and 30 respectively. The positions of the centre at mature stage using different cumulus schemes KF, BMJ, GF, G3, GD and OKF are located 87.42^{o}E and 17.61^{o}N, 89.9^{o}E and 22^{o}N, 88.45^{o}E and 18.40^{o}N, 87.6^{o}E and 17.5^{o}N, 87.36^{o}E and 18.5^{o}N respectively. The model simulated wind 47, 40, 43 , 46, 38 and 41 m/s are obtained at 0900 UTC of 14, 1500 UTC of 14, 1200 UTC of 15, 2100 UTC of 15, 1800 UTC of 14 and 0900 UTC of 14 May 2013 respectively. But the model simulated wind 44, 35, 43 , 44, 35 and 40 m/s are obtained at 0000 UTC of 15, 0900 UTC of 16, 1200 UTC of 15, 0300 UTC of 15 , 0000 UTC of 16 and 2100 UTC of 15 May 2013 respectively at mature stage (that is at the minimum SLP position). The figures demonstrate that a calm region is found inside the eye of the system and maximum wind was found in the eye wall. The simulated value of wind at the centre using different cumulus schemes has a wide variety. In Figure 29 the value is less than 11 m/s and in Figure 30 the value is less than 7 m/s. Variation of east–west and North South elongated wind at the center are clearly observed. Figures 29 and 30 all cumulus scheme show eye and eye wall clearly. The radius of maximum wind of the TC Viyaru is found to be just lower than 80 km according to the simulation. Variation of east-west and north-south elongated wind at the center is clearly observed.

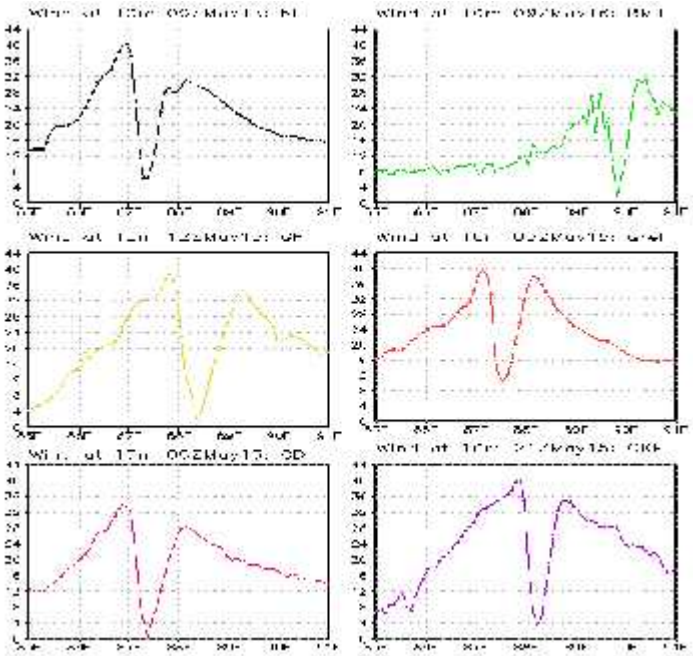

Figure 29: East west cross sectional view of WRF model simulated wind speed (m/s) of TC Viyaru at different cumulus schemes with fixed latitude.

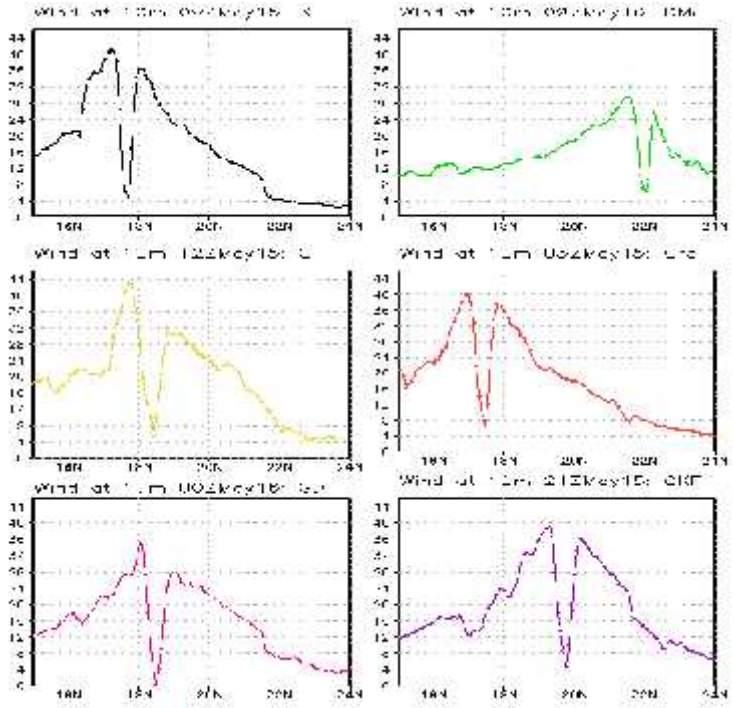

Figure 30: North south cross sectional view of WRF model simulated wind speed (m/s) of TC Viyaru at different cumulus schemes with fixed longitude.

The horizontal distribution of vector wind field at its mature stage for the levels 850, 500, 300 and 200 hPa of the TC Viyaru using different cumulus is tabulated in Table 6 and figure of this only for the levels 850 and 200 hPa are shown in Figure 31 and 32 respectively.

The horizontal distribution of vector wind field at its mature stage for the levels 850, 500, 300 and 200 hPa of the TC Viyaru using different cumulus is tabulated in Table 6 and the only results for the levels 850 and 200 hPa are shown in Figures 31 and 32 respectively.

From the Figure 31, a well organized TC circulation with strong winds encircling the centre is found at the 850 hPa levels. It is noted that the strong wind is confined to the right of the direction of the movement of the system. From the Figure 32, strong outflow is evident at 200 hPa level from the central part of the TC. So, using simulated results obtained from WRF models, Figure 31 and Figure 32 demonstrate inflow in the lower level and outflow in the upper level respectively.

WRF model simulated maximum winds at the mature stage (0000 UTC of 15, 0900 UTC of 16, 1200 UTC of 15, 0300 UTC of 15, 0000 UTC of 16 and 2100 UTC of 15 May 2013) are about 70, 60, 70, 80, 60, 80 m/s and 50, 40, 30, 40, 20, 40 m/s for different cumulus (KF, BMJ, GF, G3, GD and OKF) schemes at 850 and 200 hPa levels respectively. The wind

speed at 850 hPa levels is found minimum for BMJ and GD scheme, and maximum for OKF schemes. And the wind speed at 200 hPa levels is found minimum for GD scheme and maximum for KF schemes. The mature stages are obtained at different time and position. The values of wind speed for mature stage at the levels 500 and 300 hPa are obtained different with different cumulus schemes.

Table 6: WRF model simulated wind speed (m/s) at different cumulus schemes of 850, 500, 300 and 200 hPa pressure levels of TC Viyaru

Pressure level (hPa)	Simulated maximum Wind Speed (m/s) at different time					
	00 UTC of 15 May at KF	09 UTC of 16 May at BMJ	12 UTC of 15 May at GF	03 UTC of 15 May at Greel	00 UTC of 16 May at GD	21 UTC of 15 May at OKF
850	70	60	70	80	60	80
500	60	60	60	70	50	60
300	60	40	50	60	30	60
200	50	40	30	40	20	40

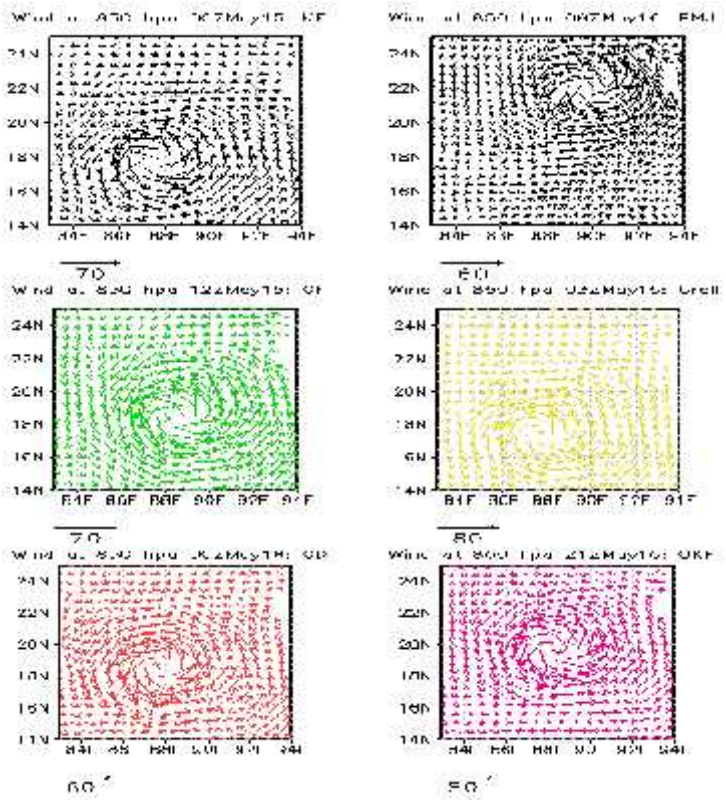

Figure 31: WRF model simulated Wind vector and magnitude at 850 hPa levels at different cumulus schemes.

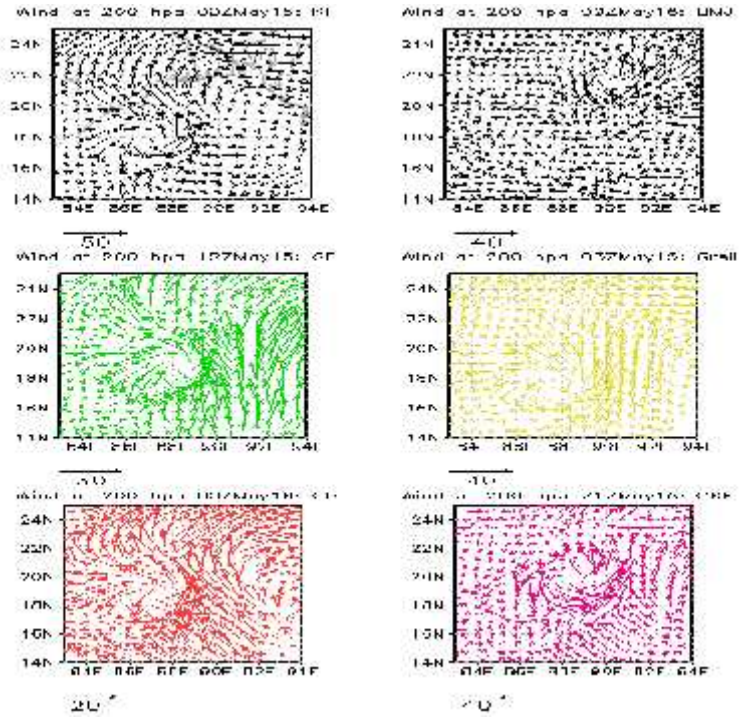

Figure 32: WRF model simulated Wind vector and magnitude at 200 hPa levels at different cumulus schemes.

The Vertical profile of Radial, Tangential, Vertical and Horizontal wind fields at its mature stage for the TC Viyaru using different cumulus schemes KF, BMJ, GF, G3, GD and OKF in WRF model are obtained at 0000 UTC of 15, 0900 UTC of 16, 1200 UTC of 15, 0300 UTC of 15, 0000 UTC of 16 and 2100 UTC of 15 May 2013 respectively and shown in Figures 33, 34, 35 and 36 respectively. Model simulated results are also tabulated in Table 7, for different cumulus schemes mentioned in the Table. From the table it is clear that the value of the vertical profiles of radial, tangential, vertical and horizontal wind of TC Viyaru obtained using different cumulus (KF, BMJ, GF, G3, GD and OKF) schemes are different for different cumulus schemes. The strong wind with different speeds (Table 7) is confined to different levels in lower troposphere and extended up to 100 hPa level in the left side of the system.

From the Figure 33, it is found that vertical profile of radial wind is much more organized and it is also clearly seen that the system has strong inflow in the lower levels which bring the air to the system through the boundary level and lower level and outflow in the upper level. The Radial wind is found minimum for Kain-Fritsch and Old Kain-Fritsch scheme and maximum for Grell-Fritsch schemes.

The vertical profile of tangential wind flows in a northerly direction at the eastern side of the system and in a southerly direction at the western side. For this reason, tangential wind

shows positive value at the right side (east side) of the centre and negative value at the left side (west side) of the centre. The Tangential wind is found minimum for Grell-Denenyi scheme and maximum for Grell-Fritsch schemes.

The values of vertical wind are different in magnitude for different cumulus schemes and are 0.4, 1.0, 1.5, 0.8, 1.0 and 0.6 m/s ~~are~~ simulated by KF, BMJ, GF, G3, GD and OKF cumulus schemes respectively. It indicates that the vertical wind is found minimum for KF scheme and maximum for GF scheme. These values are along the eye wall and other parts of the system which feed moisture into the system. It is noted that Virayu has very weak updraft motion at the eye wall throughout middle and upper troposphere. The downward motion is visible in the central parts of the TC and other areas in between rain bands.

The vertical profile of horizontal wind of the system at its mature stage shows the distribution of strong winds up to 100 hPa for KF, GF, G3 and OKF cumulus schemes and up to 200 hPa for BMJ and GD cumulus schemes around the centre of TC. It further confirms that the maximum winds are confined to the right of the direction of the movement of the system. This value decreases with the radial distance from both side of the eye. Calm wind zone is sharp and narrow and little bit tilted to the westward and get expanded towards upper levels. This is in agreement with the previous studies of Rao and Prasad (2006) and Goswami *et al.* (2006) on Orissa TC. Cyclonic circulation is generally seen up to about 300 hPa level and anticyclonic circulation with divergence fields aloft. In case of TC Viyaru, cyclonic circulation is also seen up to about 200 hPa level for all cumulus scheme and anticyclonic circulation with divergence fields aloft. And the horizontal wind is found minimum for GD scheme and maximum for GF scheme.

Table 7: WRF model simulated radial wind, tangential wind, vertical velocity and horizontal wind (m/s) of TC Viyaru at different cumulus schemes.

Component of wind	Simulated maximum wind speed (m/s) at different time					
	00 UTC of 15 May at KF	09 UTC of 16 May at BMJ	12 UTC of 15 May at GF	03 UTC of 15 May at G3	00 UTC of 16 May at GD	21 UTC of 15 May at OKF
Radial wind	15	5	15	5	10	10
Tangential wind	45	45	50	50	40	50
Vertical velocity	o.4	1	1.5	o.8	1	0.6
Horizontal wind	70	50	60	70	50	60

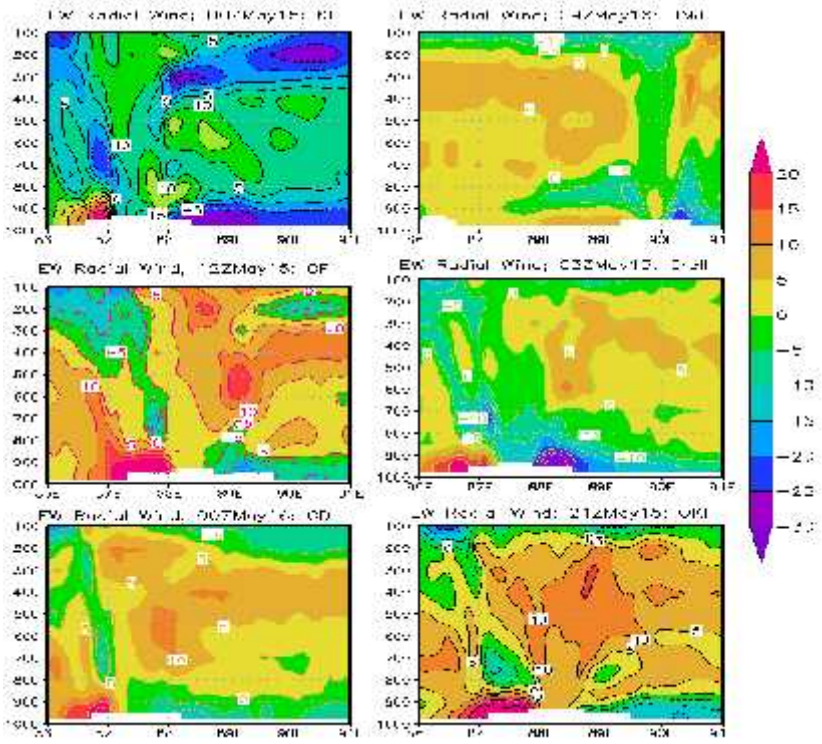

Figure 33: WRF model simulated Radial wind (m/s) of TC Viyaru at different cumulus schemes.

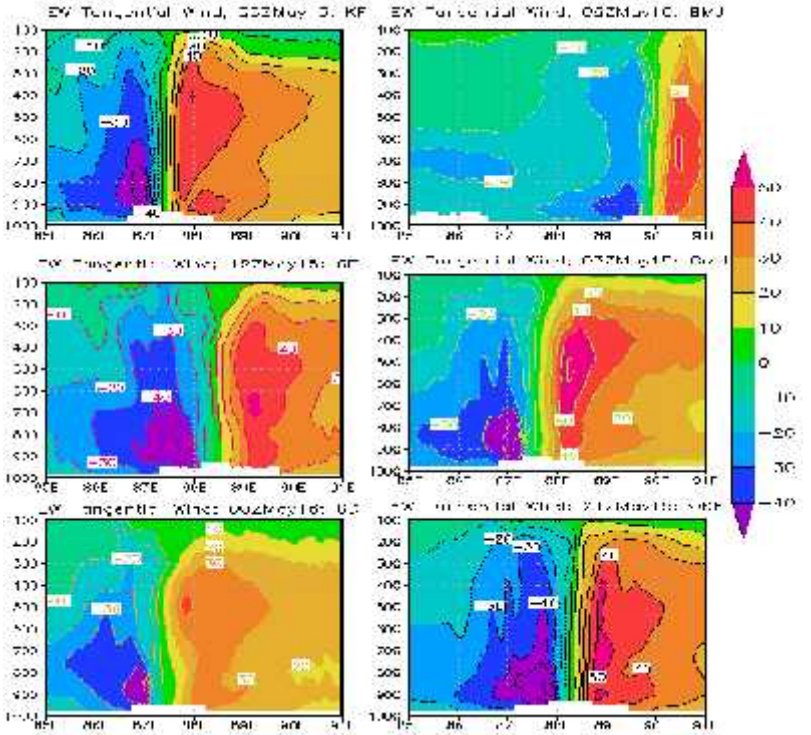

Figure 34: WRF model simulated Tangential wind (m/s) of TC Viyaru at different cumulus schemes.

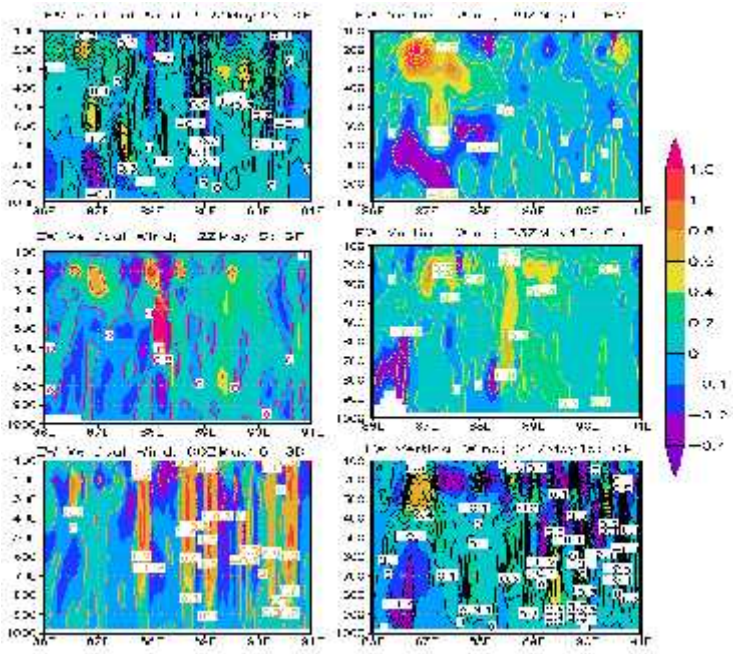

Figure 35: WRF model simulated Vertical wind (m/s) of TC Viyaru at different cumulus schemes.

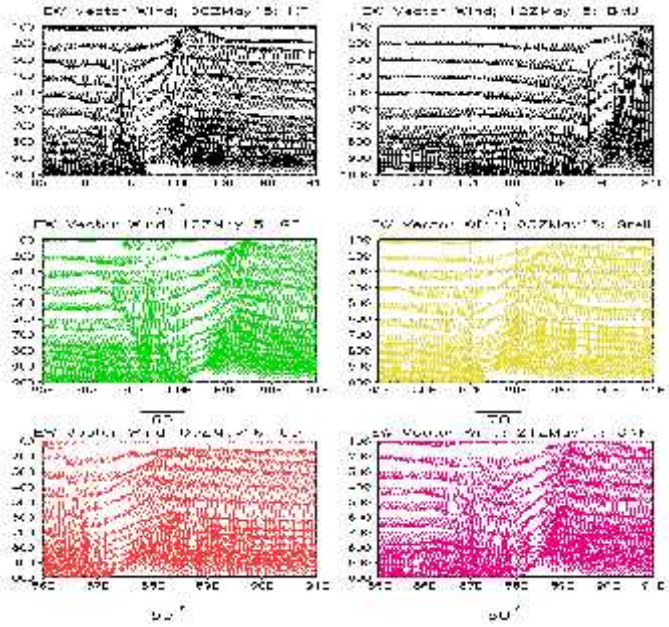

Figure 36: WRF model simulated Horizontal wind (m/s) of TC Viyaru at different cumulus schemes.

4.2.4 Vorticity

To know the evolution WRF model simulated relative vorticity at 1000, 950, 850, 500 and 300 hPa with six cumulus KF, BMJ, GF, G3, GD and OKF schemes for 96 hours (every 3 hourly) are presented in Figure 37. The value of relative vorticity is increased with the increase of time (i.e. in the development of the TC) at all levels for all cumulus schemes and

has increased to a maximum value. Thereafter, the value shows a fall. From the figure it is observed that at 850, 500 and 300 hPa, the vorticity is found maximum for cumulus KF scheme. And at 1000 hPa level, the vorticity is found maximum for cumulus BMJ scheme. At 950 hPa level, the vorticity is found maximum for cumulus G3 scheme. The vorticity is found more than zero for all levels using all schemes. So, from the simulated value of vorticity it is seen that system intensification is satisfied more or less by all cumulus schemes.

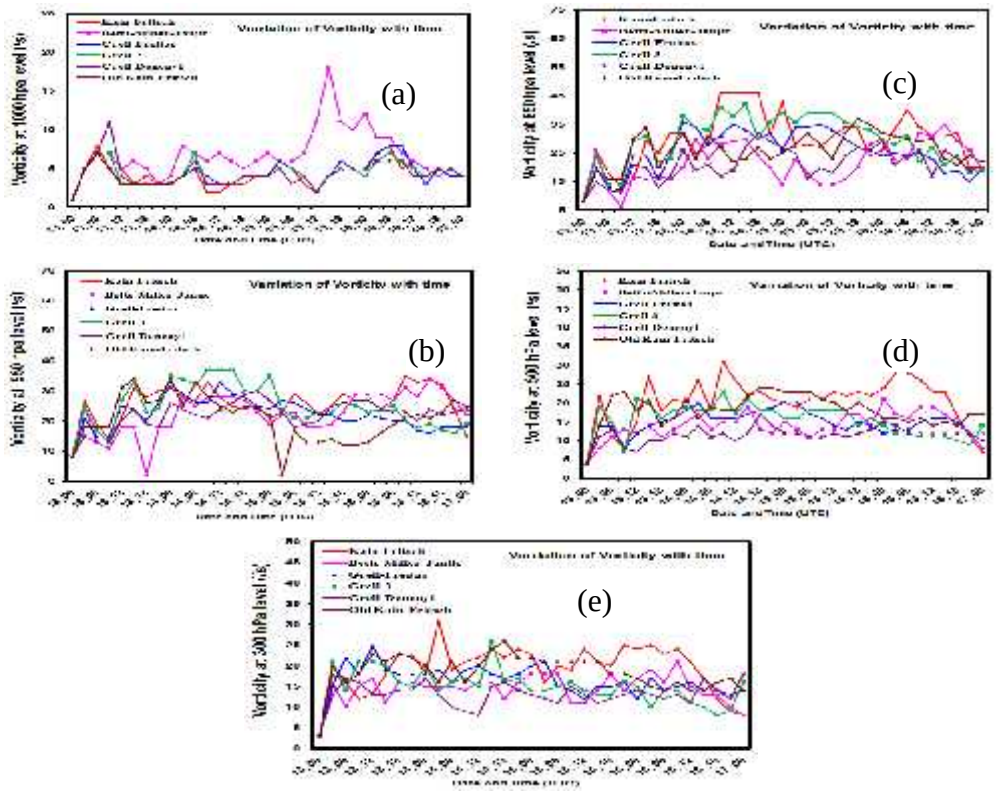

Figure 37: Evolution of model simulated vorticity with time at different cumulus schemes for 1000, 950, 850, 500 and 300 hPa level of TC Viyaru.

The horizontal distribution of the simulated relative vorticity obtained for TC Viyaru at 850 and 200 hPa levels are shown in the Figures 38 and 39 respectively. It is seen from the figures that the vorticity is distributed with maximum value at the centre and these values for the levels 850, 500, 300 and 200 hPa are tabulated in Table 8 for different cumulus (KF, BMJ, GF, G3, GD and OKF) schemes respectively. At 850 hPa, the distribution maintains circular pattern with some asymmetric features in the outer periphery. Negative vorticity fields are situated far from the centre. This distance of the negative vorticity from the centre is increased due to development of TC (not shown). Low level relative vorticity fields confirm the strong cyclonic circulation at low levels with different time and distance in feeding the moisture into the system to sustain its intensity. The values of relative vorticity are increased with the development of TC. At 200 hPa level, the weak positive vorticity embedded with negative vorticity field is visible at 200 hPa level. Negative vorticity is

found at the centre of the TC. It is clear from the figure that relative vorticity is more organized in the mature stage. The vorticity is found maximum or minimum for 850, 500, 300 and 200 levels at different time using different cumulus schemes.

Vertical distribution of the relative vorticity with fixed latitude (along east-west direction) and fixed longitude (along north-south direction) are obtained from WRF model is shown in Figures 40 and 41 respectively and the values are tabulated in Table 8.

Simulated results at 0000 UTC of 15, 0900 UTC of 16, 1200 UTC of 15, 0300 UTC of 15, 0000 UTC of 16 and 2100 UTC of 15 May 2013 for different cumulus schemes KF, BMJ, GF, G3, GD and OKF are located at 87.42^{o}E and 17.61^{o}N, 89.9^{o}E and 22^{o}N, 88.45^{o}E and 18.4^{o}N, 87.6^{o}E and 17.5^{o}N, 87.36^{o}E and 18.5^{o}N and 88.3^{o}E and 19.75^{o}N respectively. In Figure 40 the system has the positive vorticity along the centre up to 100 hPa level with higher value for all cumulus. For KF, BMJ, GF, G3, GD and OKF the higher values are found up to 180, 180, 200, 100, 100 and 150 levels respectively. So the strong cumulus scheme are G3 and GD schemes. In Figure 41, the system has the positive vorticity along the centre up to 100 hPa level with higher value for all cumulus schemes. For KF, BMJ, GF, G3, GD and OKF the higher value is up to 100 levels.

Table 8: WRF Model simulated maximum vorticity (x10^{-5} s^{-1}) at different pressure levels associated with TC Viyaru at different cumulus schemes.

Pressure level (hPa)	Vorticity (x10^{-5} s^{-1}) at different times					
	00 UTC of 15 May at KF	09 UTC of 16 May at BMJ	12 UTC of 15 May at GF	03 UTC of 15 May at Greel	00 UTC of 16 May at GD	21 UTC of 15 May at OKF
850	300	250	250	300	250	300
500	180	160	110	150	110	160
300	180	160	190	110	70	145
200	120	150	90	110	90	120
Position of TC centre	17.61^{o}N and 87.62^{o}E	22^{o}N and 89.9^{o}E	18.40^{o}N and 88.45^{o}E	17.5^{o}N and 87.6^{o}E	18.5^{o}N and 87.36^{o}E	19.75^{o}N and 88.3^{o}E
Vertical distribution with fixed latitude	22	20	12	22	22	22
Vertical distribution with fixed longitude	20	18	12	18	12	19

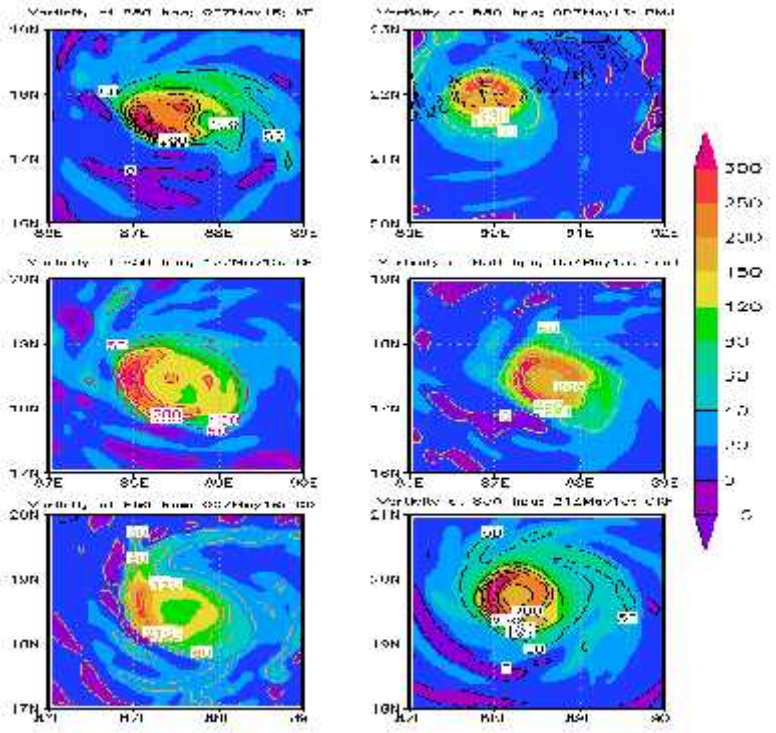

Figure 38: WRF Model simulated vorticity field of 850 hPa levels at different cumulus schemes.

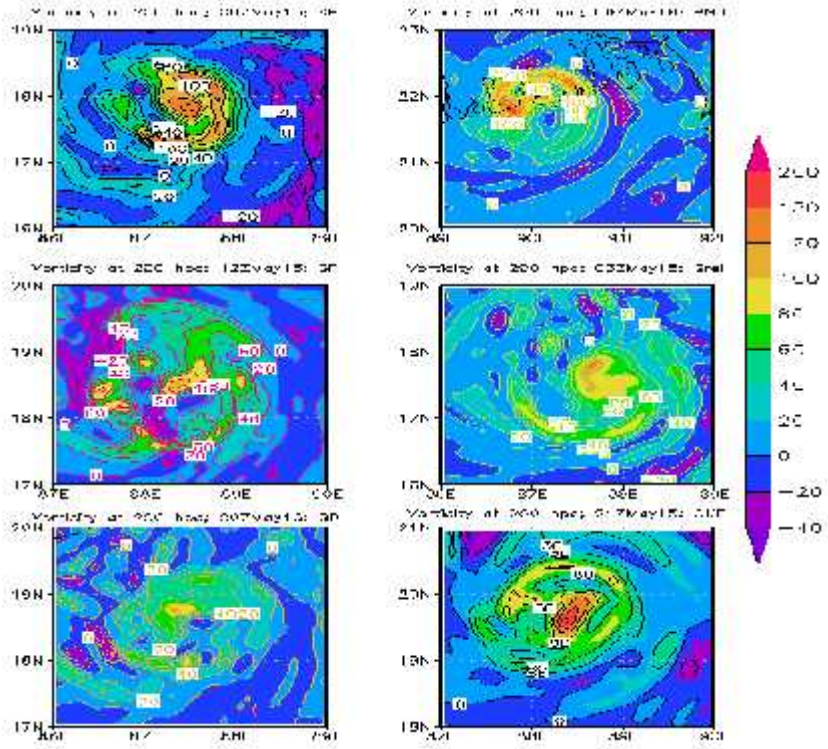

Figure 39: WRF Model simulated vorticity field of 200 hPa levels at different cumulus schemes.

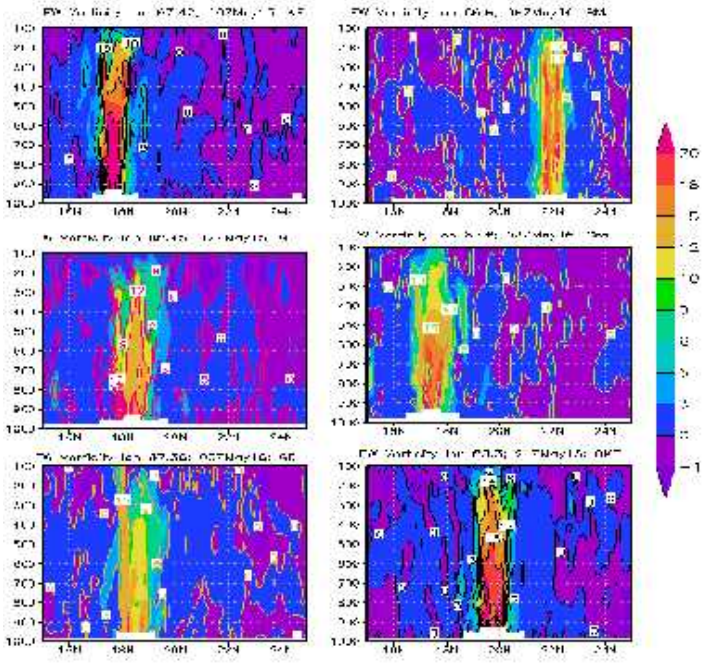

Figure 40: WRF model simulated east west vertical distribution of relative vorticity with fixed longitude of TC Viyaru through the centre at different cumulus schemes.

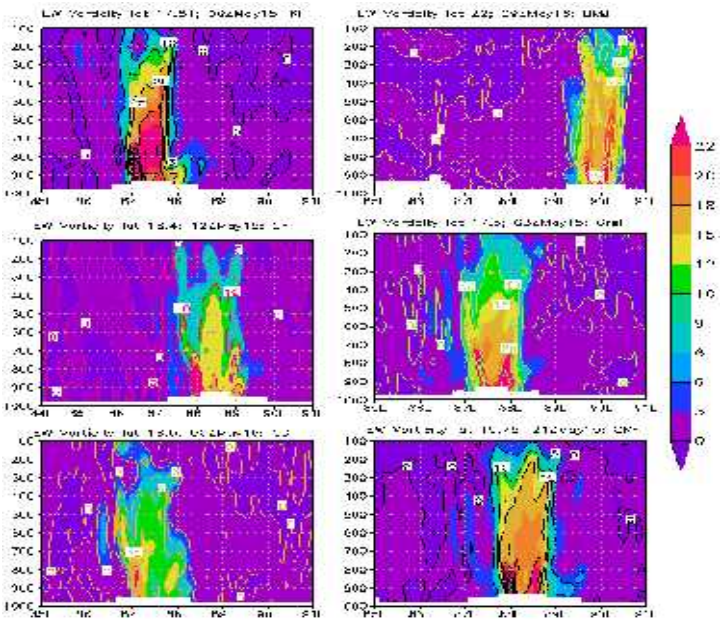

Figure 41: WRF model simulated east west vertical distribution of relative vorticity with fixed latitude of TC Viyaru through the centre at different cumulus schemes.

4.2.5 Temperature anomaly

The WRF model simulated temperature anomaly at 0000 UTC of 15, 0900 UTC of 16, 1200 UTC of 15, 0300 UTC of 15, 0000 UTC of 16 and 2100 UTC of 15 May 2013 (i.e. its

mature stage) for different cumulus (KF, BMJ, GF, G3, GD and OKF) schemes is shown in Figure 42 and the values are tabulated in Table 9. It is noted that the warm core region is slightly expanded up to 200 hPa level almost for all cumulus schemes.

For Kain-Fritsch cumulus scheme, at 0900 UTC of 14 May 2013, a warm core with 12^{o}C is observed in 480-220 hPa layer. It is noted that the warm core region is expanded outward at 500-200 hPa level. The greatest anomaly is observed around 350 hPa level. The simulated temperature anomaly demonstrates that the warm core is visible mainly at upper troposphere.

For Betts-Miller-Janjic cumulus scheme at 1500 UTC of 14 May 2013, a warm core with 9^{o}C is observed in 320-200 hPa layer. It is noted that the warm core region is expanded outward at 400-200 hPa level. The greatest anomaly is observed around 250 hPa level. The simulated temperature anomaly demonstrates that the warm core is visible mainly at upper troposphere.

For Grell-Fritsch cumulus scheme at 1200 UTC of 15 May 2013, a warm core with 10^{o}C is observed in 420-290 hPa layer. It is noted that the warm core region is expanded outward at 450-200 hPa level. The greatest anomaly is observed around 350 hPa level. The simulated temperature anomaly demonstrates that the warm core is visible mainly upper troposphere.

For Grell-3 cumulus scheme at 2100 UTC of 15 May 2013, a warm core with 11^{o}C is observed in 400-280 hPa layer. It is noted that the warm core region is expanded outward at 500-200 hPa level. The greatest anomaly is observed around 350 hPa level. The simulated temperature anomaly demonstrates that the warm core is visible mainly at upper troposphere.

For Grell-Denenyi cumulus scheme at 1800 UTC of 14 May 2013, a warm core with 7^{o}C is observed in 670-200 hPa layer. It is noted that the warm core region is expanded outward at 400-200 hPa level. The greatest anomaly is observed around 550 hPa level. The simulated temperature anomaly demonstrates that the warm core is visible mainly above middle troposphere.

For Old Kain-Fritsch cumulus scheme at 0900 UTC of 14 May 2013, a warm core with 11^{o}C is observed in 400-150 hPa layer. It is noted that the warm core region is expanded outward at 500-200 hPa level. The greatest anomaly is observed around 300 hPa level. The

simulated temperature anomaly demonstrates that the warm core is visible mainly at upper troposphere.

Finally, the greatest anomaly is occurred at cumulus KF scheme around 350 hPa levels. The simulated temperature anomaly demonstrates that the warm core is visible mainly at upper troposphere except GD cumulus scheme. Negative temperature anomalies are also seen at the lower levels.

Table 9: WRF Model simulated temperature anomaly (^{o}C), Relative Humidity (%), water vapor mixing ratio (g/kg) associated with TC Viyaru at different cumulus schemes.

Parameter	00 UTC of 15 May at KF	09 UTC of 16 May at BMJ	12 UTC of 15 May at GF	03 UTC of 15 May at Greel	00 UTC of 16 May at GD	21 UTC of 15 May at OKF
Maximum Temperature	12	9	10	11	7	11
Relative Humidity	100	100	100	100	100	100
Water vapor mixing ratio	2.2	2	2.2	2.2	2.2	2.2

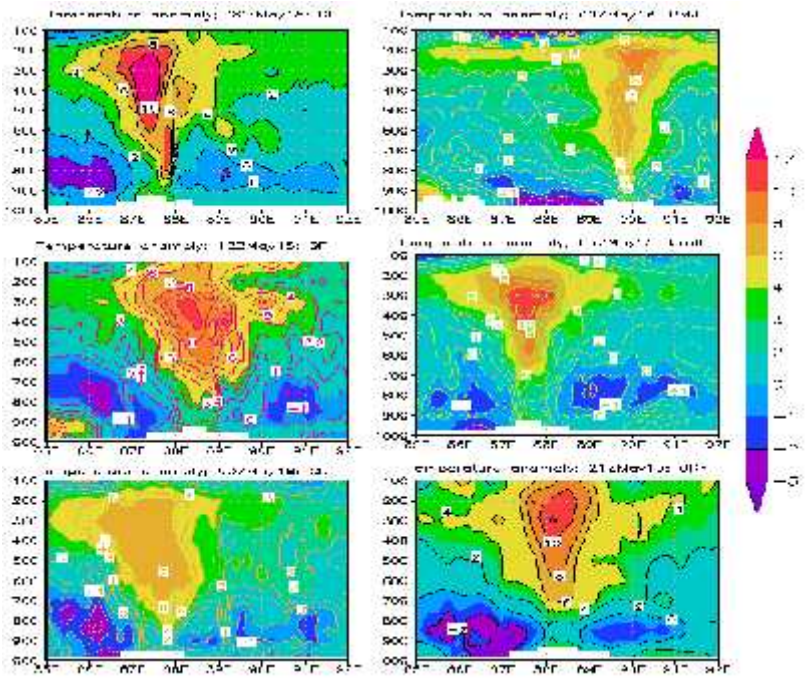

Figure 42: WRF model simulated vertical distribution of temperature anomaly in the east-west direction of TC Viyaru at different cumulus schemes.

4.2.6 Relative humidity

The Horizontal distribution of relative humidity of TC Viyaru obtained from WRF model at 0000 UTC of 15, 0900 UTC of 16, 1200 UTC of 15, 0300 UTC of 15, 0000 UTC of 16 and 2100 UTC of 15 May 2013 for different cumulus (KF, BMJ, GF, G3, GD and OKF) schemes is shown in Figure 43. Time variation of relative humidity at surface is obtained around 86-100%. But the relative humidity at 850 levels with all cumulus is 100% for all the cyclones (not shown in figure). These values satisfy the condition for the intensification of cyclone through convection.

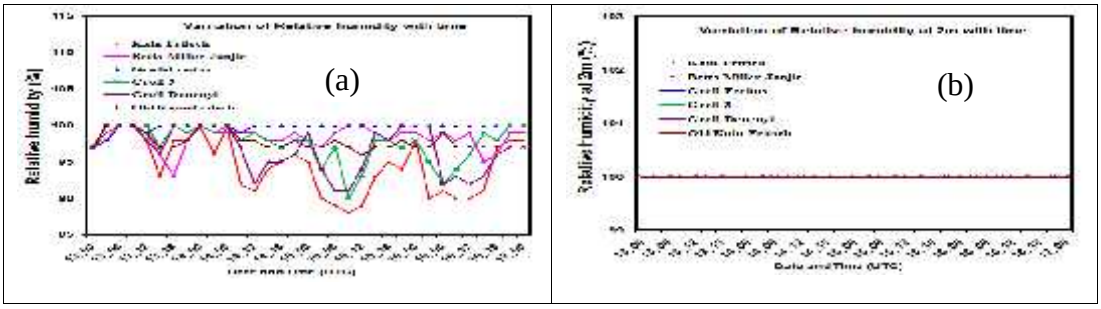

Figure 43: Evolution of model simulated (a) RH and (b) RH at 2m with time at different cumulus schemes of TC Viyaru.

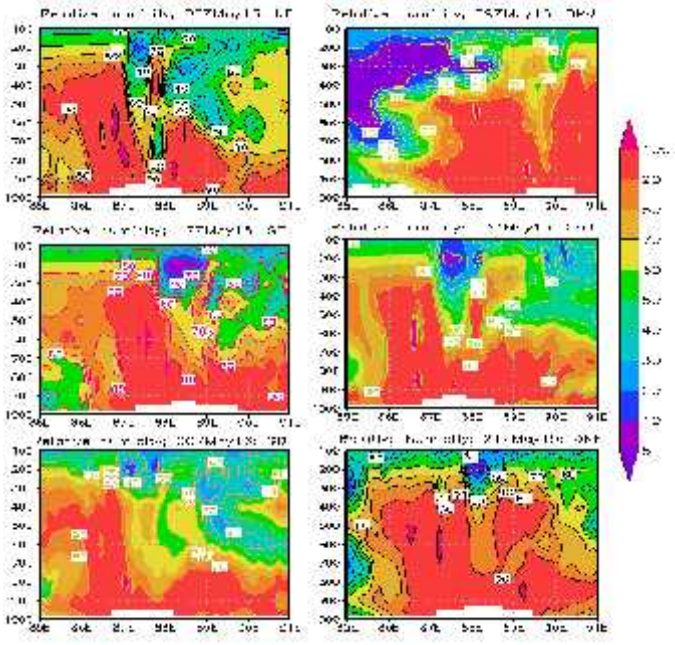

Figure 44: WRF model simulated vertical distribution of Relative humidity (%) in the east-west direction of TC Viyaru at different cumulus schemes.

The vertical cross section of relative humidity for TC Viyaru obtained from WRF model at 0000 UTC of 15, 0900 UTC of 16, 1200 UTC of 15, 0300 UTC of 15, 0000 UTC of 16 and

2100 UTC of 15 May 2013 (i.e. its mature stage) for different cumulus (KF, BMJ, GF, G3, GD and OKF) schemes from surface to 100 hPa levels is shown in Figure 44 and its values are tabulated in Table 9. It is noted that high relative humidity (more than 95%) spreads in outer range of eye wall up to 350, 500,700, 700, 720 and 400 hPa levels for the cumulus (KF, BMJ, GF, G3, GD and OKF) schemes respectively. High relative humidity bands are also found in the rain band of the system situated at both sides of the system in the wider range throughout 980-700 hPa level. From the Table 9 and the Figure 44, it is observed that highest relative humidity 100% is observed using all cumulus schemes.

4.2.7 Relative humidity at 2m

The time evolution of relative humidity at 2m of TC Viyaru obtained from WRF model at 0000 UTC of 15, 0900 UTC of 16, 1200 UTC of 15, 0300 UTC of 15, 0000 UTC of 16 and 2100 UTC of 15 May 2013 (i.e. its mature stage) for different cumulus (KF, BMJ, GF, G3, GD and OKF) scheme is shown in Figure 43. It is noted that high relative humidity at 2m (around 100%) spreads in outer range of eye wall up for all cumulus schemes without any exception. It is the good indication for the intensification of cyclone.

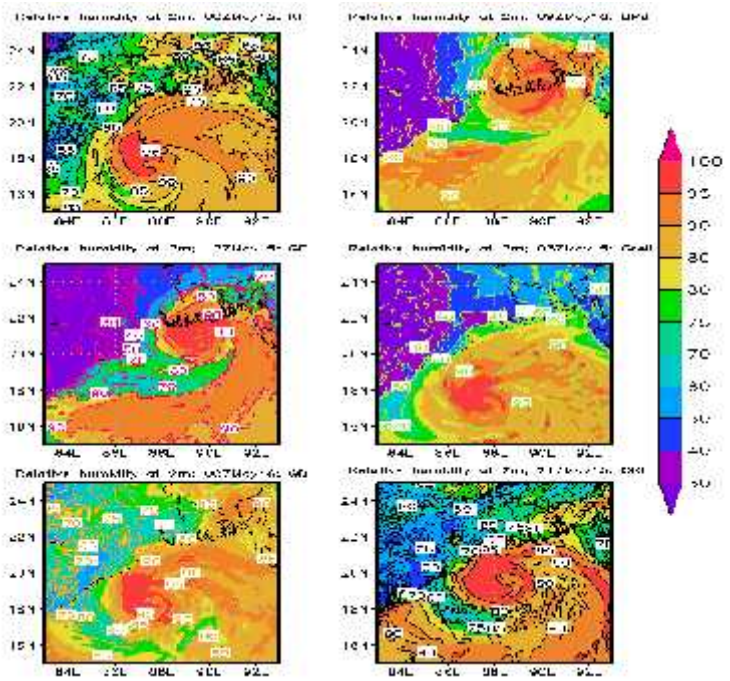

Figure 45: WRF model simulated spatial distribution of relative humidity at 2m (%) in the east-west direction of TC Viyaru at different cumulus schemes.

The spatial distribution of relative humidity at 2m of TC Viyaru obtained from WRF at 0000 UTC of 15, 0900 UTC of 16, 1200 UTC of 15, 0300 UTC of 15, 0000 UTC of 16 and

2100 UTC of 15 May 2013 (i.e. its mature stage) for different cumulus (KF, BMJ, GF, G3, GD and OKF) scheme is shown in Figure 45. The values of the relative humidity at 2m of TC Viyaru around the centre are about 100% or less for all cumulus schemes. This status of the relative humidity is satisfied the convection for the cyclone intensification.

4.2.8 Water vapor mixing ratio

The vertical distribution of water vapor mixing ratio obtained from WRF model along the east-west cross section of the centre at 0000 UTC of 15, 0900 UTC of 16, 1200 UTC of 15, 0300 UTC of 15, 0000 UTC of 16 and 2100 UTC of 15 May 2013 (i.e. its mature stage) for different cumulus (KF, BMJ, GF, G3, GD and OKF) schemes respectively for TC Viyaru from surface to 100 hPa level is shown in Figure 46 and its values are tabulated in Table 9. It shows that the highest moisture content more than around $2.2*10^{-2}$ kg/kg or more is found at the centre of the system at 900 hPa level and it decreases upwards to 400 hPa levels or more. For the development of the system this upward level goes up to 300 hPa level (i.e. its mature stage). Performance of all cumulus schemes for the simulation of vertical distribution of water vapor mixing ratio are comparable.

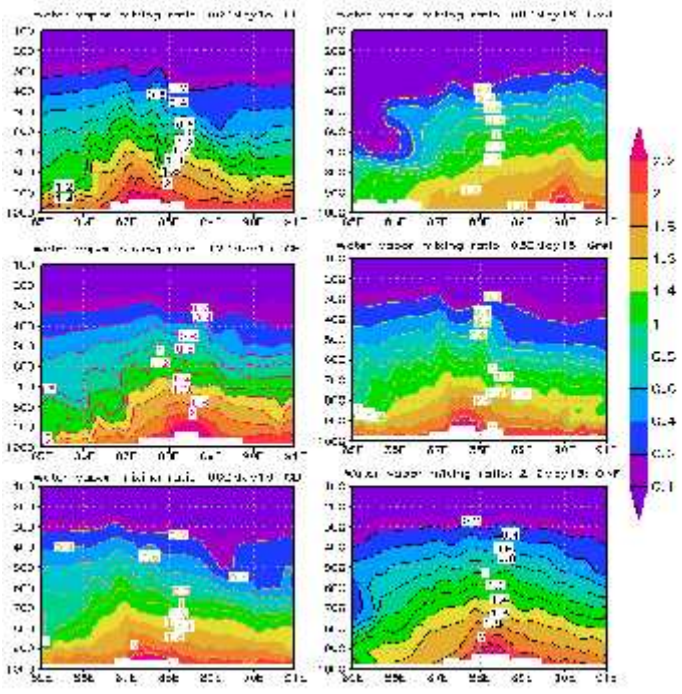

Figure 46: WRF model simulated vertical distribution of water vapor mixing ratio along the east-west cross section of the centre of TC Viyaru at different cumulus schemes.

The horizontal distribution of water vapor mixing ratio for TC Viyaru at 950 hPa level at 0000 UTC of 15, 0900 UTC of 16, 1200 UTC of 15, 0300 UTC of 15, 0000 UTC of 16 and

2100 UTC of 15 May 2013 (i.e. its mature stage) for different cumulus (KF, BMJ, GF, G3, GD and OKF) schemes respectively are obtained from WRF model is shown in the Figure 47. The maxing ratio shows a highly asymmetric character in the horizontal distribution. In Figure 47, maximum water vapor mixing ratio of 2.2 g/kg is obtained. It is noted that the highest mixing ratio is obtained at 950 hPa level close to Bangladesh.

It is noted that the high moisture flux comes from the southern side covering a large area of the Bay of Bengal which feeds the system along its southeastern side through the boundary layer. The value of high moisture flux increases slightly with development of the system.

Maximum value of water vapor mixing ratio is 2.2 gm/Kg and it is situated mainly at and around the centre of the cyclone. These maximum values cover large area of sea and small area of Bangladesh with lower value for all cumulus schemes. The south and western parts of Bangladesh cover with more value of water vapor mixing ratio (but less than 2.2 gm/Kg) finally, it may be concluded that all the schemes satisfy the intensification of the cyclone.

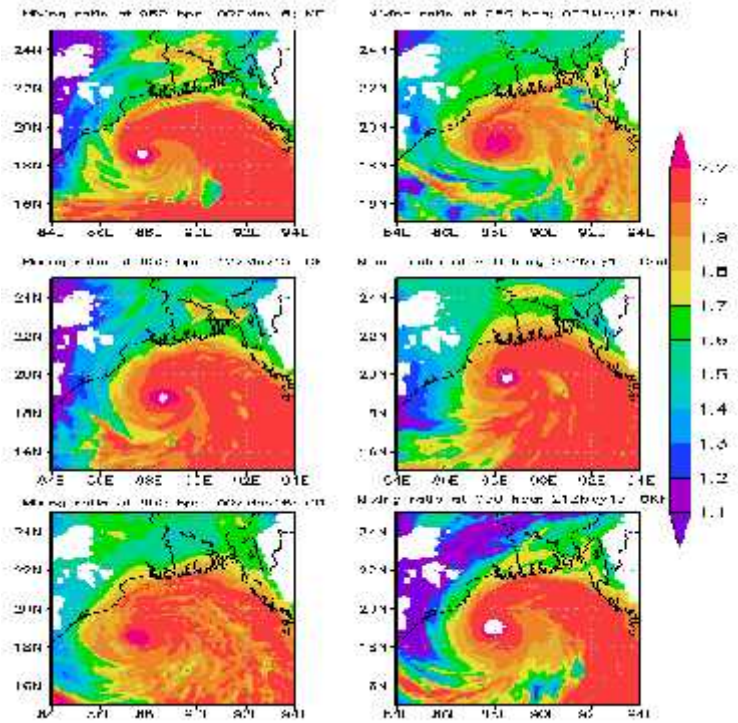

Figure 47: WRF model simulated horizontal distribution of water vapor mixing ratio at 950 hPa of TC Viyaru at different cumulus.

4.3 Tropical Cyclone Nilam

The model simulated MSLP, maximum wind at 10 m level, Vorticity, Temperature anomaly, Relative humidity, Relative humidity at 2m and Water vapor mixing ratio with six CP schemes along with synoptic situation have been discussed for the TC Nilam in the following sub-sections:

4.3.1 Description of Tropical Cyclone Nilam

To analyze the low intensity of TC Nilam, the WRF model has been run for 96 hrs with the initial field at 0000 UTC of 28 October 2012 using different cumulus. The cyclone Nilam originated over the BOB in the period from October 27, 2012 to November 01, 2012. The IMD has designated it as BOB 02 and JTWC as 02B. It was first identified as a low pressure on October 27, 2012, in south central BOB. Then, it developed into depression on October 28, 2012, at 1130 IST near 9.5°N and 86°E (550 km to the northeast of Trincomalee, Sri Lanka). It moved near 9°N and 83°E and developed into deep depression on October 29, 2012. Then, it became cyclonic storm on October 30, 2012 and lay at 110 km to the northeast of Trincomalee. Initially, the system moved westward and remained stationary near Sri Lanka coast. Then, under the influence of a low- to mid-level subtropical ridge, the system continued to move in the north-northwestward direction toward Mahabalipuram. The system made landfall on the Indian coast near Mahabalipuram on 31 October between 1600 IST and 1700 IST. During landfall, the system was very fast with maximum wind speed of 70–80 knots. Thereupon, it continued to move in the west-northwest direction up to south interior Karnataka and got weakened into a depression over land surface on November 01, 2012. Maximum rainfall occurred over southwest sector of the system center, and heavy to very heavy rainfall extended up to 300 km (IMD report, Oct. 2012). Using WRF models the different meteorological parameters are simulated and discussed for the intensity of the TC Nilam in the following sub-sections. The WRF model simulated data are compared with those obtained from Joint Typhoon Warning Centre (JTWC).

4.3.2 Minimum sea level pressure (MSLP)

The storm intensity forecasts for the TC Nilam in terms of MSLP using six different cumulus schemes KF, BMJ, GF, G3, GD and OKF for 96 hours (every 3 hourly) are presented in Figure 48. The WRF model simulated and observed MSLP gradually drops with time and attains peak intensity just before the landfall and thereafter MSLP increases. The model simulated MSLP values of 978, 997, 965, 965, 986 and 983 hPa are obtained using KF, BMJ, GF, G3, GD and OKF schemes respectively and these simulated MSLP values are obtained at 1200 UTC of 30, 1500 UTC of 30, 18 UTC of 31, 1800 UTC of 31,

2100 UTC of 31 and 1500 UTC of 31 October 2012 respectively. The observed MSLP of 987 hPa is obtained at 0300 UTC of 31 October 2012 according to IMD. So, simulated MSLP values are obtained later/earlier than that of observed. The observed MSLP is much higher than the simulated MSLP for all cumulus schemes with little exception. The pressure departure is found minimum for Grell- Fritsch and Grell-3 schemes and maximum for Betts-Miller-Janjic schemes compared with IMD observed. The simulated pressure fall for all cumulus schemes indicate that the system has attained the intensity of cyclonic storm and the observation also indicates that the system attained the intensity of cyclonic storm (987 hPa). Cumulus schemes BMJ, G3 and OKF match better than the others cumulus schemes with the observed intensity. But Cumulus schemes G3 and OKF simulate minimum MSLP (mature stage) later than that of observed and Cumulus BMJ simulates much earlier than the observed. Cumulus BMJ simulates more intensity than the observed. Intensity simulated by Cumulus schemes KF, G3 and GD has absolutely not matched with the observed value.

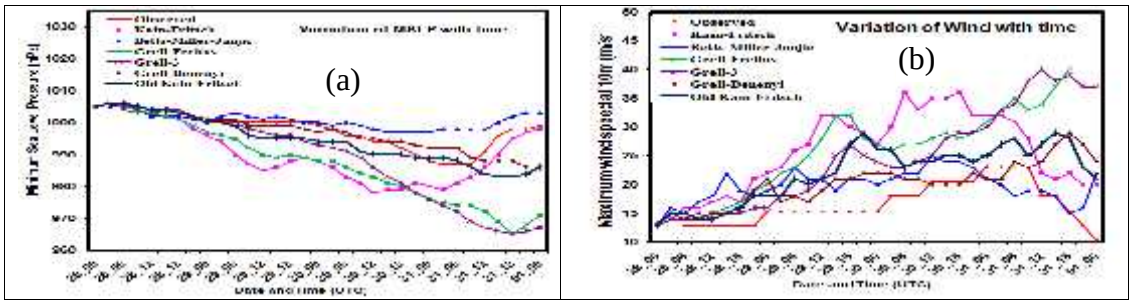

Figure 48: Evolution of WRF model simulated (a) MSLP and (b) MWS at 10m level using six different cumulus schemes and that of observed of the TC Nilam.

Figure 49 shows the mature stage of spatial distribution of sea level pressure using six different cumulus schemes and it is obtained with different time and position with different intensity. The spatial distribution of sea level pressure at its mature stage for the TC Nilam using different cumulus schemes KF, BMJ, GF, G3, GD and OKF in WRF model is obtained at 1200 UTC of 30, 1500 UTC of 30, 18 UTC of 31, 1800 UTC of 31, 2100 UTC of 31 and 1500 UTC of 31 October 2012 respectively.

The lowest simulated MSLP (i.e. mature stage) for the TC Nilam using different cumulus schemes KF, BMJ, GF, G3, GD and OKF in WRF models are 978, 997, 965, 965, 986 and 983 hPa respectively. The observation also indicates that the system attained the intensity of cyclonic storm (987 hPa). It is seen that BMJ cumulus scheme has very high intensity. The GD cumulus scheme has almost the same intensity of the observation and then the OKF

cumulus scheme has also nearly the same intensity of the observation. The KF, GF and G3 cumulus schemes have very lower intensity than the observation.

In Figure 49, it is observed that the spatial distribution of sea level pressure at mature stage using different cumulus is obtained with different times and different positions. Positions of mature stages using KF, BMJ, GF, G3, GD and OKF schemes are located at 82.45^{o}E and 9.72^{o}N at 1200 UTC of 30, 82.45^{o}E and 9.9^{o}N 72^{o}N at 1500 UTC of 26 October, 81.19^{o}E and 13.3^{o}N 72^{o}N at 1800 UTC of 31, 81.49^{o}E and 12.89^{o}N 72^{o}N at 1800 UTC of 31, 81.35^{o}E and 14^{o}N 72^{o}N at 2100 UTC of 31 and 80.93^{o}E and 12.45^{o}N 72^{o}N at 1500 UTC of 31 October 2012 respectively. Intensity, position and time of mature stages are different for different cumulus schemes used in WRF model. The isobar has circular arrangement around the TC centre with some asymmetric features in the outer periphery. The contour interval is different for different positions because of different intensity of the system. From the Figure 49, the radius of the TC eye is found to be around 90 km for all cumulus according to all simulation.

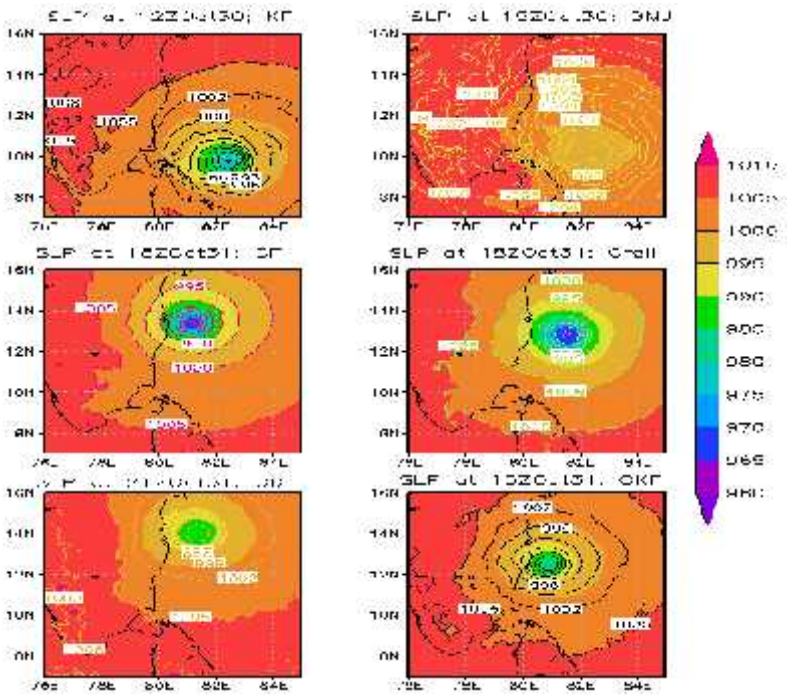

Figure 49: WRF model simulated SLP of TC Nilam at different cumulus schemes.

The distribution of the sea level pressure for the TC Nilam along east-west cross section and north-south cross section passing through its centre using different cumulus is shown in Figure 50. The positions of the centre at mature stage using different cumulus schemes KF, BMJ, GF, G3, GD and OKF are located at 82.45^{o}E and 9.72^{o}N, 82.45^{o}E and 9.9^{o}N, 81.19^{o}E and 13.3^{o}N, 81.49^{o}E and 12.89^{o}N, 81.35^{o}E and 14^{o}N and 80.93^{o}E and 12.45^{o}N respectively.

The model simulated MSLP values of 978, 997, 965, 965, 986 and 983 hPa are obtained at 1200 UTC of 30, 1500 UTC of 30, 1800 UTC of 31, 1800 UTC of 31, 2100 UTC of 31 and 1500 UTC of 31 October 2012 respectively and are shown in Figure 50. In Figure 50, the black, green, yellow, orange, magenta and the dark purple color represent KF, BMJ, GF, G3, GD and OKF schemes respectively. The figures demonstrate the moderate pressure gradient around the centre with maximum gradient at around 100 km below or above for all cumulus schemes from the centre. Variation of east-west and north-south elongated SLP at the center are clearly observed.

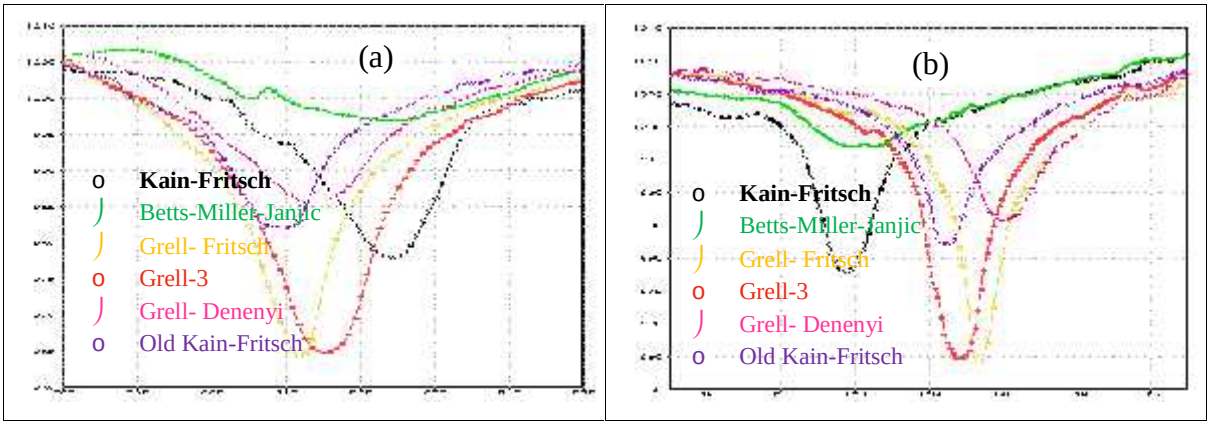

Figure 50: WRF model simulated (a) East West and (b) North South cross sectional view of SLP of TC Nilam at different cumulus schemes with fixed latitude and longitude respectively.

4.3.3 Maximum Wind speed

The storm intensity forecasts for the TC Nilam in terms of MWS using six different cumulus schemes KF, BMJ, GF, G3, GD and OKF for 96 hours (every 3 hourly) along with observed MWS are presented in Figure 48. The model simulated MWSs are obtained at the standard meteorological height of 10 m. The WRF model simulated MWSs are higher than the observed values through almost full forecast hours with a few exceptions. Model simulated highest values of MWS using six different cumulus schemes are obtained at same the time and earlier. But for ~~are~~ convenience, time of maximum intensity (mature stage) ~~are~~ is considered as the time of obtained MSLP (times are written in previous section).

The observed and simulated MWS by WRF decrease with time gradually after obtaining highest value of MWS. The highest value of MWS for the TC Nilam using different cumulus schemes KF, BMJ, GF, G3, GD and OKF in WRF models are 36, 25, 40, 40, 29 and 29 m/s respectively. Whereas the observed MWS is 23.15 m/s. the simulated and

observation value indicate that the system attained the intensity of cyclonic storm (17.5 - 24.44 m/s). WRF model using different cumulus schemes simulate higher value of MWS than that of observed value. It is seen GF and G3 cumulus schemes have very high intensity than the KF, GD and OKF cumulus schemes have also high intensity. The BMJ cumulus scheme has slightly more intensity than the observation.

Figure 51 shows the spatial distribution of the surface (10 m) wind speed at the mature stage of the TC using six different cumulus schemes and it is obtained with different times and positions with different intensities. The spatial distribution of wind speed at its mature stage for the TC Nilam using different cumulus schemes KF, BMJ, GF, G3, GD and OKF in WRF model is obtained at 1200 UTC of 30, 1500 UTC of 30, 1800 UTC of 31, 1800 UTC of 31, 2100 UTC of 31 and 1500 UTC of 31 October 2012 respectively and shown in Figure 51. The Figure 51 obtained from WRF model shows that the wind field of the TC is highly asymmetric in the horizontal distribution. At 0000 UTC of 28 October 2012 (i.e. at the initial time of simulation) the TC is in the sea with different cumulus schemes (not shown in figure). Gradually, TC is organized with strong wind bands around and the wind flow in the core region shows asymmetric feature with minimum wind speed at the centre. The spatial distribution of surface (10 m) wind speed is found maximum for GF and G3 schemes and minimum for BMJ cumulus scheme. The figure shows that the pattern has an asymmetric wind distribution with strong wind bands in the front right side, rear left and rear right sides close to the centre of north directed moving storm. In Figure 51, it is observed that the spatial distribution of wind speed at the mature stage of the TC using different cumulus schemes is obtained with different times and different positions. Positions of mature stages using KF, BMJ, GF, G3, GD and OKF schemes are located at 82.45^{o}E and 9.72^{o}N at 1200 UTC of 30, 82.45^{o}E and 9.9^{o}N at 1500 UTC of 26, 81.19^{o}E and 13.3^{o}N at 1800 UTC of 31, 81.49^{o}E and 12.89^{o}N at 1800 UTC of 31, 81.35^{o}E and 14^{o}N at 2100 UTC of 31 and 80.93^{o}E and 12.45^{o}N at 1500 UTC of 31 October respectively. At this mature stage, the wind flow in the core region shows a near circular feature with minimum wind speed at the centre.

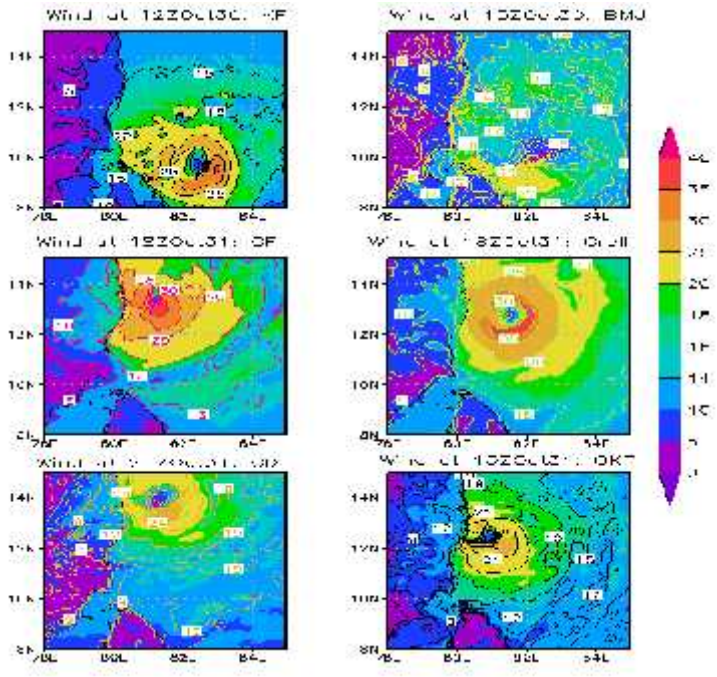

Figure 51: WRF model simulated MWS of TC Nilam at different cumulus schemes.

The distribution of the surface wind of the TC Nilam along east-west cross section and north-south cross section passing through its centre at mature stage using different cumulus schemes is shown in Figures 52 and 53 respectively. The positions of the centre at mature stage using different cumulus schemes KF, BMJ, GF, G3, GD and OKF are located at 82.45^{o}E and 9.72^{o}N, 82.45^{o}E and 9.9^{o}N, 81.19^{o}E and 13.3^{o}N, 81.49^{o}E and 12.89^{o}N, 81.35^{o}E and 14^{o}N and 80.93^{o}E and 12.45^{o}N respectively. The model simulated wind speeds of 36, 25, 40, 40, 29 and 29 m/s are obtained at 0600 UTC of 30, 1200 UTC of 30, 1800 UTC of 31, 1200 UTC of 31, 1800 UTC of 31 and 1500 UTC of 31 October 2008 respectively. But the model simulated wind of 35, 24, 40, 39, 27 and 29 m/s are obtained at 1200 UTC of 30, 1500 UTC of 30, 1800 UTC of 31, 1800 UTC of 31, 2100 UTC of 31 and 1500 UTC of 31 October 2012 respectively at mature stage (that is at the minimum SLP position). The figures demonstrate that a calm region is found inside the eye of the system and maximum wind was found in the eye wall. The simulated value of wind at centre using different schemes has a wide variation with time and place. In Figure 52, the value is less than 4 m/s and in Figure 53 the value is less than 7 m/s. In Figure 52, the KF, GF, G3 and OKF cumulus schemes show better result than the other cumulus schemes. And in Figure 53, the KF, GF and OKF cumulus schemes show better result than the other cumulus schemes. In both figures, the performance of BMJ cumulus scheme is the worst. The radius of maximum

wind of the TC Nilam is found to be just lower than 60 km according to the simulation. Variation of east-west and north-south elongated wind at the center is clearly observed.

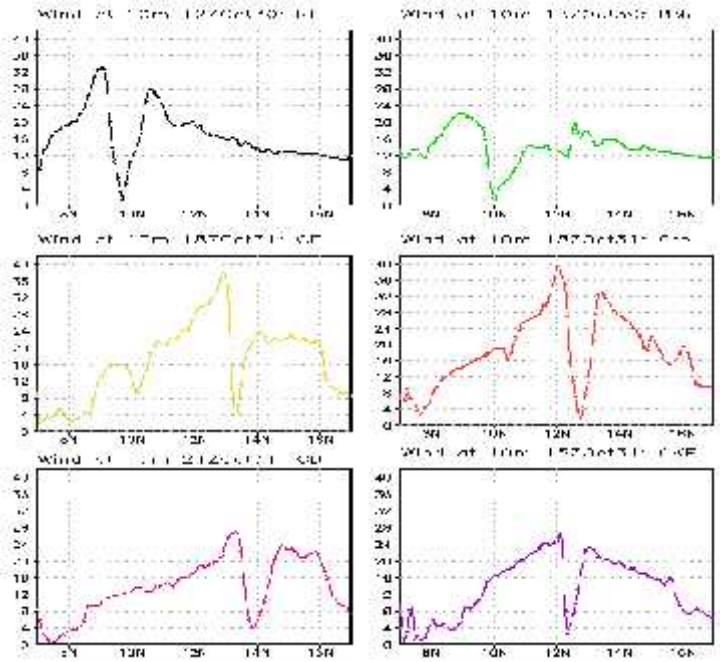

Figure 52: East West cross sectional view of WRF model simulated wind speed (m/s) of TC Nilam at different cumulus schemes with fixed longitude.

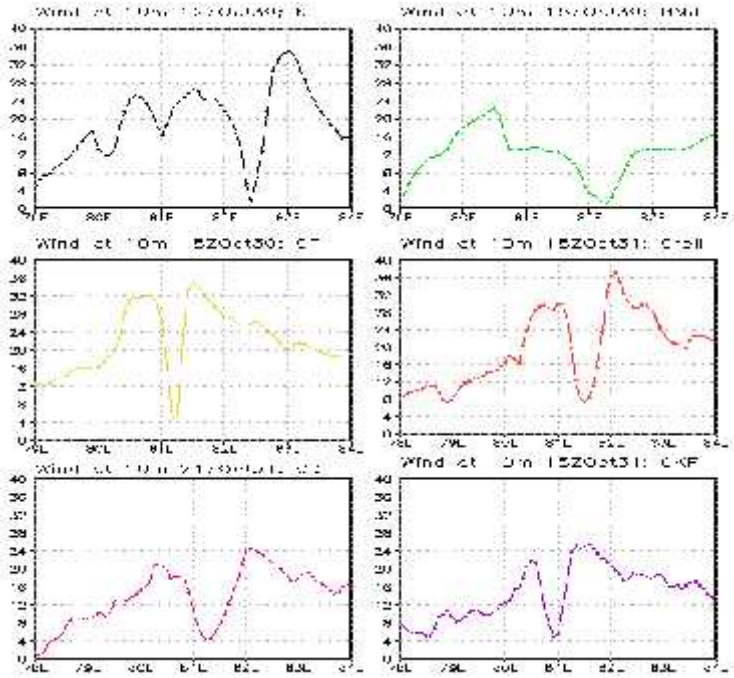

Figure 53: North-south cross sectional view of WRF model simulated Wind speed (m/s) of TC Nilam at different cumulus schemes with fixed latitude.

The horizontal distribution of vector wind field at its mature stage for the levels 850, 500, 300 and 200 hPa of the TC Nilam using different cumulus is tabulated in Table 10 and figure of this only for the levels 850 and 200 hPa are shown in Figures 54 and 55 respectively.

From the Figure 54, a well organized TC circulation with strong winds encircling the centre is found at the 850 hPa levels. It is noted that the strong wind is confined to the right of the direction of the movement of the system. From the Figure 55, at 200 hPa level strong outflow is evident from the central part of the TC. So, using simulated results obtained from WRF models, Figure 54 and Figure 55 demonstrate inflow in the lower level and outflow in the upper level respectively.

WRF model simulated maximum winds at the mature stage (1200 UTC of 30, 1500 UTC of 30, 1800 UTC of 31, 1800 UTC of 31, 2100 UTC of 31 and 1500 UTC of 31 October 2012) are about 60, 40, 60, 70, 40, 40 m/s and 30, 30, 30, 40, 20, 30 m/s for different cumulus (KF, BMJ, GF, G3, GD and OKF) schemes at 850 and 200 hPa levels respectively. The wind speed at 850 hPa level is found minimum for BMJ, GD and OKF schemes and maximum for G3 scheme. And the wind speed at 200 hPa levels is found minimum for GD scheme and maximum for G3 schemes. The mature stages are obtained at different time and position. The values of wind speed for mature stage at the levels 500 and 300 hPa are obtained different with different cumulus schemes.

Table 10: WRF model simulated maximum wind speed (m/s) at different cumulus schemes of 850, 500, 300 and 200 hPa pressure levels of TC Nilam.

Pressure level (hPa)	Maximum Wind Speed (m/s) at different time					
	12 UTC of 30 October at KF	15 UTC on 30 October at BMJ	18 UTC on 31 October at GF	18 UTC on 31 October at Greel	21 UTC on 31 October at GD	15 UTC on 31 October at OKF
850	60	40	60	70	40	40
500	40	30	40	40	30	30
300	40	30	40	40	20	30
200	30	30	30	40	20	30

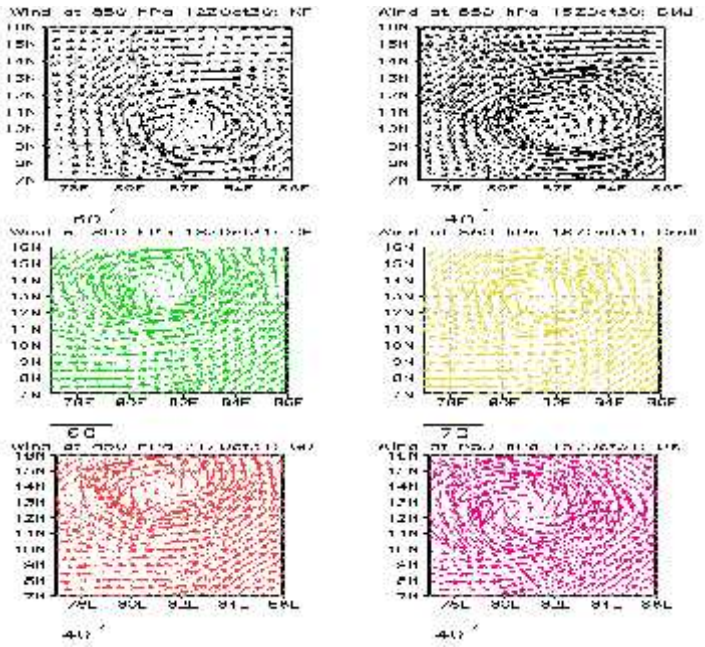

Figure 54: WRF model simulated Wind vector and magnitude at 850 hPa levels at different cumulus schemes.

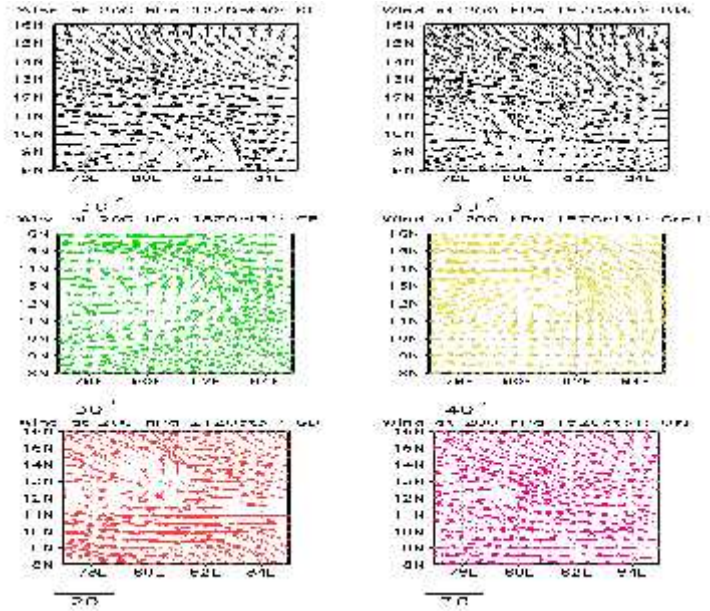

Figure 55: WRF model simulated Wind vector and magnitude at 200 hPa levels at different cumulus schemes.

The vertical profile of Radial, Tangential, Vertical and Horizontal wind field at its mature stage for the TC Nilam using different cumulus schemes KF, BMJ, GF, G3, GD and OKF in WRF model are obtained at 1200 UTC of 30, 1500 UTC of 30, 1800 UTC of 31, 1800 UTC of 31, 2100 UTC of 31 and 1500 UTC of 31 October 2012 respectively and shown in

Figures 56, 57, 58 and 59 respectively. Model simulated results are also tabulated in Table 11, for different cumulus mentioned in the Table. From the table it is clear that the value of the vertical profile of radial, tangential, vertical and horizontal wind of TC Nilam obtained using different cumulus (KF, BMJ, GF, G3, GD and OKF) schemes are different for different cumulus schemes. The strong wind with different speeds (Table 11) is confined to the different levels in lower troposphere and extended up to 100 hPa level in the left side of the system.

From the Figure 56, it is found that vertical profile of radial wind is much more organized and it is also clearly seen that the system has strong inflow in the lower levels which bring the air to the system through the boundary level and lower level and outflow in the upper level. The radial wind is found minimum for OKF scheme and maximum for KF, BMJ and GF schemes.

The vertical profile of tangential wind flows in a northerly direction at the eastern side of the system and in a southerly direction at the western side. For this reason, tangential wind shows positive value at the right side (east side) of the centre and negative value at the left side (west side) of the centre. The tangential wind is found minimum for BMJ scheme and maximum for G3 schemes.

The values of the vertical profile of vertical wind are different in magnitude for different cumulus and 2.5, 0.8, 4.0, 0.8, 1.5 and 3.5 m/s are simulated by KF, BMJ, GF, G3, GD and OKF cumulus schemes respectively. It indicates that the vertical wind is found minimum for BMJ and G3 scheme and maximum for GF schemes. These values are along the eye wall and other parts of the system which feed moisture into the system. It is noted that Nilam has very weak updraft motion at the eye wall throughout mid and upper troposphere. The downward motion is visible in the central parts of the TC and other areas in between rain bands.

The vertical profile of horizontal wind of the system at its mature stage shows the distribution of strong winds up to 100 hPa for BMJ, GF and G3 cumulus scheme, up to 150 hPa for GD cumulus scheme and up to 200 hPa for KF and OKF cumulus scheme around the centre of TC. It further confirms that the maximum winds are confined to the right of the direction of the movement of the system. This value decreases with the radial distance from both side of the eye. Calm wind zone is sharp and narrow and little bit tilted to the westward and get expanded towards upper levels. This is in agreement with the previous studies of

Rao and Prasad (2006) and Goswami *et al.* (2006) on Orissa TC. Cyclonic circulation is generally seen up to about 300 hPa level and anticyclone circulation with divergence fields aloft. In case of TC Nilam cyclonic circulation is also seen up to about 400 hPa level for cumulus KF, BMJ and GD schemes, 300 hPa levels for cumulus GF and G3 and OKF schemes and anticyclonic circulation with divergence fields aloft. And the horizontal wind is found minimum for BMJ scheme and maximum for G3 schemes.

Table 11: WRF model simulated maximum radial wind, tangential wind, vertical velocity and horizontal wind (m/s) of TC Nilam at different cumulus schemes.

Component of wind	Simulated maximum wind speed (m/s) at different time					
	12 UTC of 30 October at KF	15 UTC of 30 October at BMJ	18 UTC of 31 October at GF	18 UTC of 31 October at G3	21 UTC of 31October at GD	15 UTC of 31 October at OKF
Radial wind	25	25	25	20	20	15
Tangential wind	40	10	40	50	30	30
Vertical velocity	2.5	0.8	4.0	0.8	1.5	3.5
Horizontal wind	50	30	50	60	40	40

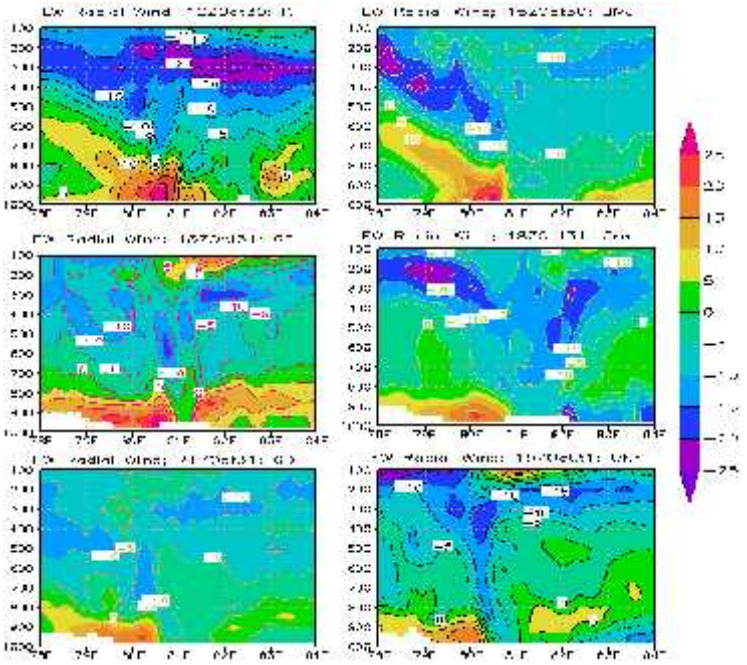

Figure 56: WRF model simulated Radial wind (cm/s) of TC Nilam at different cumulus schemes.

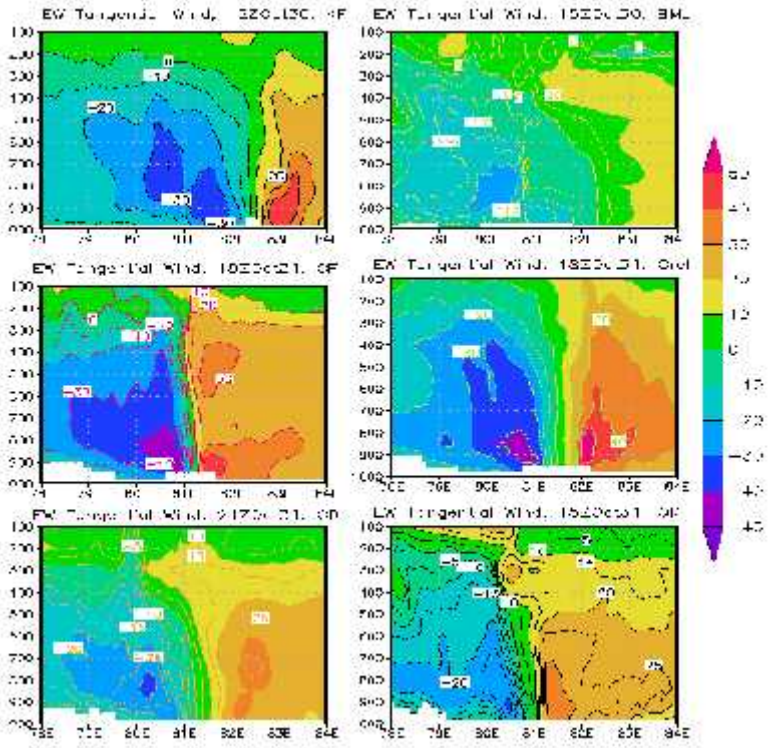

Figure 57: WRF model simulated Tangential wind (cm/s) of TC Nilam at different cumulus schemes.

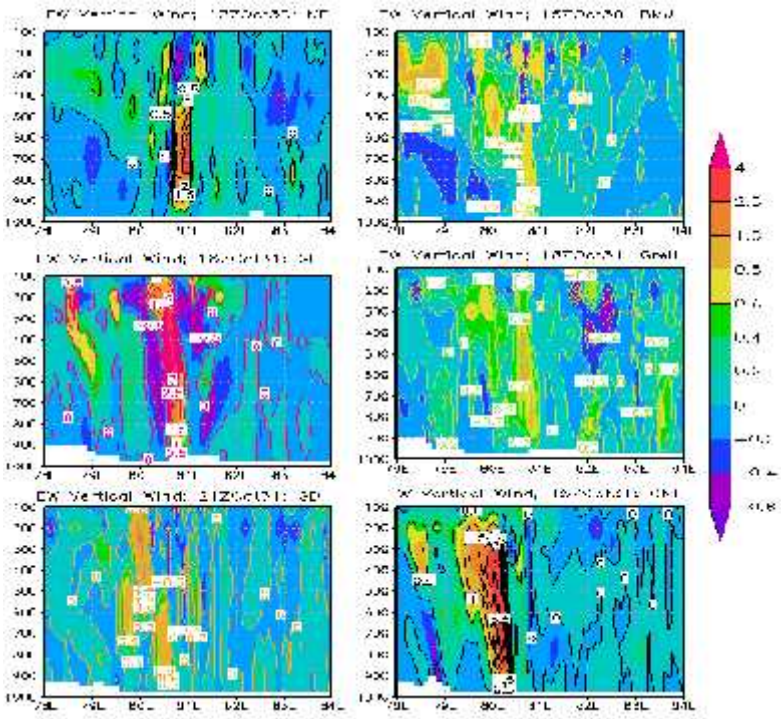

Figure 58: WRF model simulated Vertical wind (cm/s) of TC Nilam at different cumulus schemes.

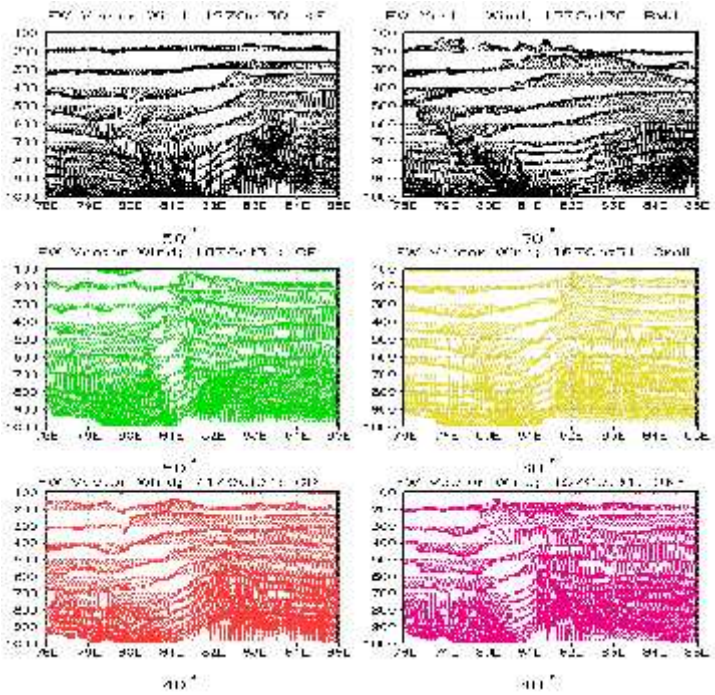

Figure 59: WRF model simulated Horizontal wind (cm/s) of TC Nilam at different cumulus schemes.

4.3.4 Vorticity

To know the evolution WRF model simulated relative vorticity at 1000, 950, 850, 500 and 300 hPa at six cumulus KF, BMJ, GF, G3, GD and OKF scheme for 96 hours (every 3 hourly) are presented in Figure 60. The values of relative vorticity are increased with the increase of time (i.e. in the development of the TC) at all levels for all cumulus schemes and increased to a maximum value. Thereafter the value shows a fall. From the figure it is observed that at 1000 hPa level the vorticity is found maximum for cumulus BMJ scheme. And at 950, 850, 500 and 300 hPa levels the vorticity is found maximum for cumulus GF scheme. The vorticity is found more than zero for all levels using all schemes. So, from the simulated value of vorticity it is seen that system intensification is satisfied more or less by all cumulus schemes.

Simulated the horizontal distribution of the relative vorticity obtained for TC Nilam at 850 and 200 hPa levels are shown in the Figures 61 and 62 respectively. It is seen from the figures that the vorticity is distributed with maximum value at the centre and these values for the levels 850, 500, 300 and 200 hPa are tabulated in Tables 12 for different cumulus

(KF, BMJ, GF, G3, GD and OKF) scheme respectively. At 850 hPa, the distribution maintains circular pattern with some asymmetric features in the outer periphery. Negative vorticity field are situated far from the centre. This distance of the negative vorticity from the centre is increased due to development of TC (not shown). Low level relative vorticity fields confirm the strong cyclonic circulation at low levels with different time and distance in feeding the moisture into the system to sustain its intensity. The values of relative vorticity are increased with the development of TC. At 200 hPa level, the weak positive vorticity embedded with negative vorticity field is visible at 200 hPa level. Negative vorticity is found at the centre of the TC. It is clear from the figure that relative vorticity is more organized in the mature stage. The vorticity is found maximum or minimum for 850, 500, 300 and 200 levels are different for different cumulus schemes.

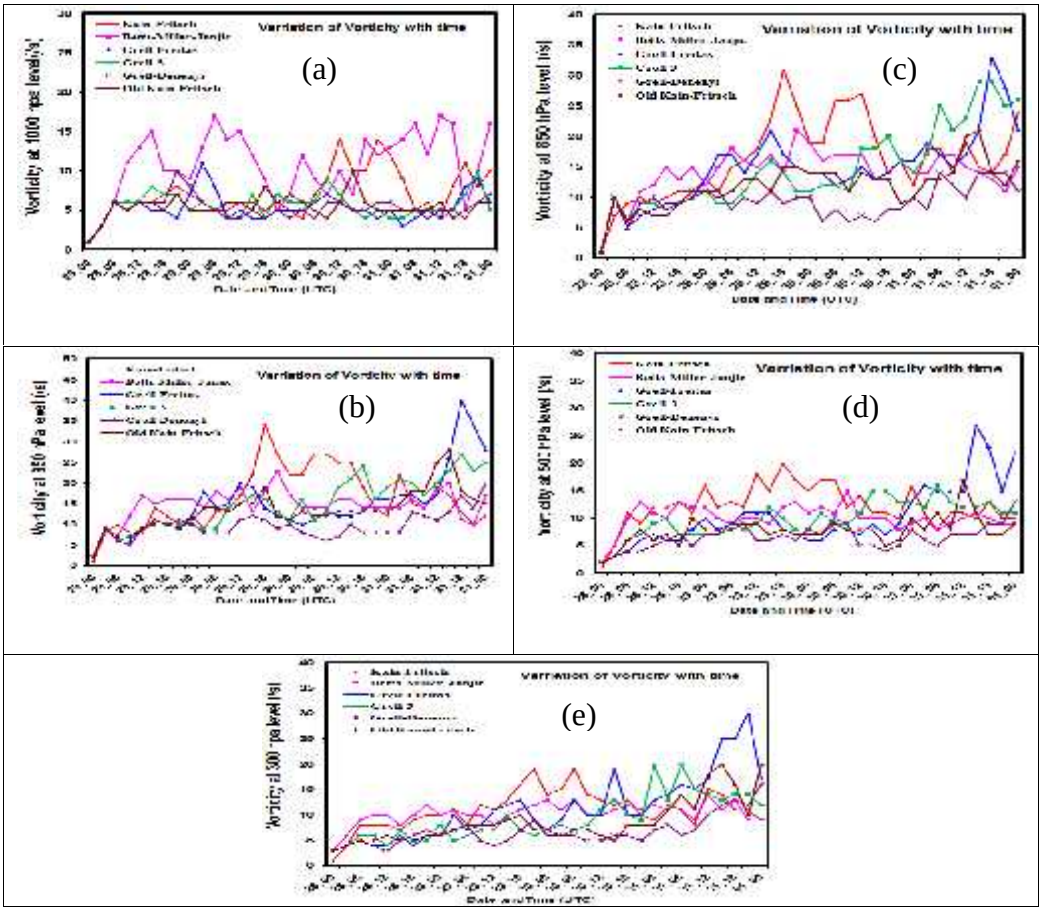

Figure 60: Evolution of model simulated vorticity with time at different cumulus scheme for 1000, 950, 850, 500 and 300 hPa level of TC Nilam.

Vertical distribution of the relative vorticity with fixed latitude (along east-west direction) and fixed longitude (along north-south direction) are obtained from WRF model is shown in Figure 63 and 64 respectively and the values are tabulated in Table 12. Simulated results at

1200 UTC of 30, 1500 UTC of 30, 1800 UTC of 31, 1800 UTC of 31, 2100 UTC of 31 and 1500 UTC of 31 October 2012 for different cumulus scheme KF, BMJ, GF, G3, GD and OKF schemes are located at 82.45^{o}E and 9.72^{o}N, 82.45^{o}E and 9.9^{o}N, 81.19^{o}E and 13.3^{o}N, 81.49^{o}E and 12.89^{o}N, 81.35^{o}E and 14^{o}N and 80.93^{o}E and 12.45^{o}N respectively.

In Figure 63 the system has the positive vorticity along the centre up to 150 hPa level with higher values for all cumulus. For KF, BMJ, GF, G3, GD and OKF schemes, the higher values are found up to 200, 200, 200, 200, 200 and 150 levels respectively. So the strong cumulus scheme is OKF scheme. In Figure 64, the system has the positive vorticity along the centre up to 100 hPa level with higher value for all cumulus schemes. For KF, BMJ, GF, G3, GD and OKF schemes, the higher values are found up to 200, 150, 150, 200, 300 and 150 levels respectively. So the strong cumulus schemes are BMJ, GF and OKF schemes.

Table 12: WRF Model simulated maximum vorticity ($x10^{-5}$ s^{-1}) at different pressure levels associated with TC Nilam at different cumulus schemes.

Pressure level (hPa)	Maximum Vorticity ($x10^{-5}$ s^{-1}) at different times					
	12 UTC of 30 October at KF	15 UTC of 30 October at BMJ	18 UTC of 31 October at GF	18 UTC of 31 October at Greel	21 UTC of 31 October at GD	15 UTC of 31 October at OKF
850	180	100	180	150	110	120
500	70	40	70	80	40	60
300	80	60	90	70	60	70
200	70	40	70	60	40	70
Position of TC centre	9.72^{o}N and 82.45^{o}E	9.9^{o}N and 82.45^{o}E	13.3^{o}N and 81.19^{o}E	12.89^{o}N and 81.49^{o}E	14^{o}N and 81.35^{o}E	12.45^{o}N and 80.93^{o}E
Vertical distribution with fixed latitude	22	20	22	22	20	22
Vertical distribution with fixed longitude	20	18	15	18	12	18

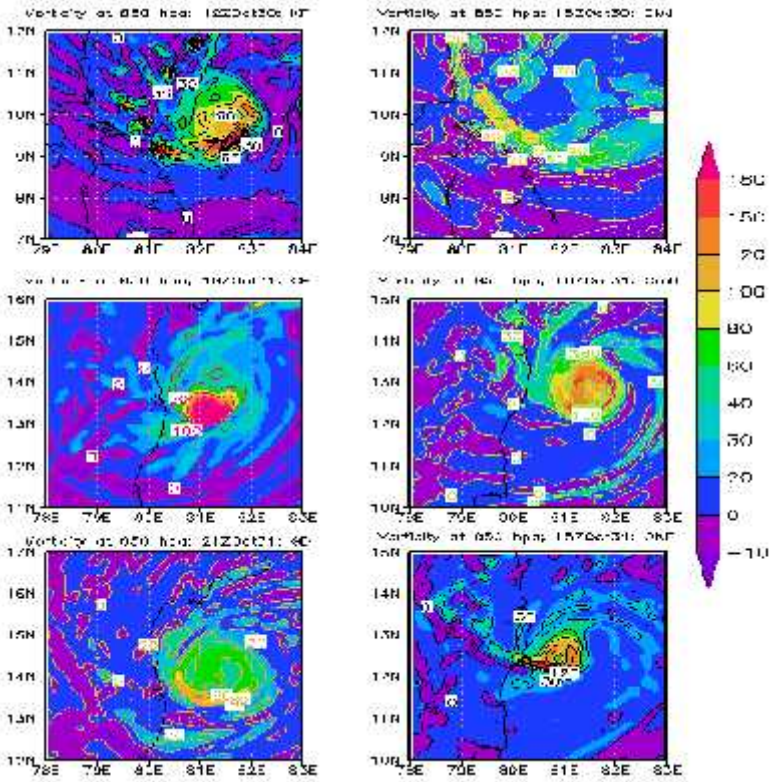

Figure 61: WRF Model simulated vorticity field of 850 hPa levels at different cumulus schemes.

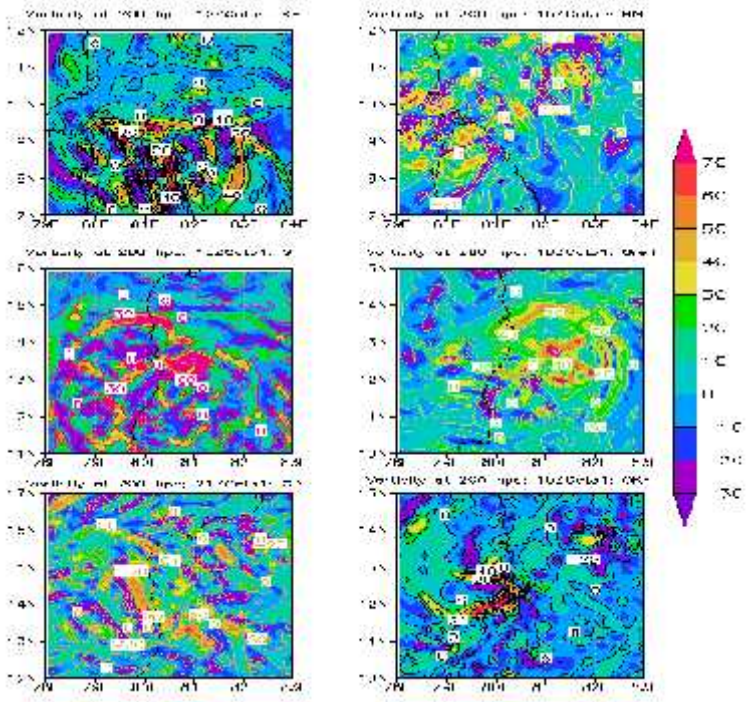

Figure 62: WRF Model simulated vorticity field of 200 hPa levels at different cumulus schemes.

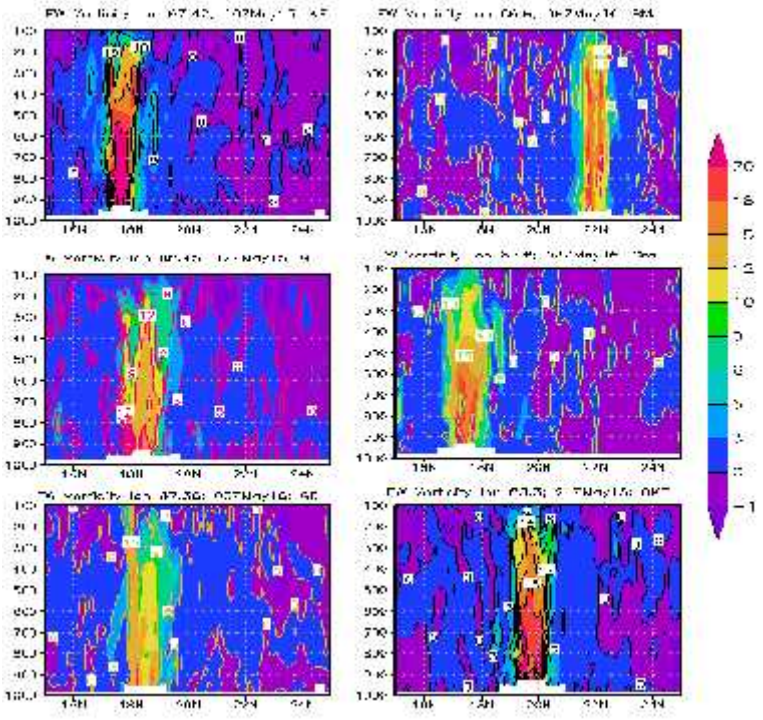

Figure 63: WRF model simulated east west vertical distribution of relative vorticity with fixed longitude of TC Nilam through the centre at different cumulus schemes.

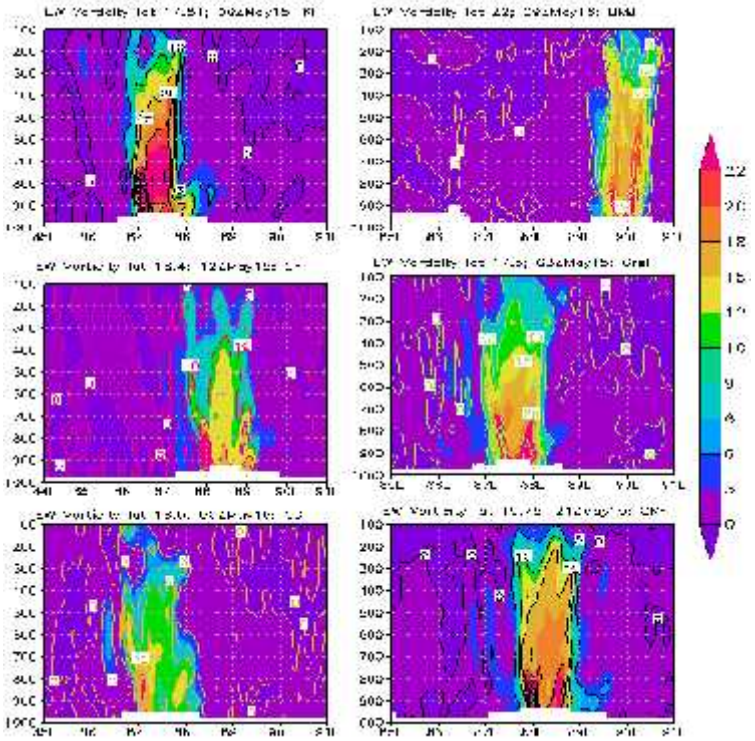

Figure 64: WRF model simulated north-south vertical distribution of relative vorticity with fixed latitude of TC Nilam through the centre at different cumulus schemes.

4.3.5 Temperature anomaly

The WRF model simulated temperature anomaly at 1200 UTC of 30, 1500 UTC of 30, 1800 UTC of 31, 1800 UTC of 31, 2100 UTC of 31 and 1500 UTC of 31 October 2012 (i.e. its mature stage) for different cumulus (KF, BMJ, GF, G3, GD and OKF) schemes is shown in Figure 65 and the values are tabulated in Table 13. It is noted that the warm core region is slightly expanded up to 200 hPa level all most for all cumulus schemes.

For KF cumulus scheme, at 1200 UTC of 30 October 2012, a warm core with 4^{o}C is observed in 950-700 hPa layer. It is noted that the warm core region is expanded outward at 980-400 hPa level. The greatest anomaly is observed around 750 and 950 hPa levels. The simulated temperature anomaly demonstrates that the warm core is visible mainly at lower troposphere.

For BMJ cumulus scheme at, 1500 UTC of 30 October 2012, a warm core with 3^{o}C is observed in 980-800 hPa layer. It is noted that the warm core region is expanded outward at 980-600 hPa level. The greatest anomaly is observed around 980 hPa level. The simulated temperature anomaly demonstrates that the warm core is visible mainly at lower troposphere.

For GF cumulus scheme at 1800 UTC of 31 October 2012, a warm core with 10^{o}C is observed in 700-550 hPa layer. It is noted that the warm core region is expanded outward at 900-200 hPa level. The greatest anomaly is observed around 600 hPa level. The simulated temperature anomaly demonstrates that the warm core is visible mainly above middle troposphere.

For G3 cumulus scheme at 1800 UTC of 31 October 2012, a warm core with 6^{o}C is observed in 400-300 hPa layer. It is noted that the warm core region is expanded outward at 710-300 hPa level. The greatest anomaly is observed around 500 hPa level. The simulated temperature anomaly demonstrates that the warm core is visible mainly at middle troposphere.

For GD cumulus scheme at 2100 UTC of 31 October 2012, a warm core with 6^{o}C is observed in 780-510 hPa layer. It is noted that the warm core region is expanded outward at 900-200 hPa level. The greatest anomaly is observed around 600 hPa level. The simulated temperature anomaly demonstrates that the warm core is visible mainly above middle troposphere.

For OKF cumulus scheme at 1500 UTC of 31 October 2012, a warm core with 6^{o}C is observed in 720-480 hPa layer. It is noted that the warm core region is expanded outward at

980-350 hPa level. The greatest anomaly is observed around 550 hPa level. The simulated temperature anomaly demonstrates that the warm core is visible mainly at above middle troposphere.

Finally, the greatest anomaly is occurred at cumulus GF scheme around 600 hPa levels. The simulated temperature anomaly demonstrates that the warm core is visible mainly at middle troposphere for all cumulus schemes with little exception. Negative temperature anomalies are also seen at the upper levels and lower levels.

Table 13: WRF Model simulated maximum temperature anomaly (ºC), Relative humitity (%) and Water vapor mixing (g/kg) ratio associated with TC Nilam at different cumulus schemes.

Parameter	12 UTC of 30 October at KF	15 UTC of 30 October at BMJ	18 UTC of 31October at GF	18 UTC of 31 October at Greel	21 UTC of 31 October at GD	15 UTC of 31 October at OKF
Maximum Temperature	4	3	10	6	6	6
Relative Humidity	100	95	100	100	100	100
Water vapor mixing ratio	2	1.8	2	2	2	2

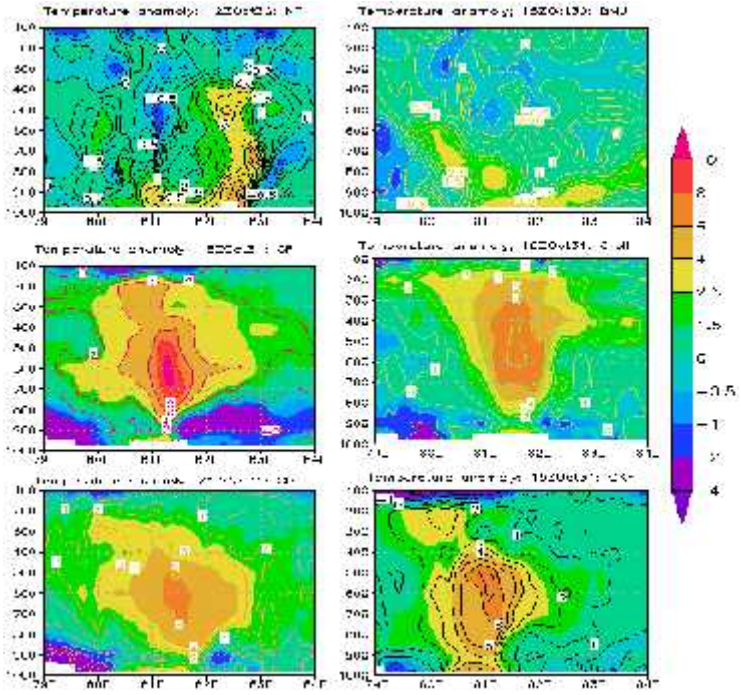

Figure 65: WRF model simulated vertical distribution of temperature anomaly in the east-west direction of TC Nilam at different cumulus schemes.

4.3.6 Relative humidity

The horizontal distribution of relative humidity for TC Nilam obtained from WRF model at 1200 UTC of 30, 1500 UTC of 30, 1800 UTC of 31, 1800 UTC of 31, 2100 UTC of 31 and 1500 UTC of 31 October 2012 (i.e. its mature stage) for different cumulus (KF, BMJ, GF, G3, GD and OKF) scheme is shown in Figure 66. Time variation of relative humidity at surface is obtained around 100% with few exceptions. But the relative humidity at 850 levels for all cumulus schemes is 100% for the cyclones (not shown in figure). These values satisfy the condition for the intensification of cyclone through convection.

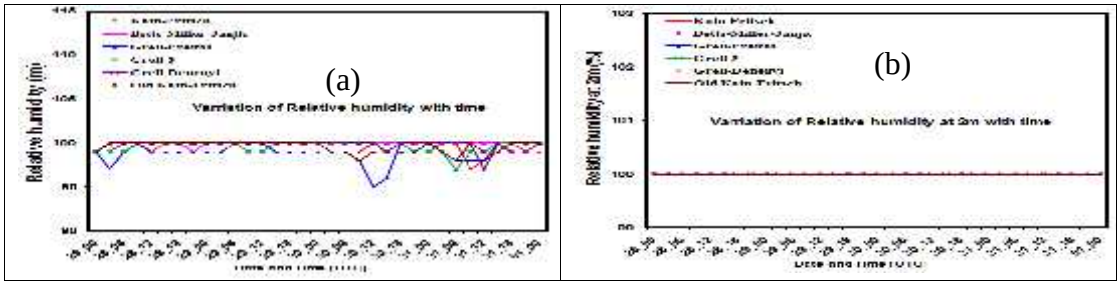

Figure 66: Evolution of model simulated (a) RH and (b) RH at 2m with time at different cumulus scheme of TC Nilam.

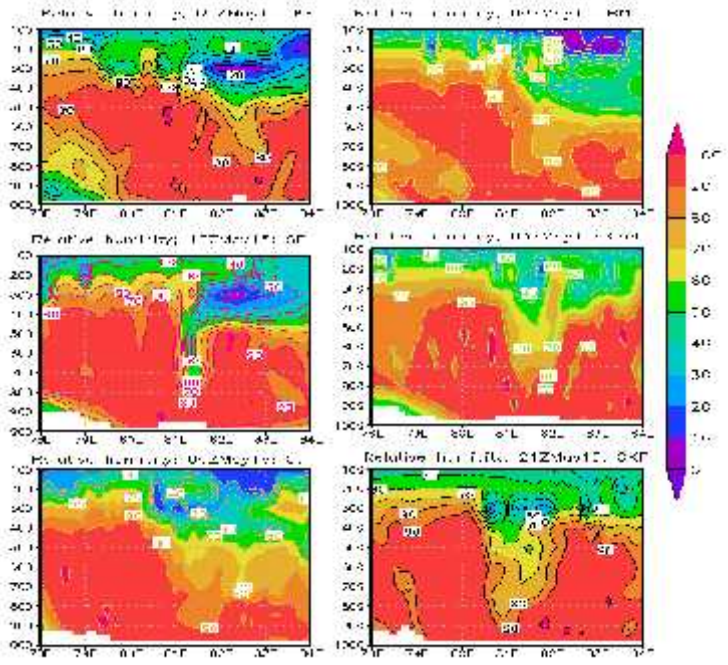

Figure 67: WRF model simulated vertical distribution of Relative humidity (%) in the east-west direction of TC Nilam at different cumulus schemes.

The vertical cross section of relative humidity for TC Nilam obtained from WRF model at 1200 UTC of 30, 1500 UTC of 30, 1800 UTC of 31, 1800 UTC of 31, 2100 UTC of 31 and

1500 UTC of 31 October 2012 (i.e. its mature stage) for different cumulus (KF, BMJ, GF, G3, GD and OKF) schemes from surface to 100 hPa levels is shown in Figure 67 and its values are tabulated in Table 13. It is noted that high relative humidity (more than 90%) spreads in outer range of eye wall up to 400, 380, 380, 400, 400 and 350 hPa levels for the cumulus (KF, BMJ, GF, G3, GD and OKF) schemes respectively. High relative humidity bands are also found in the rain band of the system situated at both sides of the system in the wider range throughout 980-400 hPa level. From the Table 13 and the Figure 67, it is observed that highest relative humidity 100% is observed using all cumulus schemes except BMJ cumulus schemes.

4.3.7 Relative humidity at 2m

The time evolution of relative humidity at 2m for TC Nilam obtained from WRF model at 1200 UTC of 30, 1500 UTC of 30, 1800 UTC of 31, 1800 UTC of 31, 2100 UTC of 31 and 1500 UTC of 31 October 2012 (i.e. its mature stage) for different cumulus (KF, BMJ, GF, G3, GD and OKF) schemes is shown in Figure 66. It is noted that high relative humidity at 2m (around 100%) spreads in outer range of eye wall up for all cumulus schemes without any exception. It is the good indication for the intensification of cyclone.

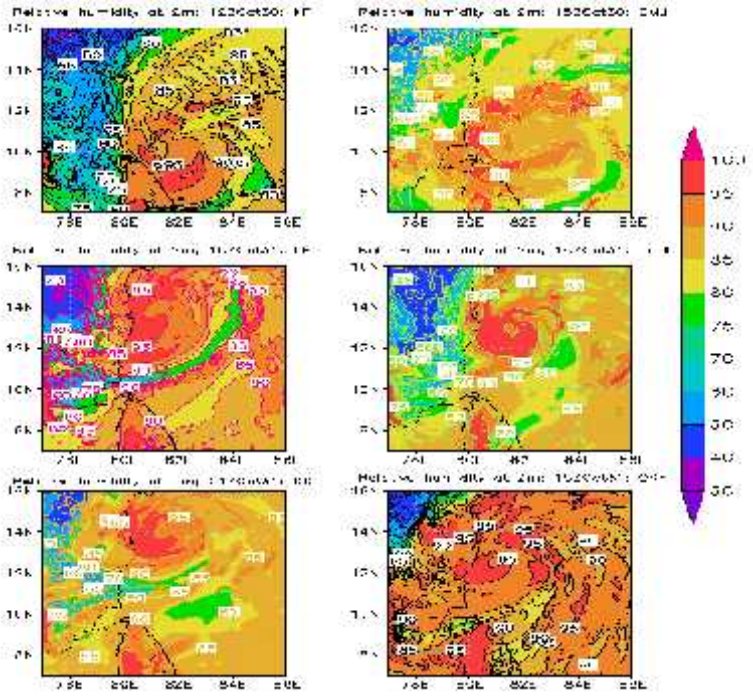

Figure 68: WRF model simulated spatial distribution of Relative humidity at 2m (%) in the east-west direction of TC Nilam at different cumulus schemes.

The spatial distribution of relative humidity at 2m for TC Nilam obtained from WRF at 1200 UTC of 30, 1500 UTC of 30, 1800 UTC of 31, 1800 UTC of 31, 2100 UTC of 31 and 1500 UTC of 31 October 2012 (i.e. its mature stage) for different cumulus (KF, BMJ, GF, G3, GD and OKF) schemes is shown in Figure 68. The values of the relative humidity at 2m for TC Nilam around the centre are about 100% or less for all cumulus schemes. This status of the relative humidity is satisfied the convection for the cyclone intensification.

4.4.8 Water vapor mixing ratio

The vertical distribution of water vapor mixing ratio obtained from WRF model along the east-west cross section of the centre at 1200 UTC of 30, 1500 UTC of 30, 1800 UTC of 31, 1800 UTC of 31, 2100 UTC of 31 and 1500 UTC of 31 October 2012 (i.e. its mature stage) for different cumulus (KF, BMJ, GF, G3, GD and OKF) schemes respectively for TC Nilam from surface to 100 hPa level is shown in Figure 69 and its values are tabulated in Table 13. It shows that the highest moisture content more than around 2 g/kg or more is found at the centre of the system at 950 hPa level and it decreases upwards to 400 hPa levels or more. For the development of the system this upward level goes up to 350 hPa level (i.e. its mature stage). Performance of all cumulus schemes for the simulation of vertical distribution of water vapor mixing ratio are comparable.

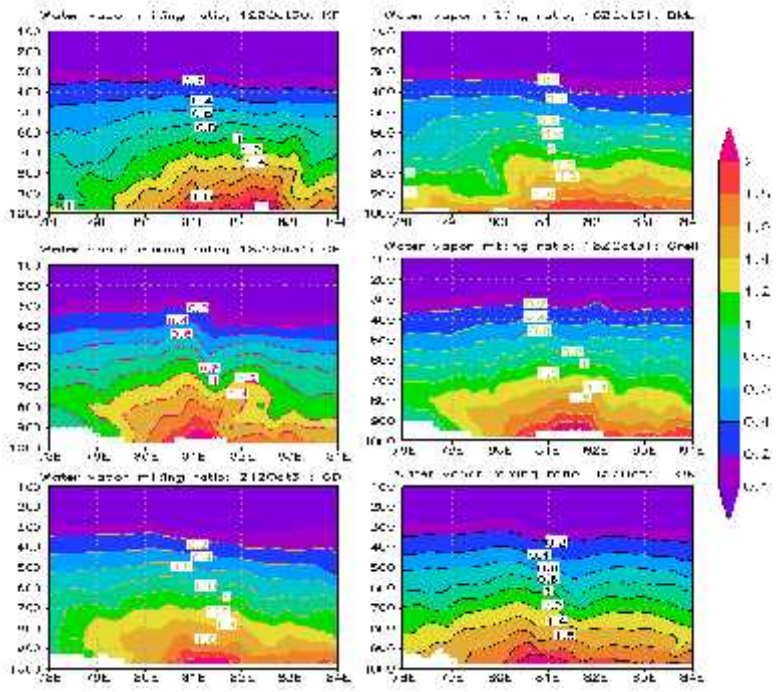

Figure 69: WRF model simulated vertical distribution of water vapor mixing ratio along the east-west cross section of the centre of TC Nilam at different cumulus schemes.

The horizontal distribution of water vapor mixing ratio for TC Nilam at 950 hPa level 1200 UTC of 30, 1500 UTC of 30, 1800 UTC of 31, 1800 UTC of 31, 2100 UTC of 31 and 1500 UTC of 31 October 2012 (i.e. its mature stage) for different cumulus (KF, BMJ, GF, G3, GD and OKF) schemes are obtained from WRF model and is shown in the Figure 70. The maxing ration shows a highly asymmetric character in the horizontal distribution. In Figure 70, maximum water vapor mixing 2 g/kg is obtained. It is noted that the highest mixing ratio are obtained at 950 hPa level close to the near of Bangladesh.

It is noted that the high moisture flux comes from the southern side covering a large area of the Bay of Bengal which feeds the system along its southeastern side through the boundary layer. The value of high moisture flux increases slightly with development of the system.

Maximum value of water vapor mixing ratio is 2.2 gm/Kg and it is situated mainly at and around the centre of the cyclone. These maximum values cover large area of sea and small area of Bangladesh for all cumulus schemes except BMJ scheme. The south and western parts of Bangladesh are covered with more values of water vapor mixing ratio (but less than 2.2 gm/Kg). Finally, it may be concluded that all the schemes satisfy the intensification of the cyclone.

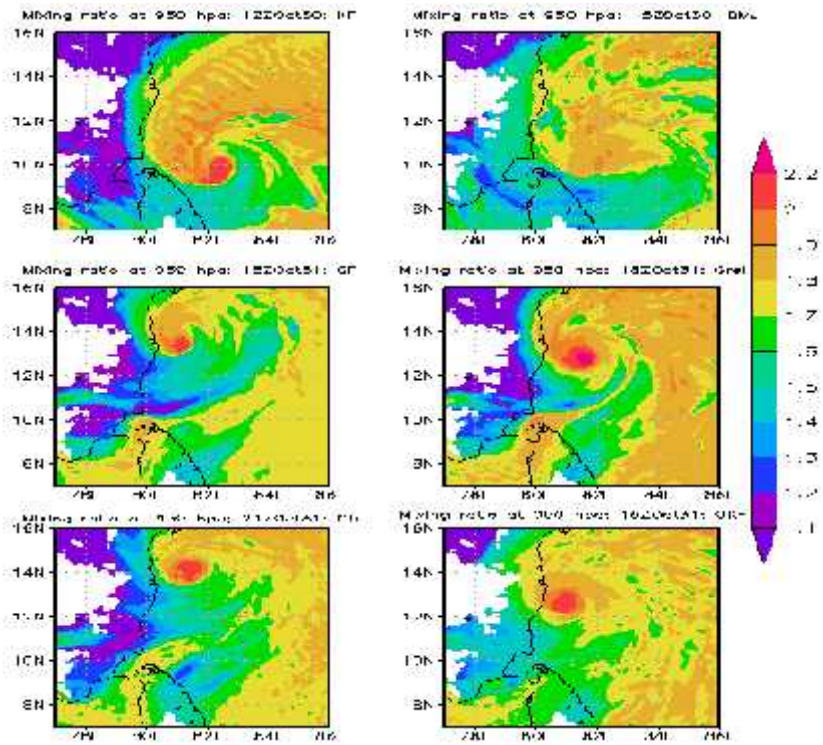

Figure 70: WRF model simulated horizontal distribution of water vapor mixing ratio at 950 hPa of TC Nilam at different cumulus schemes.

4.4 Tropical Cyclone Khaimuk

The model simulated MSLP, maximum wind at 10 m level, Vorticity, Temperature anomaly, Relative humidity, Relative humidity at 2m and Water vapor mixing ratio with six CP schemes along with synoptic situation have been discussed for the TC Khaimuk in the following sub-sections:

4.4.1 Discription of Tropical Cyclone khaimuk

Cyclone Khaimuk originated as a low pressure on 12 November 2008 in the southeast BOB, intensified into a strong cyclone on 14 November over the west-central BOB and crossed the coast of south Andhra Pradesh on 15 November 2008. On November 13, a low pressure area identified by the India Meteorological Department over southeast Bay of Bengal and adjoining areas concentrated into a depression east-southeast of Chennai, India. The IMD expected the system to intensify further and move towards north Tamil-Nadu/south Andhra Pradesh coasts. The Joint Typhoon Warning Center issued a tropical cyclone warning on the tropical cyclone early on November 14 naming it as Tropical Cyclone 05B. A few hours later the IMD upgraded the system to a deep depression issuing a Cyclone Watch for Andhra Pradesh as intensification into a cyclonic storm was possible. By mid morning the IMD advised the eastern coast of India that the system was expected to cross Andhra Pradesh by noon the next day (local time). Later that morning the deep depression intensified into a cyclonic storm and was named Khai Muk and the cyclone watch was raised to a warning for Andhra Pradesh coast with Khai Muk forecast to intensify even further before it made landfall on November 15 in south Andhra Pradesh coast close to the north of Kavali. However, the system became sheared to the western periphery and the IMD downgraded it back into a deep depression. Khai-Muk headed northwest and then northwards after making landfall in Andhra Pradesh. The name Khai Muk was contributed by Thailand, it means pearl in Thai.

By November 15, all ports in Andhra Pradesh were under cautionary signal number three. All fishermen were advised to remain at port due to rough seas. Residents along the shore were urged to evacuate as waves up to 2 m (6.5 ft) were forecast to impact the coast.

High winds knocked down trees and power lines causing traffic jams throughout the Andhra Pradesh. Boats and fishing nets were washed away by high waves produced by Khai-muk, costing Rs. 2 cores ($430,000 USD). An average of 53.5 mm (2.1 in) of rain fell throughout

the state. The highest rainfall was recorded in Polavaram at 230 mm on 17 November. An estimated 1.2 million hectares of crops were damaged or destroyed by the storm leading to Rs. 10 cores ($1.9 million USD) in agricultural losses. A total of 148 homes were destroyed and another 23 were damaged, amounting to Rs. 4 crores ($780,000 USD) in monetary losses. A 5 km (3.1 mi) stretch of highway was washed out by the storm and damages to the road amounted to Rs. 4 crores ($780,000 USD).

4.4.2 Minimum sea level pressure (MSLP)

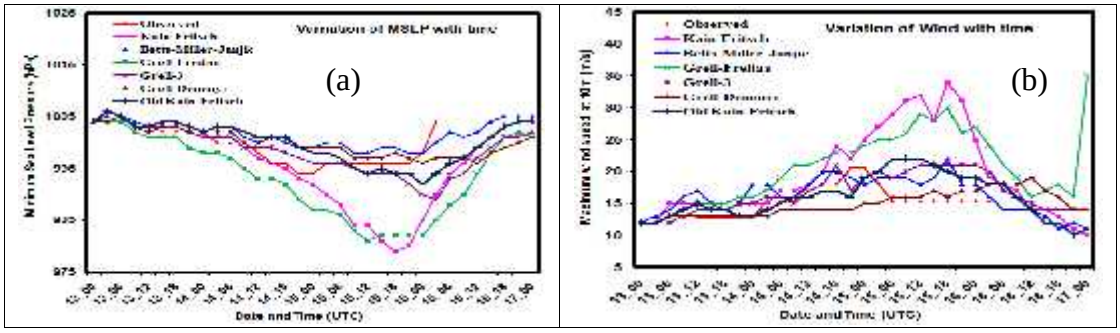

Figure 71: Evolution of WRF model simulated (a) MSLP and (b) MWS at 10m level using six different cumulus schemes and that of observed of the TC Khaimuk.

The storm intensity forecasts for the TC Khaimuk in terms of MSLP using six different cumulus schemes KF, BMJ, GF, G3, GD and OKF for 96 hours (every 3 hourly) are presented in Figure 71. The WRF model simulated and observed MSLP gradually drops with time and attains peak intensity just before the landfall and thereafter MSLP increases. The model simulated MSLP values of 979, 988, 981, 989, 996 and 992 hPa are obtained using KF, BMJ, GF, G3, GD and OKF schemes respectively and these simulated MSLP values are obtained at 1800 UTC of 15, 0900 UTC of 15, 12 UTC of 15, 0300 UTC of 16, 0000 UTC of 16 and 0000 UTC of 16 November 2008 respectively. The observed MSLP 996 hPa is obtained at 2100 UTC of 15 November 2008 according to IMD. So, simulated MSLP values are obtained later/earlier than that of observed. The observed MSLP is much higher than the simulated MSLP for all cumulus schemes with little exception. The pressure departure is found minimum for Kain-Fritsch scheme and maximum for Betts-Miller-Janjic schemes compared with IMD observed. The simulated pressure fall for all cumulus schemes indicate that the system has attained the intensity of cyclonic storm and the observation also indicates that the system attained the intensity of cyclonic storm (996 hPa). Cumulus schemes BMJ, GD and OKF match better than the others cumulus schemes with the observed intensity. But Cumulus schemes BMJ and GD simulate later than the observed and

KF, GF, G3 and OKF simulate earlier than the observed. Intensity simulated by Cumulus BMJ and G3 is absolutely not matched with the observed value.

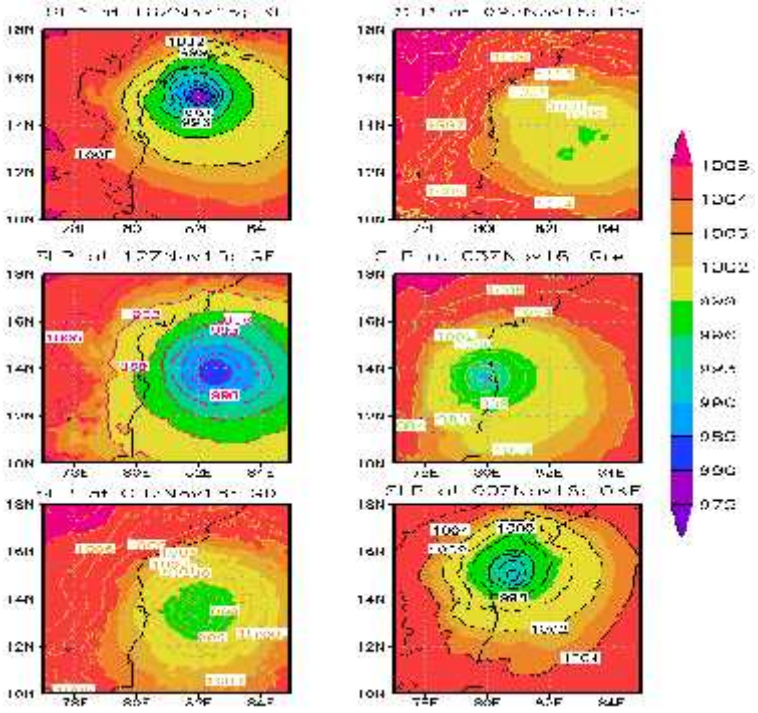

Figure 72: WRF model simulated SLP of TC Khaimuk at different cumulus schemes.

Figure 72 shows the mature stage of spatial distribution of sea level pressure using six different cumulus schemes and it is obtained with different time and position with different intensity. The spatial distribution of sea level pressure at its mature stage for the TC Khaimuk using different cumulus schemes KF, BMJ, GF, G3, GD and OKF in WRF model is obtained at 1800 UTC of 15, 0900 UTC of 15, 1200 UTC of 15, 0300 UTC of 16, 0000 UTC of 16 and 0000 UTC of 16 November 2008 respectively. The observed MSLP of 996 hPa is obtained at 2100 UTC of 15 November 2008 respectively.

The lowest simulated MSLP (i.e. mature stage) for the TC Khaimuk using different cumulus schemes KF, BMJ, GF, G3, GD and OKF in WRF models are 979, 988, 981, 989, 996 and 992 hPa respectively. The observation also indicates that the system attained the intensity of cyclonic storm (996 hPa,). The GD cumulus scheme has the same intensity as the observation. It is seen that KF cumulus scheme has very high intensity, and then the GF cumulus scheme has also very high intensity. The OKF, BMJ and G3 cumulus schemes have lower intensity than the observation.

In Figure 72, it is observed that mature stage of spatial distribution of sea level pressure using different cumulus is obtained with different times and different positions. Positions of mature stages using KF, BMJ, GF, G3, GD and OKF schemes are located at 81.99^{o}E and 15.20^{o}N at 1800 UTC of 15, 82.55^{o}E and 12.7^{o}N at 0900 UTC of 15, 82.34^{o}E and 13.88^{o}N at 1200 UTC of 15, 79.95^{o}E and 13.75^{o}N at 0300 UTC of 16, 81.84^{o}E and 13.30^{o}N at 0000 UTC of 16 and 80.79^{o}E and 15.02^{o}N with time at 0000 UTC of 16 November respectively. Intensity, position and time of mature stages are different for different cumulus schemes used in WRF model. The isobar has circular arrangement around the TC centre with some asymmetric features in the outer periphery. The contour interval is different for different positions because of different intensity of the system. From the Figure 72, the radius of the TC eye is found to be around 100 km for all cumulus according to all simulation

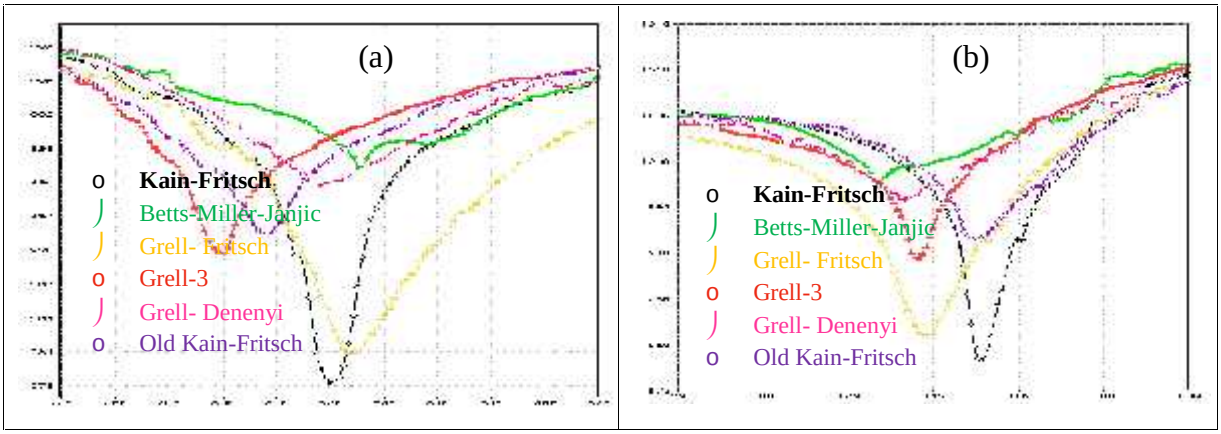

Figure 73: WRF model simulated (a) East West and (b) North South cross sectional view of SLP of TC Khaimuk at different cumulus schemes with fixed latitude and longitude respectively.

The distribution of the sea level pressure of the TC Khaimuk along east-west cross section and north-south cross section passing through its centre using different cumulus is shown in Figure 73. The positions of the centre at mature stage using different cumulus schemes KF, BMJ, GF, G3, GD and OKF are located at 81.99^{o}E and 15.20^{o}N, 82.55^{o}E and 12.7^{o}N, 82.34^{o}E and 13.88^{o}N, 79.95^{o}E and 13.75^{o}N, 81.84^{o}E and 13.30^{o}N and 80.79^{o}E and 15.02^{o}N respectively. The model simulated MSLP 979, 988, 981, 989, 996 and 992 hPa are obtained at 1800 UTC of 15, 0900 UTC of 15, 1200 UTC of 15, 0300 UTC of 16, 0000 UTC of 16 and 0000 UTC of 16 November 2008 respectively and shown in Figure 73. In Figure 73, the black, green, yellow, orange, magenta and the dark purple color represent KF, BMJ, GF, G3, GD and OKF schemes respectively.

The figures demonstrate the moderate pressure gradient around the centre with maximum gradient at around 120 km below or above for all cumulus schemes from the centre. Variation of east-west and north-south elongated SLP at the center are clearly observed.

4.4.3 Maximum Wind speed

The storm intensity forecasts for the TC Khaimuk in terms of MWS using six different cumulus schemes KF, BMJ, GF, G3, GD and OKF for 96 hours (every 3 hourly) along with observed MWS are presented in Figure 71. The model simulated MWSs are obtained at the standard meteorological height of 10 m. The WRF model simulated MWSs are higher than the observed values through almost full forecast hours with a few exceptions. Model simulated highest values of MWS using six different cumulus schemes are obtained at same the time and earlier. But for convenience, time of maximum intensity (mature stage) are considered as the time of obtained MSLP (this time are written in previous section).

The observed and simulated MWS by WRF decrease with time gradually after obtained highest value of MWS. The highest values of MWS for the TC Khaimuk using different cumulus schemes KF, BMJ, GF, G3, GD and OKF in WRF models are 34, 19, 29, 20, 17 and 19 m/s respectively. Whereas the observed MWS is 20.56 m/s. The simulated and observation values indicate that the system has attained the intensity of cyclonic storm (17.5 - 24.44 m/s). WRF model using different cumulus schemes simulate more or less the same value of MWS than that of observed value. It is seen KF cumulus scheme has very high intensity, the GF cumulus scheme has also high intensity. The GF, G3 and OKF cumulus schemes has almost same intensity as the observation. Finally, GD cumulus scheme has lower intensity than the observation.

Figure 74 shows that the mature stage of spatial distribution of surface (10 m) wind speed using six different cumulus schemes and it is obtained with different times and positions with different intensities. The spatial distribution of wind speed at its mature stage for the TC Khaimuk using different cumulus schemes KF, BMJ, GF, G3, GD and OKF in WRF model is obtained at 1800 UTC of 15, 0900 UTC of 15, 1200 UTC of 15, 0300 UTC of 16, 0000 UTC of 16 and 0000 UTC of 16 November 2008 respectively and shown in Figure 74. The Figure 74 obtained from WRF model shows that the wind field of the TC is highly asymmetric in the horizontal distribution. At 0000 UTC of 13 November 2008 (i.e. at the initial time of simulation) the TC is in the sea with different cumulus schemes (not shown in

figure). Gradually, TC is organized with strong wind bands around and the wind flow in the core region shows asymmetric feature with minimum wind speed at the centre. The spatial distribution of surface (10 m) wind speed is found maximum for KF scheme and minimum for BMJ, GD and OKF scheme. The figure shows that the pattern has an asymmetric wind distribution with strong wind bands in the front right side, rear left and rear right sides close to the centre of north directed moving storm. In Figure 74, it is observed that mature stage of spatial distribution of wind speed using different cumulus is obtained with different times and different positions. Positions of mature stages using KF, BMJ, GF, G3, GD and OKF are located at 81.99^{o}E and 15.20^{o}N at 1800 UTC of 15, 82.55^{o}E and 12.7^{o}N at 0900 UTC of 15, 82.34^{o}E and 13.88^{o}N at 1200 UTC of 15, 79.95^{o}E and 13.75^{o}N at 0300 UTC of 16, 81.84^{o}E and 13.30^{o}N at 0000 UTC of 16 and 80.79^{o}E and 15.02^{o}N at 0000 UTC of 16 November 2008 respectively. At this mature stage, the wind flow in the core region shows a near circular feature with minimum wind speed at the centre.

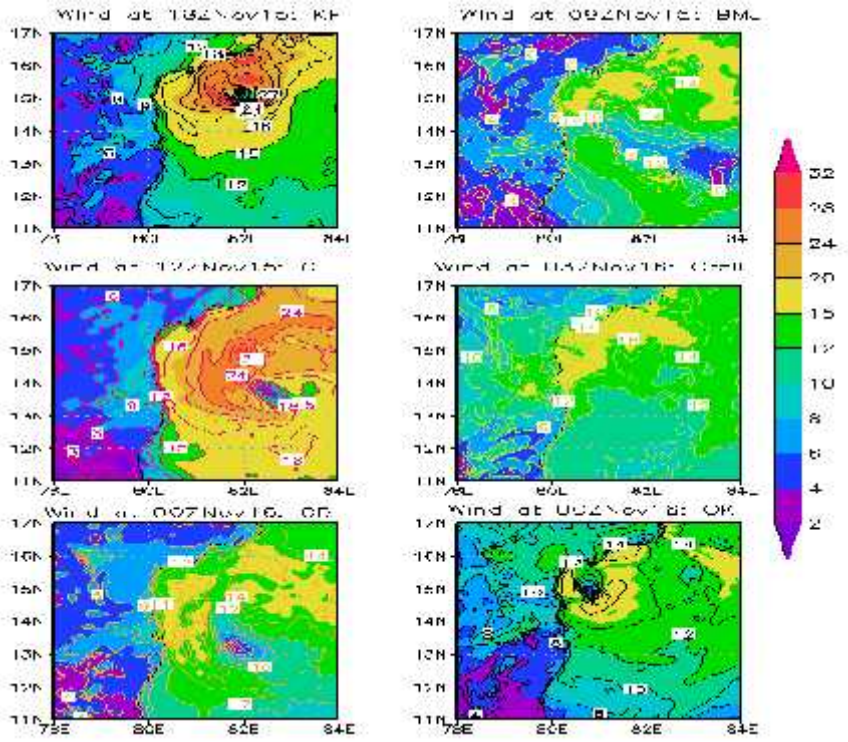

Figure 74: WRF model simulated MWS of TC Khaimuk at different cumulus schemes.

The distribution of the surface wind of the TC Khaimuk along east-west cross section and north-south cross section passing through its centre at mature stage using different cumulus is shown in Figures 75 and 76 respectively. The position of the centre at mature stage using different cumulus schemes KF, BMJ, GF, G3, GD and OKF are located at 81.99^{o}E and

15.20°N, 82.55°E and 12.7°N, 82.34°E and 13.88°N, 79.95°E and 13.75°N, 81.84°E and 13.30°N and 80.79°E and 15.02°N respectively. The model simulated wind speeds of 34, 22, 35, 21, 19 and 22 m/s are obtained at 1800 UTC of 15, 1800 UTC of 15, 0000 UTC of 17, 1200 UTC of 15, 1200 UTC of 16 and 0600 UTC of 26 November 2008 respectively. But the model simulated wind speeds of 34, 19, 29, 20, 17 and 19 m/s are obtained at 1800 UTC of 15, 0900 UTC of 15 November, 1200 UTC of 15, 0300 UTC of 16, 0000 UTC of 16 and 0000 UTC of 16 November 2008 respectively at mature stage (that is at the minimum SLP position). The figures demonstrate that a calm region is found inside the eye of the system and maximum wind was found in the eye wall. The simulated value of wind at the centre using different cumulus schemes has a wide variety. In Figure 75, the value is less than 6 m/s and in Figure 76 the value is less than 11 m/s. In both Figures the KF, GF and OKF cumulus scheme show better result than the other cumulus schemes. In Figure 75, the performance of BMJ and G3 cumulus scheme is worst and Figure 76, the performance of G3 cumulus scheme is worst. The radius of maximum wind of the TC Khaimuk is found to be just lower than 100 km according to the simulation. Variation of east-west and north-south elongated wind at the center is clearly observed.

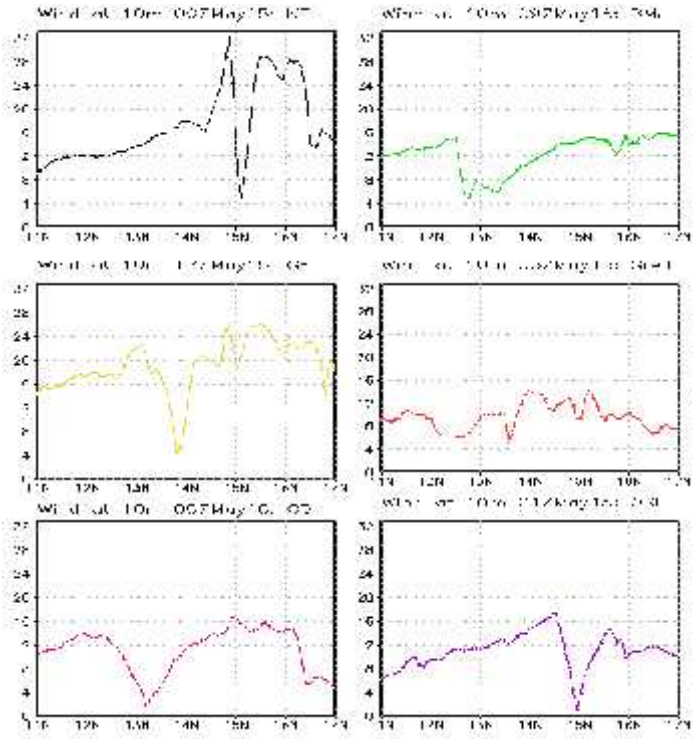

Figure 75: East West cross sectional view of WRF model simulated wind speed (m/s) of TC Khaimuk at different cumulus schemes with fixed longitude.

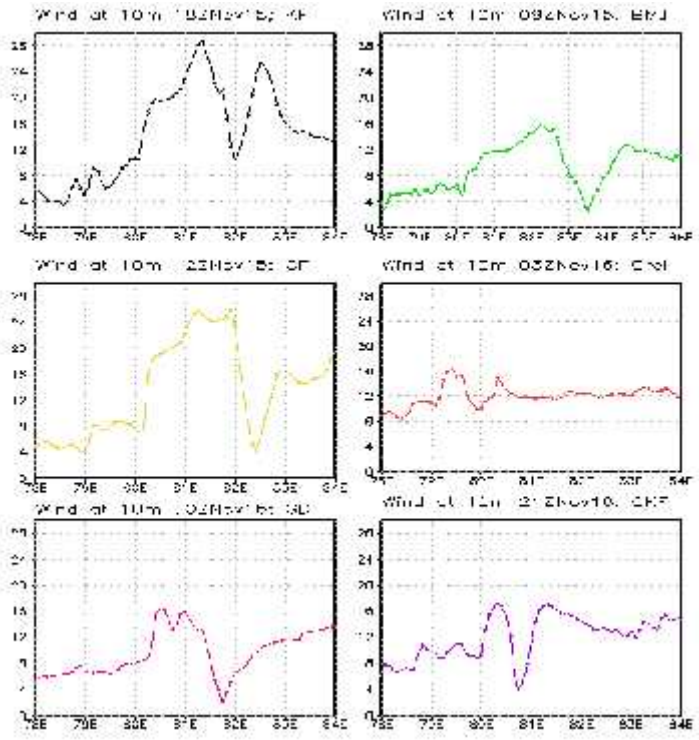

Figure 76: North south cross sectional view of WRF model simulated Wind speed (m/s) of TC Khaimuk at different cumulus schemes with fixed latitude.

The horizontal distribution of vector wind field at its mature stage for the levels 850, 500, 300 and 200 hPa of the TC Khaimuk using different cumulus is tabulated in Table 13 and figure of this only for the levels 850 and 200 hPa are shown in Figure 77 and 78 respectively.

From the Figure 77, a well organized TC circulation with strong winds encircling the centre is found at the 850 hPa levels. It is noted that the strong wind is confined to the right of the direction of the movement of the system. From the Figure 78, at 200 hPa level strong outflow is evident from the central part of the TC. So, using simulated results obtained from WRF models, Figure 77 and Figure 78 demonstrate inflow in the lower level and outflow in the upper level respectively.

WRF model simulated maximum winds at the mature stage (1800 UTC of 15, 0900 UTC of 15, 1200 UTC of 15, 0300 UTC of 16, 0000 UTC of 16 and 0000 UTC of 16 November 2008) are about 60, 30, 50, 40, 30, 40 m/s and 30, 20, 30, 20, 20, 20 m/s for different cumulus (KF, BMJ, GF, G3, GD and OKF) scheme at 850 and 200 hPa levels respectively. The wind speed at 850 hPa levels is found minimum for BMJ and GD scheme and maximum for KF schemes. And the wind speed at 200 hPa levels is found minimum for

BMJ, G3, GD amd OKF scheme and maximum for KF and GF schemes. The mature stages are obtained at different time and position. The values of wind speed for mature stage at the levels 500 and 300 hPa are obtained different with different cumulus schemes.

Table 14: WRF model simulated wind speed (m/s) at different cumulus schemes at 850, 500, 300 and 200 hPa pressure levels of TC Khaimuk.

Pressure level (hPa)	Maximum Wind Speed (m/s) at different time					
	18 UTC of 15 November at KF	09 UTC of 15 November at BMJ	12 UTC of 15 November at GF	03 UTC of 16 November at Greel	00 UTC of 16 November at GD	00 UTC of 16 November at OKF
850	60	30	50	40	30	40
500	40	20	40	30	20	30
300	30	20	30	20	20	20
200	30	20	30	20	20	20

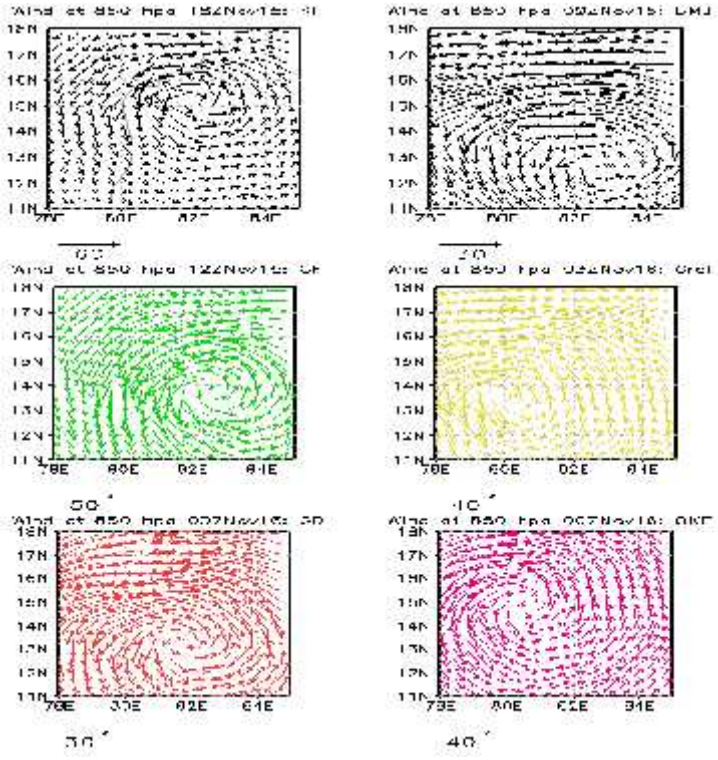

Figure 77: WRF model simulated Wind vector and magnitude at 850 hpa levels at different cumulus schemes.

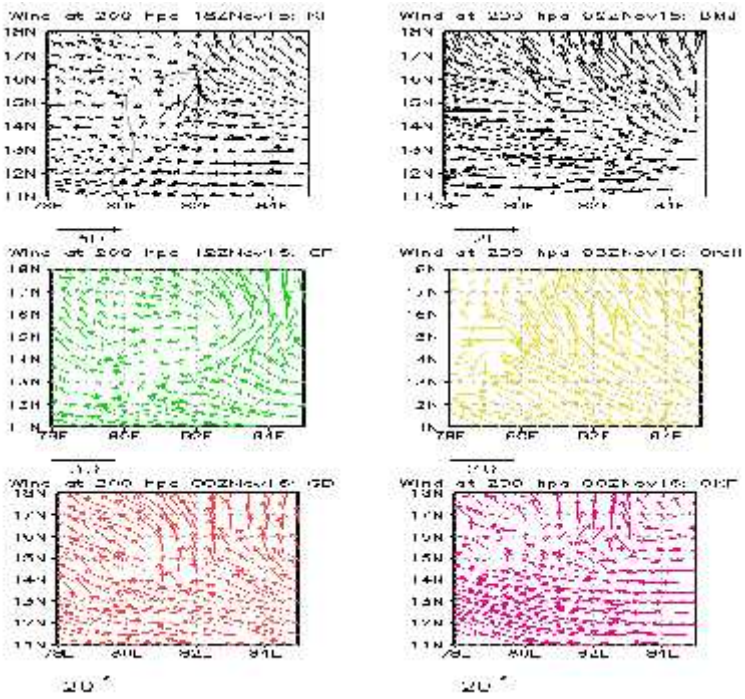

Figure 78: WRF model simulated Wind vector and magnitude at 200 hpa levels at different cumulus schemes.

The Vertical profile of Radial, Tangential, Vertical and Horizontal wind field at its mature stage for the TC Khaimuk using different cumulus schemes KF, BMJ, GF, G3, GD and OKF in WRF model are obtained at 1800 UTC of 15, 0900 UTC of 15, 1200 UTC of 15, 0300 UTC of 16, 0000 UTC of 16 and 0000 UTC of 16 November 2008 respectively and shown in Figures 79, 80, 81 and 82 respectively. Model simulated results are also tabulated in Table 15, for different cumulus mentioned in the Table. From the table, it is clear that the value of the vertical profile of radial, tangential, vertical and horizontal wind of TC Khaimuk obtained using different cumulus (KF, BMJ, GF, G3, GD and OKF) schemes are different for different cumulus schemes. The strong wind with different speeds (Table 15) is confined to the different levels in lower troposphere and extended up to 100 hPa level in the left side of the system.

From the Figure 79, it is found that vertical profile of radial wind is much more organized and it is also clearly seen that the system has strong inflow in the lower levels which bring the air to the system through the boundary level and lower level and outflow in the upper level. The Radial wind is found minimum for Old Kain-Fritsch scheme and maximum for all cumulus except Old Kain-Fritsch schemes.

The vertical profile of tangential wind flows in a northerly direction at the eastern side of the system and in a southerly direction at the western side. For this reason, tangential wind shows positive value at the right side (east side) of the centre and negative value at the left

side (west side) of the centre. The Tangential wind is found minimum for BMJ scheme and maximum for KF schemes.

The values of the vertical profile of vertical wind are different in magnitude for different cumulus and 3.5, 2.0, 4.0, 1.5, 2.5 and 0.3 m/s are simulated by KF, BMJ, GF, G3, GD and OKF cumulus schemes respectively. It indicates that the vertical wind is found minimum for OKF scheme and maximum for KF schemes. These values are along the eye wall and other parts of the system which feed moisture into the system. It is noted that Khaimuk has very weak updraft motion at the eye wall throughout mid and upper troposphere. The downward motion is visible in the central parts of the TC and other areas in between rain bands.

The vertical profile of horizontal wind of the system at its mature stage shows the distribution of strong winds up to 100 hPa for GF, G3 and GD cumulus schemes, up to 150 hPa for OKF and up to KF and BMJ cumulus scheme around the centre of TC. It further confirms that the maximum winds are confined to the right of the direction of the movement of the system. This value decreases with the radial distance from both side of the eye. Calm wind zone is sharp and narrow and little bit tilted to the westward and get expanded towards upper levels. This is in agreement with the previous studies of Rao and Prasad (2006) and Goswami *et al.* (2006) on Orissa TC. Cyclonic circulation is generally seen up to about 300 hPa level and anticyclone circulation with divergence fields aloft. In case of TC Khaimuk, cyclonic circulation is also seen up to about 500 hPa level for cumulus BMJ and OKF scheme, 400 hPa levels for cumulus KF and GD scheme, 300 hPa levels for GF and G3 cumulus schemes and anticyclone circulation with divergence fields aloft. And the horizontal wind is found minimum for GD and BMJ scheme and maximum for KF schemes.

Table 15: WRF model simulated maximum radial wind, tangential wind, vertical velocity and horizontal wind (m/s) of TC Khaimuk at different cumulus schemes.

Component of wind	Simulated maximum wind speed (m/s) at different times					
	18 UTC of 15 November at KF	09 UTC of 15 November at BMJ	12 UTC of 15 November at GF	03 UTC of 16 November at Greel	00 UTC of 16 November at GD	00 UTC of 16 November at OKF
Radial wind	9	9	9	9	9	6
Tangential wind	25	12	20	15	15	20
Vertical velocity	3.5	2	4	1.5	2.5	0.3
Horizontal wind	50	20	40	30	20	30

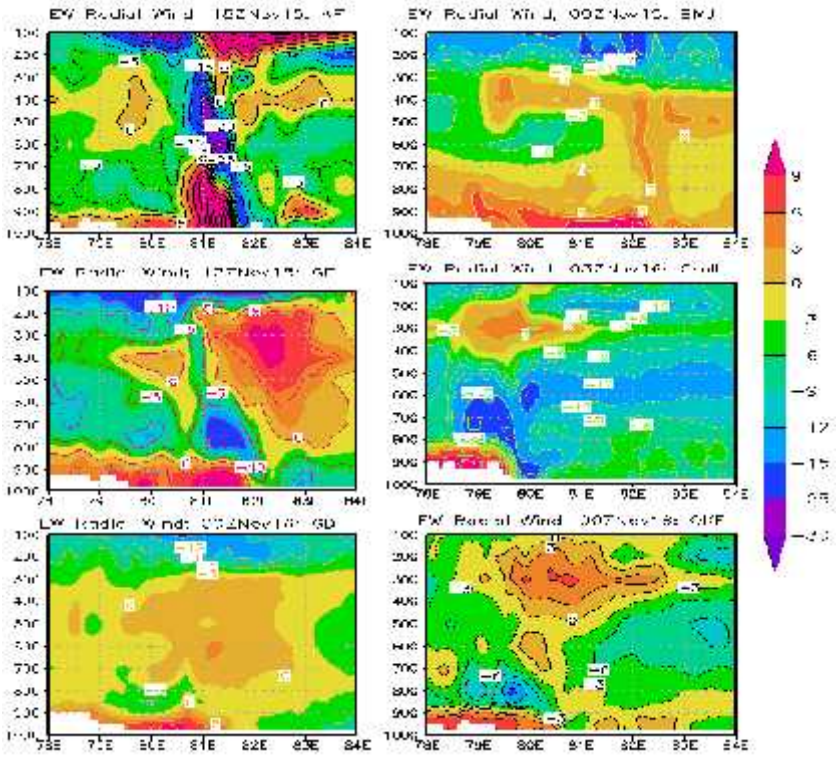

Figure 79: WRF model simulated Radial wind (cm/s) of TC Khaimuk at different cumulus schemes.

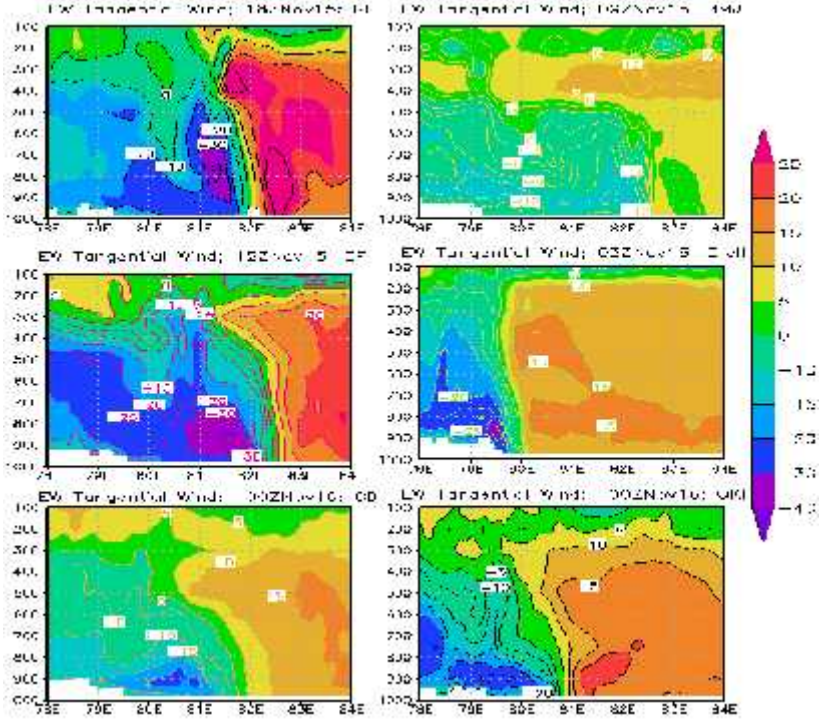

Figure 80: WRF model simulated Tangential wind (cm/s) of TC Khaimuk at different cumulus schemes.

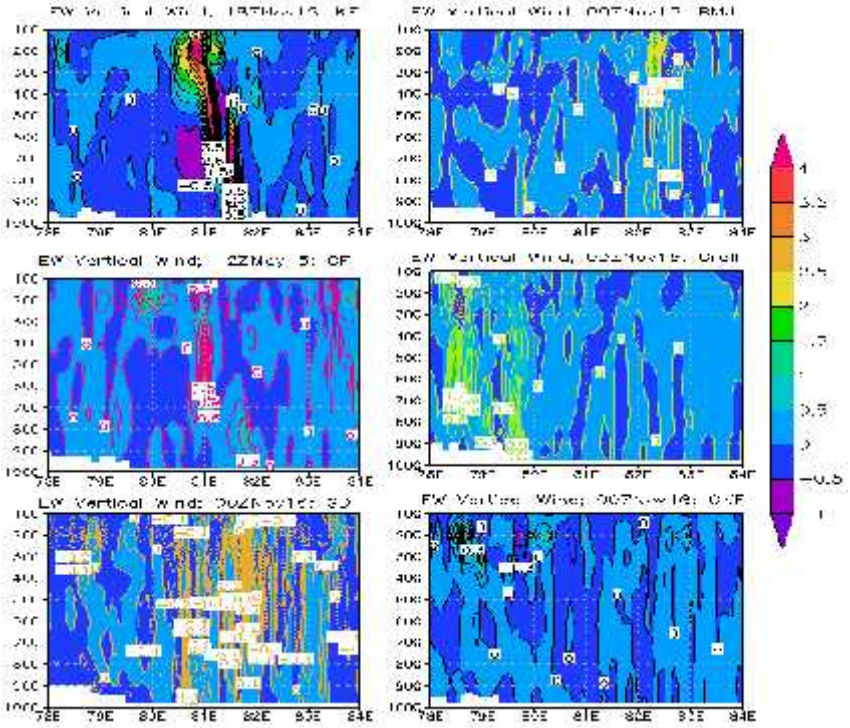

Figure 81: WRF model simulated Vertical wind (cm/s) of TC Khaimuk at different cumulus schemes.

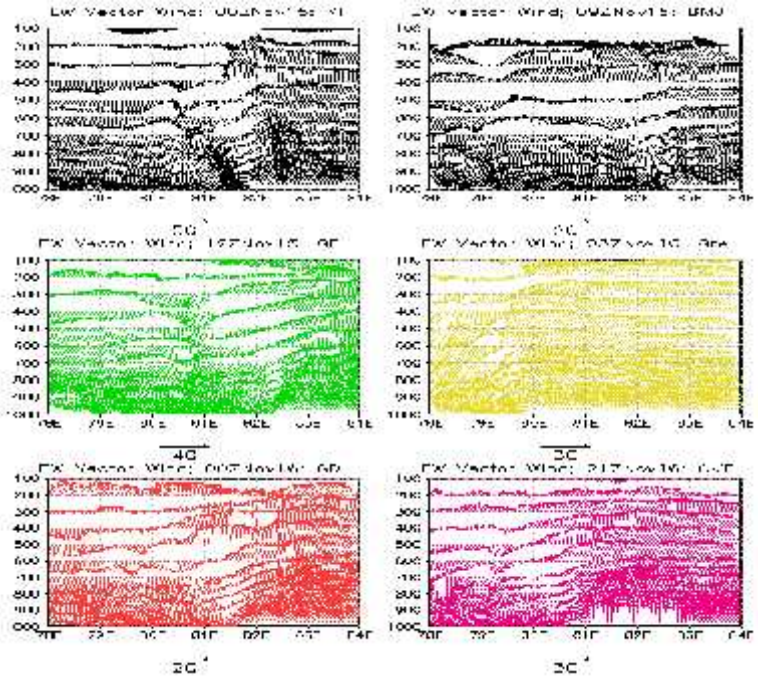

Figure 82: WRF model simulated Horizontal wind (cm/s) of TC Khaimuk at different cumulus schemes.

4.4.4 Vorticity

To know the evolution WRF model simulated relative vorticity at 1000, 950, 850, 500 and 300 hPa at six cumulus KF, BMJ, GF, G3, GD and OKF schemes for 96 hours (every 3 hourly) are presented in Figure 83. The values of relative vorticity are increased with the increase of time (i.e. in the development of the TC) at all levels for all cumulus schemes and increased to a maximum value. Thereafter the value shows a fall. From the figure it is observed that at 950, 850 and 500 hPa the vorticity is found maximum for cumulus KF scheme. And 1000 hPa level the vorticity is found maximum for cumulus BMJ scheme. And 300 hPa level the vorticity is found maximum for cumulus GF scheme. The vorticity is found more than zero for all levels using all schemes. So, from the simulated value of vorticity it is seen that system intensification is satisfied more or less by all cumulus schemes.

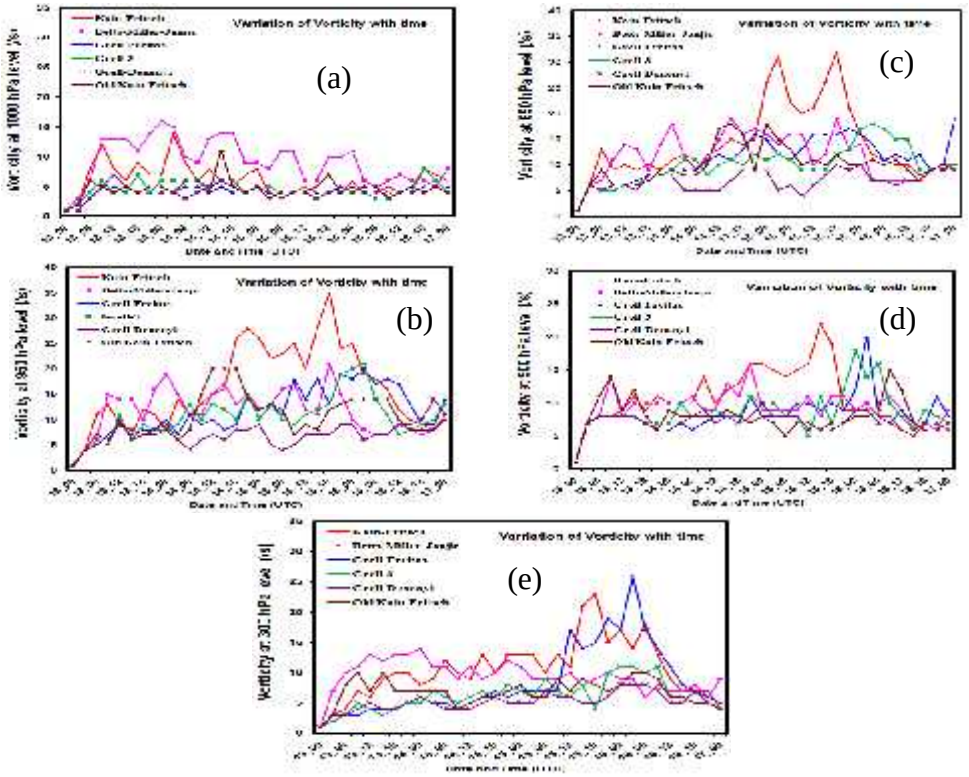

Figure 83: Evolution of model simulated vorticity with time at different cumulus schemes for 1000, 950, 850, 500 and 300 hPa level of TC Khaimuk.

Vertical distribution of the relative vorticity with fixed latitude (along east-west direction) and fixed longitude (along north-south direction) are obtained from WRF model is shown in Figures 86 and 87 respectively and the values are tabulated in Table 16. Simulated results at 1800 UTC of 15, 0900 UTC of 15, 1200 UTC of 15, 0300 UTC of 16, 0000 UTC of 16 and

0000 UTC of 16 November 2008 for different cumulus schemes KF, BMJ, GF, G3, GD and OKF are located at 81.99°E and 15.20°N, 82.55°E and 12.7°N, 82.34°E and 13.88°N, 79.95°E and 13.75°N, 81.84°E and 13.30°N and 80.79°E and 15.02°N respectively.

In figure 86 the system has the positive vorticity along the centre up to 500 hPa level with higher value for all cumulus. For KF, BMJ, GF, G3, GD and OKF the higher value up to 700, 750, 500, 600, 600 and 800 levels respectively. So the strong cumulus scheme is GF scheme. The greatest vorticity is KF and GF cumulus scheme. In figure 87 the system has the positive vorticity along the centre up to 200 hPa level with higher value for all cumulus. For KF, BMJ, GF, G3, GD and OKF the higher value up to 700, 800, 800, 500, 550 and 900 levels respectively. So the strong cumulus scheme is Grell scheme.

Table 16: WRF Model simulated maximum vorticity ($x10^{-5}$ s^{-1}) at different pressure levels associated with TC Khaimuk at different cumulus schemes.

Pressure level (hPa)	Maximum Vorticity ($x10^{-5}$ s^{-1}) at different times					
	18 UTC of 15 November at KF	09 UTC of 15 November at BMJ	12 UTC of 15 November at GF	03 UTC of 16 November at Greel	00 UTC of 16 November at GD	00 UTC of 16 November at OKF
850	150	90	150	150	50	70
500	100	40	40	70	50	70
300	110	40	30	70	40	30
200	100	30	20	30	30	30
Position of TC centre	15.20°N and 81.99°E	12.7°N and 82.55°E	13.88°N and 82.34°E	13.75°N and 79.95°E	13.30°N and 81.84°E	15.02°N and 80.79°E
Vertical distribution with fixed latitude	15	12	15	12	9	10
Vertical distribution with fixed longitude	16	10	18	9	5	8

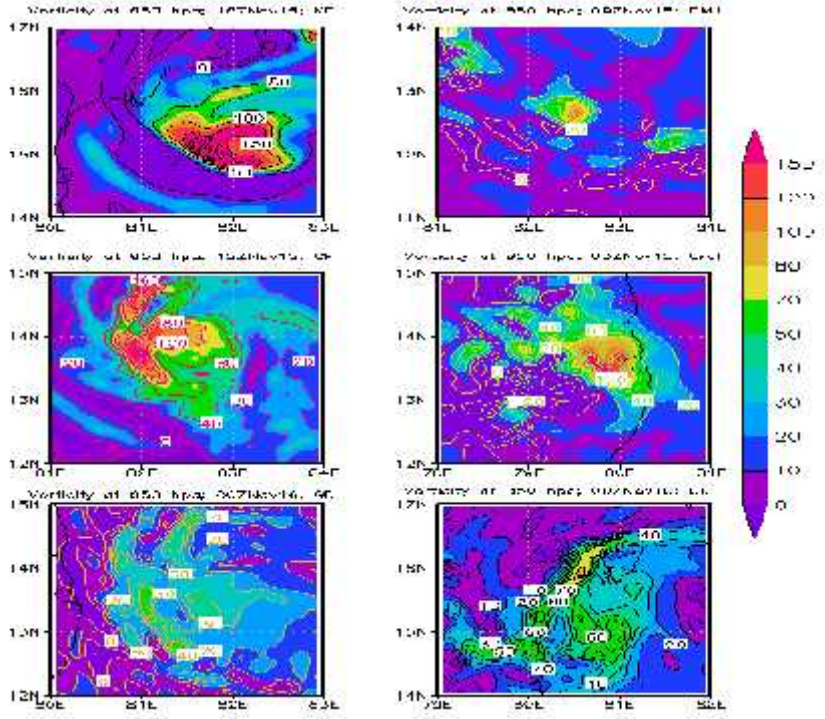

Figure 84: WRF Model simulated vorticity field of 850 hPa levels at different cumulus schemes.

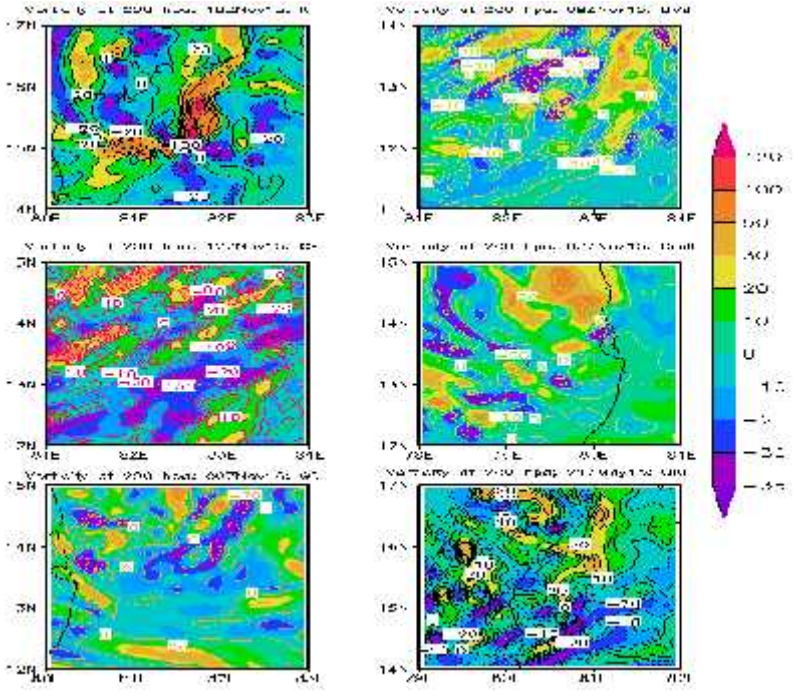

Figure 85: WRF Model simulated vorticity field of 200 hPa levels at different cumulus schemes.

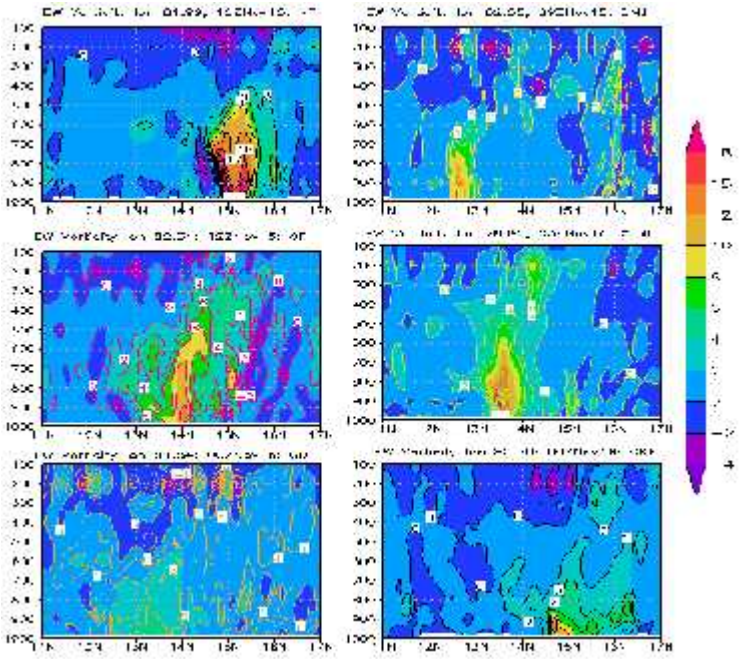

Figure 86: WRF model simulated east west vertical distribution of relative vorticity with fixed longitude of TC Khaimuk through the centre at different cumulus schemes.

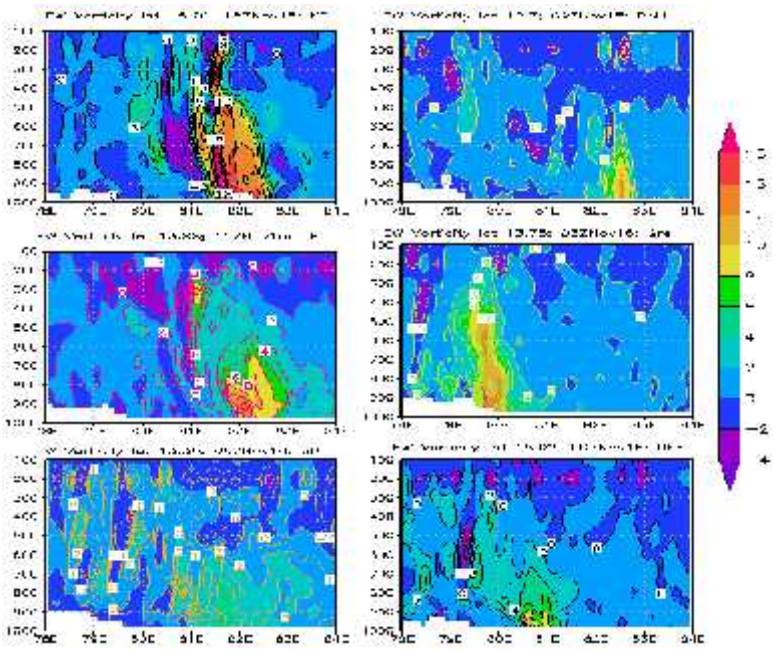

Figure 87: WRF model simulated north-south vertical distribution of relative vorticity with fixed latitude of TC Khaimuk through the centre at different cumulus schemes.

4.4.5 Temperature anomaly

The WRF model simulated temperature anomaly at 1800 UTC of 15, 0900 UTC of 15, 1200 UTC of 15, 0300 UTC of 16, 0000 UTC of 16 and 0000 UTC of 16 November 2008 (i.e. its

mature stage) for different cumulus (KF, BMJ, GF, G3, GD and OKF) schemes is shown in Figure 87 and the values are tabulated in Table 16. It is noted that the warm core region is slightly expanded up to 200 hPa level all most for all cumulus schemes.

For Kain-Fritsch cumulus scheme at1800 UTC of 15 November 2008, a warm core with 7^{o}C is observed in 880-220 hPa layer. It is noted that the warm core region is expanded outward at 880-200 hPa level. The greatest anomaly is observed around 800 hPa level. The simulated temperature anomaly demonstrates that the warm core is visible mainly at middle troposphere.

For Betts-Miller-Janjic cumulus scheme at 0900 UTC of 15 November 2008, a warm core with 4^{o}C is observed in 920-750 hPa layer. It is noted that the warm core region is expanded outward at 950-600 hPa level. The greatest anomaly is observed around 850 hPa level. The simulated temperature anomaly demonstrates that the warm core is visible mainly at lower troposphere.

For Grell-Fritsch cumulus scheme at 1200 UTC of 15 November 2008, a warm core with 6^{o}C is observed in 740-590 hPa layer. It is noted that the warm core region is expanded outward at 950-200 hPa level. The greatest anomaly is observed around 650 hPa level. The simulated temperature anomaly demonstrates that the warm core is visible mainly below the middle troposphere.

For Grell-3 cumulus scheme at 0300 UTC of 16 November 2008, a warm core with 5^{o}C is observed in 990-700 hPa layer. It is noted that the warm core region is expanded outward at 900-200 hPa level. The greatest anomaly is observed around 800 hPa level. The simulated temperature anomaly demonstrates that the warm core is visible mainly at lower troposphere.

For Grell-Denenyi cumulus scheme at 0000 UTC on 16 November 2008, a warm core with 3^{o}C is observed in 730-590 hPa layer. It is noted that the warm core region is expanded outward at 980-200 hPa level. The greatest anomaly is observed around 650 hPa level. The simulated temperature anomaly demonstrates that the warm core is visible mainly below the middle troposphere.

For Old Kain-Fritsch cumulus scheme at 0000 UTC of 16 November 2008, a warm core with 5^{o}C is observed in 880-550 hPa layer. It is noted that the warm core region is expanded outward at 880-200 hPa level. The greatest anomaly is observed around 800 hPa level. The

simulated temperature anomaly demonstrates that the warm core is visible mainly at lower troposphere.

Finally, the greatest anomaly is occurred at cumulus KF scheme around 800 hPa levels. The simulated temperature anomaly demonstrates that the warm core is visible mainly at lower and middle troposphere for all cumulus schemes. Negative temperature anomalies are also seen at the upper levels and lower levels.

Table 17: WRF Model simulated maximum temperature anomaly (^{o}C), Relative Humidity (%) and water vapor mixing ratio (g/kg) associated with TC Khaimuk at different cumulus schemes.

Parameter	18 UTC of 15 November at KF	09 UTC of 15 November at BMJ	12 UTC of 15 November at GF	03 UTC of 16 November at G3	00 UTC on 16 November at GD	00 UTC of 16 November at OKF
Maximum Temperature	7	4	6	5	3	5
Relative Humidity	95	100	100	100	100	95
Water vapor mixing ratio	2	2	2	1.8	1.8	2

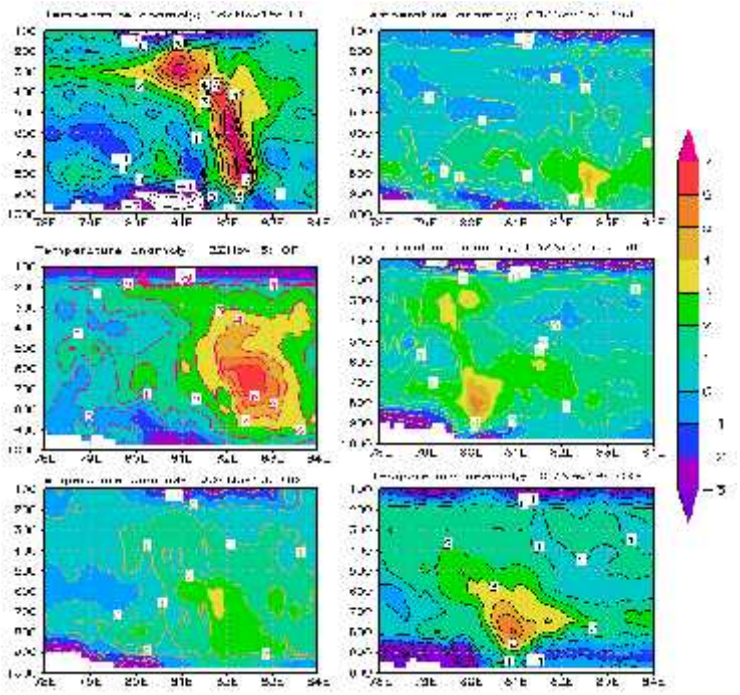

Figure 88: WRF model simulated vertical distribution of temperature anomaly in the east-west direction of TC Khaimuk at different cumulus schemes.

4.4.6 Relative humidity

The Horizontal distribution of relative humidity of TC Khaimuk obtained from WRF model at 1800 UTC of 15, 0900 UTC of 15, 1200 UTC of 15, 0300 UTC of 16, 0000 UTC of 16 and 0000 UTC of 16 November 2008 (i.e. its mature stage) for different cumulus (KF, BMJ, GF, G3, GD and OKF) schemes is shown in Figure 89. Time variation of relative humidity at surface is obtained around 90-100%. But the relative humidity at 850 levels for all cumulus is 100% of the cyclone (not shown). These values satisfy the condition for the intensification of cyclone through convection.

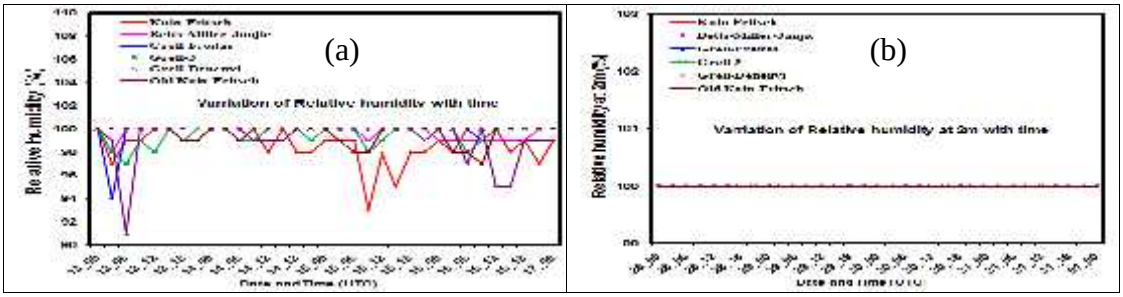

Figure 89: Evolution of model simulated (a) RH and (b) RH at 2m with time at different cumulus schemes of TC Khaimuk.

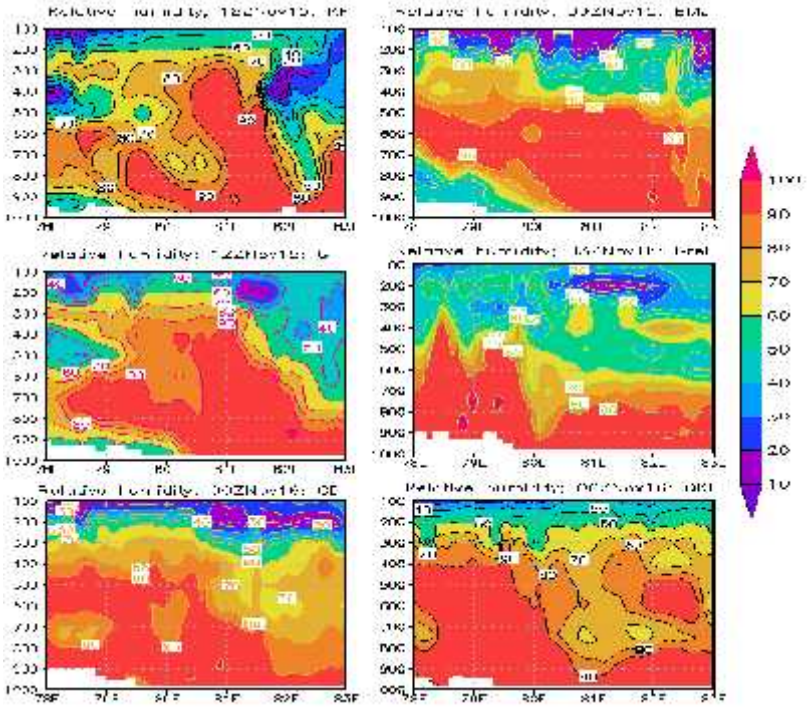

Figure 90: WRF model simulated vertical distribution of Relative humidity (%) in the east-west direction of TC Khaimuk at different cumulus schemes.

The vertical cross section of relative humidity of TC Khaimuk obtained from WRF model at 1800 UTC of 15, 0900 UTC of 15, 1200 UTC of 15, 0300 UTC of 16, 0000 UTC of 16 and

0000 UTC of 16 November 2008 (i.e. its mature stage) for different cumulus (KF, BMJ, GF, G3, GD and OKF) scheme from surface to 100 hPa levels is shown in Figure 90 and its values are tabulated in Table 17. It is noted that high relative humidity (more than 90%) spreads in outer range of eye wall up to 300, 500, 400, 500, 480 and 400 hPa levels for the cumulus (KF, BMJ, GF, G3, GD and OKF) scheme respectively. High relative humidity bands are also found in the rain band of the system situated at both sides of the system in the wider range throughout 980-350 hPa level. From the Table 17 and the Figure 90, it is observed that highest relative humidity 100% is observed using almost all cumulus schemes except KF and OKF cumulus schemes.

4.4.7 Relative humidity at 2m

The time evolution of relative humidity at 2m of TC Khaimuk obtained from WRF model at 1800 UTC of 15, 0900 UTC of 15, 1200 UTC of 15, 0300 UTC of 16, 0000 UTC of 16 and 0000 UTC of 16 November 2008 (i.e. its mature stage) for different cumulus (KF, BMJ, GF, G3, GD and OKF) schemes is shown in Figure 89. It is noted that high relative humidity at 2m (around 100%) spreads in outer range of eye wall up for all cumulus schemes without any exception. It is the good indication for the intensification of cyclone.

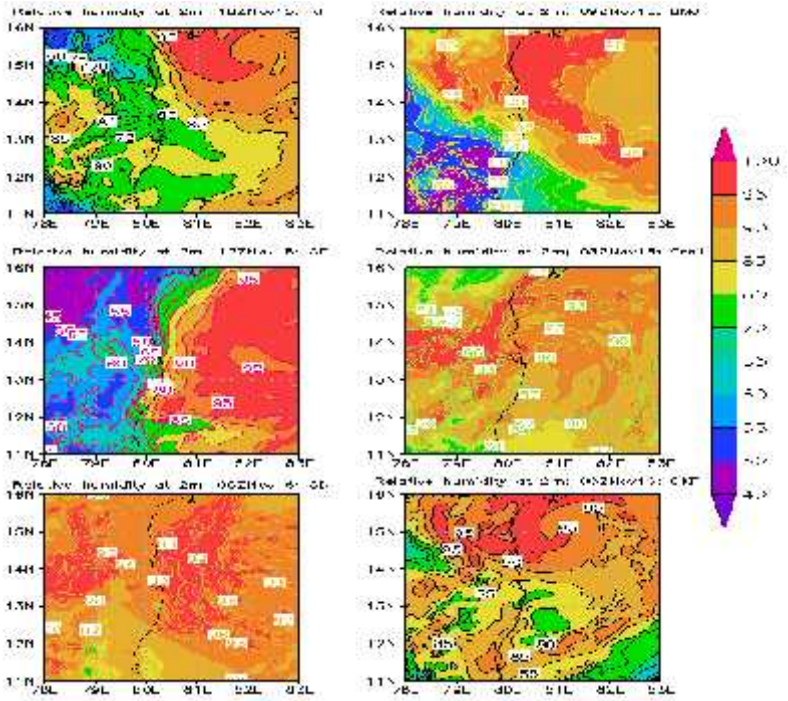

Figure 91: WRF model simulated spatial distribution of Relative humidity at 2m (%) in the east-west direction of TC Khaimuk at different cumulus schemes.

The spatial distribution of relative humidity at 2m of TC Khaimuk obtained from WRF at 1800 UTC of 15, 0900 UTC of 15, 1200 UTC of 15, 0300 UTC of 16, 0000 UTC of 16 and 0000 UTC of 16 November 2008 (i.e. its mature stage) for different cumulus (KF, BMJ, GF, G3, GD and OKF) schemes is shown in Figure 91. The values of the relative humidity at 2m of TC Khaimuk around the centre are about 100% or less for all cumulus schemes. This status of the relative humidity is satisfied the convection for the cyclone intensification.

4.4.8 Water vapor mixing ratio

The vertical distribution of water vapor mixing ratio obtained from WRF model along the east-west cross section of the centre at 1800 UTC of 15, 0900 UTC of 15, 1200 UTC of 15, 0300 UTC of 16, 0000 UTC of 16 and 0000 UTC of 16 November 2008 (i.e. its mature stage) for different cumulus (KF, BMJ, GF, G3, GD and OKF) schemes respectively of TC Khaimuk from surface to 100 hPa level is shown in Figure 92 and its values are tabulated in Table 17. It shows that the highest moisture content more than around 2 g/kg or more is found at the centre of the system at 950 hPa level and it decreases upwards to 400 hPa levels or more. For the development of the system this upward level goes up to 350 hPa level (i.e. its mature stage). Performance of all cumulus schemes for the simulation of vertical distribution of water vapor mixing ratio are comparable.

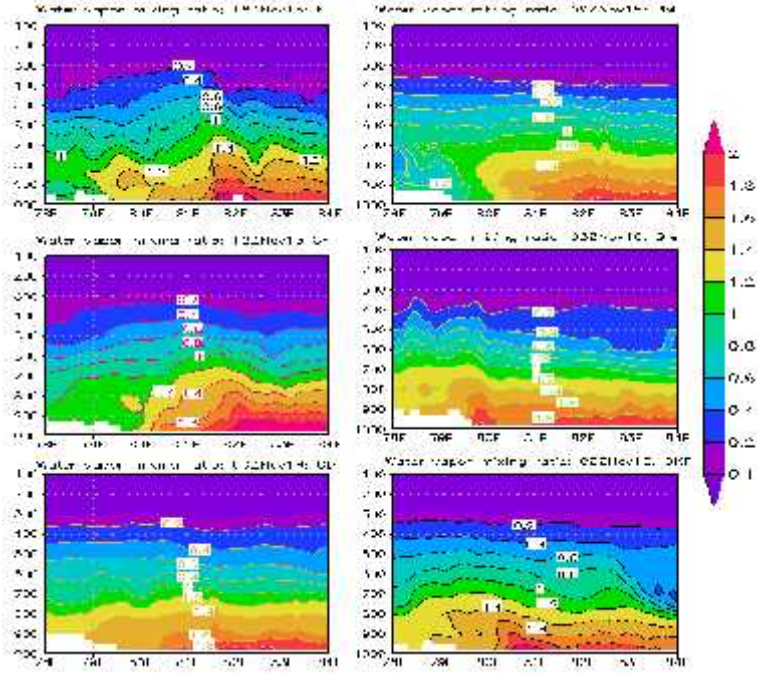

Figure 92: WRF model simulated vertical distribution of water vapor mixing ratio along the east-west cross section of the centre of TC Khaimuk at different cumulus schemes.

The horizontal distribution of water vapor mixing ratio of TC Khaimuk at 950 hPa level at 1800 UTC of 15, 0900 UTC of 15, 1200 UTC of 15, 0300 UTC of 16, 0000 UTC of 16 and 0000 UTC of 16 November 2008 (i.e. its mature stage) for different cumulus (KF, BMJ, GF, G3, GD and OKF) schemes are obtained from WRF model is shown in the Figure 93. The maxing ration shows a highly asymmetric character in the horizontal distribution. In Figure 93, maximum water vapor mixing 2 g/kg is obtained. It is noted that the highest mixing ratio are obtained at 950 hPa level close to the near of Bangladesh.

It is noted that the high moisture flux comes from the southern side covering a large area of the Bay of Bengal which feeds the system along its southeastern side through the boundary layer. The value of high moisture flux increases slightly with development of the system.

Maximum value of water vapor mixing ratio is 2 gm/Kg and it situated mainly at and around the centre of the cyclone. These maximum values cover large area of sea and small area of Bangladesh for all cumulus schemes. The south and western part of Bangladesh is cover with more value of water vapor mixing ratio (but less than 2 gm/Kg) finally, it may be concluded that all the schemes satisfy the intensification of the cyclone.

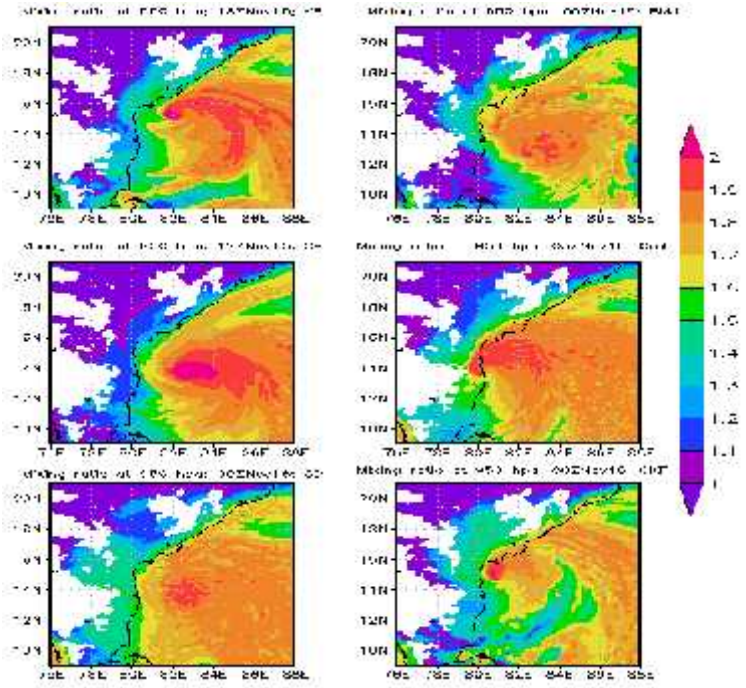

Figure 93: WRF model simulated horizontal distribution of water vapor mixing ratio at 950 hPa of TC Khaimuk at different cumulus schemes.

Chapter V

Conclusions

Four TC Rashmi, Viyaru, Nilam and Khaimuk have been simulated using six cumulus (Kain-Fritsch (KF), Betts-Miller-Janjic (BMJ), Grell–Freitas (GF), Grell-Devenyi (GD), Grell-3 and Old Kain-Fritsch (OKF) schemes option in ARW model and the following conclusion are made:

- Minimum sea level pressure (MSLP) for Rashmi using cumulus G3, OKF and BMJ match better than the others cumulus with the observed intensity (MSLP). For Viyaru, the observed MSLP is higher than the simulated MSLP for all cumulus schemes but intensity (MSLP) using BMJ and GD cumulus schemes is a little bit close to the observed value. For Nilam, intensity (MSLP) using cumulus BMJ, G3 and OKF match better than the others cumulus with the observed intensity. For khaimuk the intensity (MSLP) using GD cumulus is almost match the observed value.

- Variation of east–west elongated SLP and wind at the center are clearly observed for six cumulus scheme. For Rashmi and Nilam, the maximum intensity is obtained using GF cumulus scheme, for Viyaru the maximum intensity is obtained using OKF and for Khaimuk the maximum intensity is obtained using KF. For horizontal distribution, the performance of cumulus is same as above.

- The magnitude of maximum winds with different cumulus scheme is close to each other but more or less than the observed maximum wind.

- The simulated central pressure and maximum sustained wind at 10 m level are closed to the observed pressure and 10 m wind speed and intensified earlier or later time.

- Simulated vorticity, temperature anomaly, mixing ratio, relative humidity at different levels with change of time are satisfied the system intensification.

- The model has successfully simulated the strong relative vorticity at lower level spreading over the strong convective region of each cyclone. Simulated low level vorticity fields at 850 hPa level demonstrate the size of the system with strong convective regions of each cyclone, which are in agreements with the observations. For the weak systems the lower positive vorticity is found to extend up to 100 hPa level with exception.

- The warm core characteristics with maximum temperature anomaly simulated in the middle and upper troposphere successfully by all the cumulus. This warm core has the vertical extends from the lower level to tropopause.

- The high relative humidity is found in the eye wall of the TC and low relative humidity at the center. For all cumulus, it is observed that highest relative humidity more than 90% of the cyclones. But the relative humidity at 850 levels for all cumulus is 100% of the cyclones. And the relative humidity at 2m it is 100% for all cumulus of the cyclones.

- From the analysis of water vapor maxing ratio, it is found that moisture flux comes from the southern side covering a large area of the Bay of Bengal which feeds the system along its southeastern side through the boundary layer.

- Using different CP options, variation of MSLP is around -20 to 10 hPa compared to observed value for all cyclones except Viyaru. Temperature anomaly from 3-12 ^{0}C is obtained. Around 100 km cyclone eye is also observed. It may be concluded that the different CP options have their impact on the simulation of cyclonic Rashmi, Viyaru, Nilam and Khaimuk with more or less value with the observed value.

Reference

Akhter Md A.E, Md. M. Alam and M. A. K. Mallik, 2017: Impacts of Cumulus Physics for the Track Prediction of Tropical Cyclone Roanu, Dew Drop 3, 66-72.

Akhter Md A.E, Hossain, Alam, Md. M.; 2011: Sensititivity study of the cumulus parameterization schemes with planetary boundary layer option in estimating rainfall in Bangladesh using MM5, Prime University Journal of Multidisciplinary Quest, Volume-5, Number-1.

Arakawa, A.; V. R. Lamb, 1977: Computational design of the basic dynamical processes of the UCLA general circulation mode, Methods of Computational Physics, New York: Academic Press, 17, 173–265.

Betts, and M. J. Miller, 1986: A new convective adjustment scheme. Part II: Single column tests using GATE wave, BOMEX, ATEX and arctic air-mass data sets. Quart. J. Roy. Meteor. Soc., 112,693–709.

Bechtold P, Bazile E, Guichard F, Mascart P, Richard E (2001) A mass-flux convection scheme for regional and global models. Q J R Meteorol soc 127(573): 869-886.

Charney,J.G. and Eliassen, A. (1964) On the Growth of the Hurricane Depression. Journal of the Atmospheric Sciences, 21, 68-75.

Craig, G.C. and Gray, S.L., 1996: CISK or WISHE as the Mechanism for Tropical Cyclone Intensification. Journal of the Atmospheric Sciences, 53, 3528-3540.

Deardorff, J. W., 1972: Parameterization of the planetary boundary layer for use in general circulation models, Mon. Wea. Rev., 100, 93–106.

Deshpande M, Pattnaik S and Salvekar P 2010 Impact of physical parameterization schemes on numerical simulation of super cyclone Gonu; Natural Hazards 55(2) 211–231.

Deshpande, M., Pattnaik, S. and Salvekar, P.S. (2012) Impact of Cloud Parameterization on the Numerical Simulation of a Super Cyclone. Annales Geophysicae, 30, 775-795.

Dudhia, J., 1989: Numerical study of convection observed during the winter monsoon experiment using a mesoscale two-dimensional model, J. Atmos. Sci., 46, 3077-3107.

Dudhia, J, Hong, S .Y and Lim, K. S., 2008: A new method for representing mixed-phase particle fall speeds in bulk microphysics parameterizations. J. Meteo. Soc. of Japan, Vol 86A, 33-44

Efstathiou, G.A., Zoumakis, N.M., Melas, D. and Kassomenos, P., 2012: Impact of Precipitating Ice on the Simulation of a Heavy Rainfall Event with Advanced Research WRF Using Two Bulk Microphysical Schemes. Asia-Pacific Jour- nal of Atmospheric Sciences, 48, 357-368

Emanuel K.A 1983: On assessing local Condition Symmetric in stability from atmospheric sounding Mon .Web. Rev. 111, 2016-2033.

Evans, J.L., 1992: Comment on "Can existing climate models be used to study anthropogenic changes in tropical cyclone climate?". Geophys. Res. Lett., **19**, 1523-1524.

Fritsch J.M and C.F Chappell, 1980: Numerical Prediction of Convective Driven Mesoscale Pressure Systems, Part I: onvectiveParameterization.J.Atoms.sci.37, 1722-1733.

Gray, W.M., 1968: Global View of the Origin of Tropical Disturbances and Storms. Monthly Weather Review, 96, 669-700.

Grell, G. A., and D. Devenyi, 2002: A generalized approach to parameterize convection combining ensemble and data assimilation techniques. Geophysics. Res. Lett., 29(14), Article 1693

Grell, G.A., Freitas, S.R., Stuefer, M. and Fast, J.D. (2011) Inclusion of Biomass Burning in WRF-Chem: Impact on Wildfires on Weather Forecasts. Atmosphere Chemistry Physics,11,5289-5303. http://dx.doi.org/10.5194/acp-11-5289-2011

Henderson-Sellers, A., H. Zhang, G. Berz, K. Emanuel, W. Gray, C. Landsea, G. Holland, J. Lighthill, S.-L. Shieh, P. Webster, and K. McGuffie, 1998: Tropical Cyclones and Global Climate Change: A Post-IPCC Assessment. Bull. Amer. Meteor. Soc., **79**, 19-38.

Holland, G.J. and Merill, R.T., 1984: On the Dynamics of Tropical Cyclone Structural Changes. Quarterly Journal of the Royal Meteorological Society, 110, 723-745.

Holland, G.J., 1983: Tropical Cyclone Motion: Environmental Interaction plus a Beta Effect. Journal of the Atmospheric Sciences, 40, 328-342.

Hong S.Y., Y. Noh and J., Dudhia 2006: A new vertical diffusion package with an explicit treatment of entrainment processes. Mon. Wea. Rev., 134, 2318-2341

Hong, S.Y and Lim, J 2006: The WRF Single-Moment 6-Class Microphysics Scheme (WSM6) J. Korean Meteor. Soc., 42, 129–151.

Janjic, Z. I., 1994: The step-mountain Eta coordinate model: further developments of the convection, viscous sub layer and turbulence closure schemes. Monthly Weather Review, Vol. 122, 927-945.

Janjic, Z. I., 2000: Comments on 'Developments and evaluation of a convection scheme for use in climate models'. J. Atmos. Sci., 57, 3686.

Kain, J. S., J. M. Fritsch, 1990: A one-dimensional entraining/detraining plume model and its application in convective parameterization. J. Atmos. Sci., 47, 1184-1202.

Kain, J. S., J. M. Fritsch, 1993: Convective parameterization for mesoscale models: the Kain-Fritsch scheme. The representation of cumulus convection in numerical models, Meteo. Monogr, No. 46 Amer. Meteor. Soc., pp 165 – 170.

Kain, J. S., 2004: The Kain-Fritsch convective parameterization: An update. J. Appl. Meteor., 43, 170-181.Lin, Y.-L., R.D. Farley, and H. D. Orville, 1983: Bulk parameterization of the snow field in a cloud model. J. Climate Appl. Meteor., 22, 1065-1092.

Kanase, R.D. and Salvekar, P.S., 2011: Numerical Simulation of Severe Cyclonic Storm LAILA (2010): Sensitivity to Initial and Cumulus Parameterization Schemes. Proceedings of Disaster Risk Vulnerability Conference, 1, 165-170.

Kreitzberg, C. W., and D. J. Perkey, 1976: Release of potential in-stability: Part I. A sequential plume model within a hydrostatic primitive equation model. J. Atmos. Sci., 33,456–475.

Lighthill, J., G. J. Holland, W.M. Gray, C. Landsea, K.Emanul, G.Craig, J.Evans.

Li, X. and Pu, Z., 2008: Sensitivity of Numerical Simulation of Early Rapid Intensification of Hurricane Emily (2005) to Cloud Microphysical and Planetary Boundary Layer Parameterizations. Monthly Weather Review, 136, 4819-4838.

Mlawer, E. J., S. J. taubman, P.D. Brown, M. J. Lacono, and S. A. Clough, 1997: Radiative transfer for inhomogeneous atmosphere: RRTM, a validated correlated-k model for the longwave. J. Geophys. Res., 102(D14), 16663-16682.

Mukhopadhyay, P., Taraphdar, S. and Goswami, B.N., 2011: Influence of Moist Processes on Track and Intensity Forecast of Cyclones over the Indian Ocean. Journal of Geophysical Research: Atmospheres, 116, Published Online.

Pattanayak S. and Mohanty, U.C. (2008) A Comparative Study on Performance of MM5 and WRF Models in Simulation of Tropical Cyclones over Indian Seas. Current Science, 95, 923-936

Osuri, K.K., Mohanty, U.C., Routray, A., Kulkarni, M.A. and Mohapatra, M. (2012) Customization of WRF-ARW Model with Physical Parameterization Schemes for the Simulation of Tropical Cyclones over North Indian Ocean. Natural Hazards, 63, 1337-1359.

Raju, P. V. S., J. Potty, U. C. Mohanty, 2011: Sensitivity of physical parameterizations on prediction of tropical cyclone Nargis over the Bay of Bengal using WRF Model, Meteorol. Atmos. Phys. 113, 125-137.

Rao, D.V.B., Prasad, D.H. and Srinivas, D. (2009) Impact of Horizontal Resolution and the Advantages of the Nested Domains Approach in the Prediction of Tropical Cyclone Intensification and Movement. Journal of Geophysical Research: Atmospheres, 114, Published Online

Srinivas, C.V., Venkatesan, R., Rao, D.V.B. and Prasad, D.H., 2007: Numerical Simulation of Andhra Severe Cyclone (2003) Model Sensitivity to Boundary Layer and Convection Parameterization. Pure and Applied Geophysics, 164, 1- 23.

Shin, H. H., and S. Y., Hong, 2011: Inter-comparison of Planetary Boundary-Layer Parametrizations in the WRF Model for a Single Day from CASES-99, Boundary-Layer Meteorol, 139, 261–281.

Simpson, J., 1983: Cumulus clouds: Interactions between laboratory experiments and observations as foundations for models. Me-soscale Meteorology, D. K. Lilly and T. Gal-Chen, Eds., Reidel, 399–412 and V. Wiggert, 1969: Models of precipitating cumulus towers. Mon. Wea. Rev., 97, 471–489.

Srinivas, V., Venkatesan, R., Yesubabu, V. and Ramarkrishna, S.S.V.S., 2010: Impact of Assimilation of Conventional and Satellite Meteorological Observations on the Numerical Simulation of a Bay of Bengal Tropical Cyclone of Nov 2008 near Tamilnadu Using WRF Model. Meteorology and Atmospheric Physics, 110, 19-44.

Tao, W. K., J. Simpson, S. Lang, M. McCumber, R Adler and R. Penc, 1990: An algorithm to estimate the heating budget from vertical hydrometeor profiles. J. Appl. Meteor., 29, 1232-1244.

Trivedi, D.K., Mukhopadhyay, P. and Vaidya, S.S. (2006) Impact of Physical Parameterization Schemes on the Numerical Simulation of Orissa Super Cyclone (1999). Mausam, 57, 97-110.

Turner, J.A.; Lawson, B.D. 1978. Weather in the Canadian Forest Fire Danger Rating System. A user guide to national standards and practices. Environment Canada, Pacific Forest Research Centre, Victoria, BC. BC-X-177.

Conference Presentation

Flora Rahman, M. A. E. Akhter and M. M. Alam: Study on the structure of low intensity tropical cyclones of Bay of Bengal using WRF model, presented at the National conference on physics - 2017, Bangladesh physical society, Atomic Energy Center, Dhaka, 5-7 January 2017.